**Chemical conversion in piston engines for hydrogen and syngas production**

Von der Fakultät für Ingenieurwissenschaften, Abteilung Maschinenbau und Verfahrenstechnik der
Universität Duisburg-Essen
zur Erlangung des akademischen Grades

eines

Doktors der Ingenieurwissenschaften

Dr.-Ing.

genehmigte Dissertation

von

Kai Banke
aus
Essen

Gutachter: Univ.-Prof. Dr.-Ing. Sebastian Kaiser
Univ.-Prof. Dr. rer. nat. Tina Kasper

Tag der mündlichen Prüfung: 23.04.2024

**DOI:** 10.17185/duepublico/81908
**URN:** urn:nbn:de:hbz:465-20240516-083046-8

# Acknowledgements

This thesis was written during my employment as a research assistant at the Institute for Energy and Materials Processes – Reactive Fluids, EMPI-RF, formerly IVG-RF) at the University of Duisburg-Essen. The research was funded by the Deutsche Forschungsgemeinschaft under project ID 229243862 as part of the Research Unit FOR 1993.

First and foremost, I would like to thank my doctoral supervisor Prof. Dr. Sebastian Kaiser, who always supported me during this time. I learned a lot from him, especially about researching and publishing research papers. Thanks to him, I had the opportunity to work on an interesting project and I had the necessary freedom to shape the research according to my ideas.

I would also like to thank Prof. Dr. Burak Atakan, without whom this project would never have happened. Working with him and his group is an important part of this work and I learned a lot from it.

I would like to thank my colleagues Robert Hegner, Dominik Freund, Charlotte Rudolph and Dennis Kaczmarek for the good cooperation and for the exchange about the research and the many good ideas that came up and motivated me. I would like to thank my predecessor Dr. Sebastian Wiemann for his work in the initial phase of the project and the careful handover to me, which enabled me to quickly familiarize myself with the project and start the research.

I would also like to thank my parents who have always supported me and made it possible for me to follow my path to this point.

# Kurzfassung

Die Welt steht vor einer umfassenden Umstellung ihrer durch die Industrialisierung geprägten Energieinfrastruktur. Von der Verbrennung fossiler Energieträger muss ein Wechsel hin zu nachhaltigeren Alternativen vollzogen werden, um den Klimawandel zu stoppen und die Energieversorgung in der Zukunft zu gewährleisten. Um dies zu erreichen, ist die Erforschung von Übergangstechnologien, die die Umwandlung fossiler Brennstoffe mit hoher Effizienz ermöglichen und sich gleichzeitig flexibel an die Nachfrage anpassen, besonders wichtig. Diese Technologien müssen in der Lage sein, die starken Schwankungen in der Bereitstellung der Sonnen- und Windenergie zu bewältigen, die durch die vorhandenen Speicherkapazitäten nicht ausgeglichen werden können. Durch die Flexibilisierung der fossilen Energieumwandlung kann der Ausbau der nachhaltigen Energiequellen weiter vorangetrieben werden, ohne die Netzstabilität zu gefährden.

Eine Möglichkeit die Effizienz von Energiewandlungsprozessen zu erhöhen ist die sogenannte Polygeneration. Dabei wird die Wandlung von Primärenergieträgern zu mechanischer Energie oder Strom, Wärme und die stoffliche Umsetzung, z.B. zu Nutzchemikalien, in einem Prozess gekoppelt. Bei dem in dieser Arbeit untersuchten Konzept wird ein brennstoffreich betriebener Verbrennungsmotor als Reaktor eingesetzt, um durch die partielle Oxidation von Methan bzw. Erdgas gleichzeitig Strom, Wärme und Nutzchemikalien zu erzeugen. Durch diese Art von Prozess wird ein flexibles Wechseln zwischen maximaler Stromerzeugung (konventioneller Motorbetrieb) und reduzierter Leistungs- und Wärmeabgabe bei gleichzeitiger Nutzchemikalienproduktion (brennstoffreicher Betrieb) ermöglicht.

In dieser Arbeit wird der Einfluss unterschiedlicher Betriebsstrategien auf den brennstoffreichen Betrieb des Verbrennungsmotors untersucht. Dafür dient ein modifizierter BASF-Oktanzahlprüfmotor als Versuchsträger. Dieser wird entweder homogen selbstzündend (HCCI) unter Nutzung der zündbeschleunigenden Additive n-Heptan, Dimethylether, Diethylether und Ozon, oder durch Nutzung von reinem Sauerstoff als Oxidator fremdgezündet betrieben. Neben unterschiedlichen Additivgehalten und Äquivalenzverhältnissen ($\Phi$ = 0,5 bis 12) werden außerdem das Verdichtungsverhältnis ($\varepsilon$ = 4,5 bis 20) und die Einlasstemperatur ($T_{in}$ = 50°C bis 190°C) variiert. Eine Zugabe von $CO_2$ im Bereich von 0 bis 33 mol-% des Einlassgemischs wird ebenfalls untersucht. Der Einfluss auf Leistungs- und Wärmeabgabe, Betriebsstabilität, Produktgaszusammensetzung, Rußbildung und den Verbrennungsverlauf wird für den noch wenig erforschten brennstoffreichen Motorbetrieb untersucht.

Die Ergebnisse zeigen, dass der HCCI-Betrieb generell mit verschiedenen Additiven und Betriebsparametern realisiert werden kann. Gegenüber dem mageren HCCI-Betrieb ist der brennstoffreiche Betrieb deutlich weniger anfällig für hohe Druckanstiegsraten und Klopfen, da der hohe Brennstoffanteil als thermischer Puffer wirkt. Der Additivanteil, die Vorwärmtemperatur und das Verdichtungsverhältnis können effektiv genutzt werden, um die Lage der Verbrennung zu beeinflussen und einen stabilen Motorbetrieb einzustellen. Bei der Wahl von Additiven spielen in erster Linie die Reaktivität und die Wärmekapazität eine wichtige Rolle. Als sehr wirksam zeigt sich die Zugabe von kleinen Mengen Ozon als Additiv. Durch nur 75 ppm Ozon im Gesamtgemisch kann der für den stabilen Betrieb benötigte DME-Anteil im Experiment von 11% auf 5.3% des Gesamtkraftstoffs gesenkt werden. Hohe Verdichtungsverhältnisse führen im HCCI-Betrieb insgesamt zu deutlich reduzierten Additivanteilen und können sogar den HCCI-Betrieb ohne Additiv bei ansonsten konstanten Parametern ermöglichen. Während sich bei der Verwendung von Luft als Oxidator der HCCI-Betrieb als zuverlässiges Mittel für stabilen Motorbetrieb bei Äquivalenzverhältnissen im Bereich von $\Phi > 1{,}5$ erweist, wird für einige Untersuchungen mit der Zugabe von $CO_2$ zum Edukt der fremdgezündete Betrieb mit reinem Sauerstoff als Oxidator genutzt. Der hohe Sauerstoffanteil ermöglicht durch die Erhöhung der Flammengeschwindigkeit im Fremdgezündeten Betrieb einen stabilen Betrieb auch bei hohen Äquivalenzverhältnissen im Bereich $1{,}9 < \Phi < 2{,}5$. Bei dieser Art von Betrieb werden in einigen Betriebspunkten bis zu 40% des zugegebenen $CO_2$ umgesetzt. Außerdem kann bei dieser Betriebsart bei einem niedrigen Verdichtungsverhältnis von $\varepsilon = 4{,}5$ bei $\Phi = 2{,}3$ die mit 62% höchste Wasserstoffausbeute erreicht werden.

# Abstract

The world is facing a major transformation of its energy infrastructure shaped by industrialization. A shift from burning fossil fuels to more sustainable alternatives is now needed to stop climate change and ensure energy supply in the future. To achieve this, research into transition technologies that can convert fossil fuels with high efficiency while flexibly adapting to demand is particularly important. These technologies must be able to cope with the large fluctuations in the supply of solar and wind energy that cannot be compensated by existing storage capacities. By making fossil fuel energy conversion more flexible, the expansion of sustainable energy sources can continue without jeopardizing grid stability.

One way of increasing the efficiency of energy conversion processes is polygeneration. In such a process, the conversion of primary energy sources to mechanical energy or electricity, heat and the material conversion, e.g., to useful chemicals, are coupled in one process. In the concept investigated in this work, a fuel-rich internal combustion engine is used as a reactor to simultaneously generate electricity, heat and useful chemicals through the partial oxidation of methane or natural gas. This type of process allows flexible switching between maximum power generation (conventional engine operation) and reduced power and heat output with simultaneous chemical production (fuel-rich operation).

In this work, the influence of different operating strategies on the fuel-rich operation of an internal combustion engine is investigated. A modified BASF octane test engine is used as the test carrier. It is operated either in HCCI mode using the ignition-accelerating additives n-heptane, dimethyl ether, diethyl ether and ozone, or in spark ignition mode using pure oxygen as oxidizer. In addition to varying additive fractions and equivalence ratios ($\Phi$ = 0.5 to 12), the compression ratio ($\varepsilon$ = 4.5 to 20) and inlet temperature ($T_{in}$ = 50°C to 190°C) are also varied. Addition of $CO_2$ ranging from 0 to 33 mol% of the inlet mixture is also investigated. The influence on power and heat release, operating stability, product gas composition, soot formation and the combustion process will be investigated. The aim is to identify framework conditions and useful operating parameters for fuel-rich engine operation, which is still little researched.

The results show that HCCI operation can generally be realized with different additives and operating parameters. Compared to lean HCCI operation, fuel-rich operation is much less susceptible to high pressure rise rates and knocking because the high fuel content acts as a thermal buffer. It is shown that additive fraction, intake temperature, and compression ratio can be effectively used to shift the combustion phasing and induce stable engine operation. Reactivity and heat capacity are the primary factors in the choice of additives. The addition of small amounts of ozone as an additive is shown to be very effective. By adding only 75 ppm ozone to the total mixture, the DME content required for stable operation can be reduced in the experiment from 11% to 5.3% of the total fuel. High compression ratios result in significantly reduced additive fractions overall in HCCI operation and can even allow HCCI operation without additive while maintaining otherwise constant parameters. While HCCI operation is shown to be a reliable way for stable engine operation at equivalence ratios in the range of $\Phi > 1.5$ when air is used as the oxidizer, for some studies with the addition of $CO_2$ to the feedstock, spark ignited operation with pure oxygen as the oxidizer is used. The high oxygen content enables stable operation even at high equivalence ratios in the range $1.9 < \Phi < 2.5$ by increasing the flame speed in the spark ignited mode. In this type of operation, up to 40% of the added $CO_2$ is converted at some operating points. Moreover, with this type of operation, the highest hydrogen yield of 62% can be achieved at a low compression ratio of $\varepsilon = 4.5$ at $\Phi = 2.3$.

# Table of Contents

# List of figures

# List of tables

# List of symbols

### Latin symbols

| Symbol | Unit | Description |
|---|---|---|
| *C, C1, C2* | - | Constants in the Woschni equation |
| *CA20* | °CA | Crank angle at which 20% of the heat has been released |
| *CA50* | °CA | Crank angle at which 50% of the heat has been released |
| $E_l$ | J | Exergy loss |
| *PB* | - | Blackening value |
| *Q* | J | Heat |
| *R* | kJ / (kg K) | Ideal gas constant |
| $R_F$ | - | Reflectometer value of unblackened paper |
| $R_R$ | - | Relative brightness |
| *S* | - | Selectivity |
| $S_{irr}$ | J / K | Irreversible entropy generation |
| *T* | K | Temperature |
| *V* | m³ | Volume |
| *W* | J | Work |
| *X* | - | Conversion |
| *Y* | - | Yield |
| *H* | J | Enthalpy |
| $c_p$ | kJ / (kg K) | Isobaric heat capacity |
| $c_v$ | kJ / (kg K) | Isochoric heat capacity |
| *d* | m | Bore of the cylinder |
| *D* | m³ | Displacement |
| *d* | - | Normalized distance |
| *e* | kJ / kg | Specific chemical exergy |
| *e* | - | Energy fraction |
| *f* | Hz | Frequency |
| *m* | kg | Mass |
| *n* | mol | Number of moles |
| *p* | bar | Pressure |
| *r* | - | Temperature parameter in the Woschni equation |
| *s* | m | Stroke |
| *w* | - | Mass fraction |
| *w* | - | Corrected velocity factor |
| *x* | - | Mole fraction |
| *y* | - | Mass fraction |
| $h_i$ | J / kg | Specific enthalpy |
| $h_{L,i}$ | J / kg | Specific lower heating value of species i |
| $h^0_{f,i}$ | J / kg | Specific standard enthalpy of formation of species i |
| *u* | J / kg | Specific internal energy |

| | | |
|---|---|---|
| $\tilde{u}$ | m/s | Mean piston speed |

**Greek symbols**

| Symbol | Unit | Description |
|---|---|---|
| $\alpha$ | W / (m² K) | Heat transfer coefficient |
| $\gamma$ | - | Specific heat capacity ratio |
| $\varepsilon$ | - | Compression ratio |
| $\eta$ | - | Efficiency |
| θ | °CA | Crank angle |
| $\nu$ | - | Stoichiometric coefficient |
| $\sigma$ | - | Standard deviation |
| Φ | - | Equivalence ratio |
| $\omega$ | kmol / (m³ s) | Molar net production rate |

**Abbreviations**

| Symbol | Description |
|---|---|
| aTDC | After top dead center |
| ATR | Auto thermal reforming |
| bTDC | Before top dead center |
| CAD | Crank angle degree |
| CFD | Computational fluid dynamics |
| CHP | Combined heat and power |
| CI | Compression ignition |
| CoV | Coefficient of variation |
| CPO | Catalytical partial oxidation |
| DEE | Diethyl ether |
| D-EGR | Dedicated exhaust gas recirculation |
| DME | Dimethyl ether |
| DR | Dry reforming |
| EGR | Exhaust gas recirculation |
| EVC | Exhaust valve close |
| EVO | Exhaust valve open |
| EXP | Experiment |
| FSN | Filter smoke number |
| FT | Fischer-Tropsch |
| HC | Hydrocarbon |
| HCCI | Homogeneous charge compression ignition |
| HRA | Heat release analysis |
| ICE | Internal combustion engine |
| IMEP | Indicated mean effective pressure |
| IR | Infrared |
| IVC | Intake valve close |

| | |
|---|---|
| IVO | Intake valve open |
| LHV | Lower heating value |
| LTC | Low temperature combustion |
| LTHR | Low temperature heat release |
| MBF | Mass burn function |
| MFC | Mass flow controller |
| MFM | Mass flow meter |
| MON | Motor octane number |
| NDIR | Nondispersive infrared absorption |
| NG | Natural gas |
| NTC | Negative temperature coefficient |
| POX | Partial oxidation |
| PRF | Primary reference fuel |
| PRR | Pressure rise rate |
| PTFE | Polytetrafluoroethylene |
| RCM | Rapid compression machine |
| RON | Research octane number |
| S/C | Steam to carbon ratio |
| SI | Spark ignition |
| SIM | Simulation |
| slm | Standard liters per minute |
| SMR | Steam methane reforming |
| SOFC | Solid oxide fuel cell |
| SR | Steam reforming |
| ST | Spark timing |
| TDC | Top dead center |
| TTL | Transistor–transistor logic |
| UV | Ultra violette |
| WGS | Water gas shift |

# 1 Introduction

The world is facing a major transformation of its energy infrastructure, and this brings many challenges. To ensure energy supply in the future and halt climate change, research into technologies that convert fossil fuels with high efficiency, adapt flexibly to demand, and cope with large fluctuations in the supply of solar and wind energy is necessary. High-efficiency storage using batteries or pumped hydro storage is limited by cost and potential. As more renewable energy sources are used, it becomes increasingly important to make the remaining share of fossil energy conversion as flexible as possible to meet demand at any time.

An important fossil fuel that will continue to be used is methane, or natural gas. It will most likely remain an important energy source for at least some decades. When methane is converted to electricity, in conventional piston engines and gas turbine processes often only around 35% thermodynamic efficiency is reached while in combined cycles efficiencies over 60% can be achieved. Traditional combined-cycle power plants do not lend themselves to load-flexible operation. There are processes that achieve higher exergetic efficiencies by using waste heat or other otherwise unused waste gas streams [1,2]. In these cases, however, the processes are usually statically linked, with each individual process having fixed, optimized operating parameters. Instead, implementing a single, flexible process and thus being able to adapt production to demand would be of great advantage. Such a process could entail high exergetic efficiencies on the one hand, and on the other hand could be shifted towards the current demand, which would be beneficial for both economy and the environment.

Such a process could be implemented e.g., in gas turbines [3], or in piston engines. Piston engines offer the advantage that the possible size of the process is very well scalable, and both very small and large processes can be realized. Engines are attractive as chemical reactors because they cannot only achieve good turnovers as high-temperature and high-pressure reactors due to high possible speeds but also can stop the reaction quickly due to the rapid expansion of the mixture and the associated drop in temperature. This may allow freezing of certain reactions that could otherwise lead to the degradation of possibly desirable reaction products when equilibrium is reached.

Traditionally, piston engines are used to provide kinetic or electrical energy, i.e., for propulsion or for electric power generation. It is important that engines emit as few pollutants as possible. For this reason, they are usually operated stoichiometrically or lean, because in these cases mostly the complete reaction products $CO_2$ and $H_2O$ are formed. A large part of engine research in recent decades has focused on optimizing engines and their operation so that as little as possible of the substances harmful to humans and the environment, such as carbon monoxide, unburned hydrocarbons, nitrogen oxides or soot, are emitted. If, on the other hand, an engine is used as a polygeneration reactor, it is operated very fuel-rich and the substances resulting from incomplete combustion, such as carbon dioxide, hydrogen or hydrocarbons, are instead viewed as a product of the process. The main product is a mixture of CO and $H_2$ (also called synthesis gas or syngas) which can be further utilized in downstream processes such as Fischer-Tropsch synthesis, methanol synthesis or ammonia synthesis. Additionally, depending on the operating conditions, smaller amounts of hydrocarbons such as ethylene are produced, which could potentially be separated from the product stream. While stoichiometric and lean-burn operation of reciprocating engines are now very well studied, there is comparatively very little research on fuel-rich engine operation.

In 1957, Szeszich was the first to demonstrate syngas production using a spark-ignition (SI) engine with partial oxidation of methane/oxygen mixtures [4]. McMillian and Lawson subsequently investigated the combustion of fuel-rich natural-gas mixtures in SI engines through a combination of experiments and simulations [5]. Lim et al. further developed this research by preheating the intake mixture [6]. Karim et al. investigated partial oxidation in a Diesel engine by igniting fuel-rich mixtures of methane and oxygen-enriched air through a very short diesel fuel injection [7]. The state of the art will be reviewed in more detail in chapters 5 to 8.

From 2013 to 2023 the German Research Foundation DFG funded the Research Unit FOR 1993, “Multifunctional Material and Energy Conversion" that investigated the use of internal combustion engines for polygeneration, the simultaneous production of mechanical work, heat, and basic chemicals from methane. This research unit includes

various subprojects that cover theoretical and experimental aspects of the topic, including creation and reduction of reaction mechanisms for chemical kinetics, simulations and experiments in reactors, shock wave tubes, rapid compression machine and engines. This thesis work was funded by the project MM2 with the topic “chemical conversion in combustion engines under unusual operating conditions”, the most application-oriented project within FOR 1993.

The focus here is on experimental investigation of fuel-rich engine operation and identification of suitable operating ranges and parameters for polygeneration mostly using homogeneous charge compression ignition (HCCI) operation, which has been identified as advantageous for stable fuel-rich combustion in previous investigations by Wiemann [8]. It is important to understand what effects the different operating strategies might have on important process parameters like work, heat and chemical outputs. The effects of fuel composition, preheating, and compression ratio on parameters such as indicated mean effective pressure, combustion phasing, heat production, efficiency, conversions, yields, and soot production will be studied in order to establish a basis for possible process control strategies in fuel-rich HCCI operation, which is a challenging issue with very limited existing studies or strategies.

To explore possible process control strategies, the first step was to develop an operating stability scan and establish limits for CoV (Coefficient of Variation) and maximum rate of pressure rise, which determine an acceptable operating range. This scan serves as a reference for setting comparable operating points. The initial investigations utilized the experimental setup from a previous work by Wiemann [9]. A comparison is made between traditional spark ignition operation and HCCI operation in the fuel-rich regime, focusing on the overall impact of equivalence ratio ranging from 0.5 to 12 on syngas yield, methane conversion, work, and efficiencies. Furthermore, the influence of compression ratio on syngas production is examined. To increase the compression ratio, the engine was modified and metal inserts were placed in the combustion chamber which reduce the compressed volume and hence allow the compression ratio to be set from $\varepsilon = 4.5$ to 20 instead of $\varepsilon = 4$ to 12 as before. The inserts make the combustion chamber geometry slightly more cylindrical to minimize heat losses. These investigations are presented and discussed in chapter 4.

In a further step, using DME as an additive, the equivalence ratio and intake temperature are varied to understand how changing these parameters affect operating stability, combustion characteristics, syngas production, and soot formation. In addition, collaborators in FOR 1993 performed simulations for selected operating points that provide insight into the chemical conversion to understand the mechanisms in more detail. This investigation is discussed in Chapter 5.

Another objective of this work is to determine a basis for the selection of additives for fuel-rich HCCI operation. Since it is not possible to investigate all possible additives with reasonable effort, the approach is instead to investigate a few different additives and to understand exactly how they work, so that conclusions can also be drawn about the suitability of other additives. To compare the additives n-heptane, diethyl ether and dimethyl ether, a small fuel injector was installed so that liquid additives could be accurately dosed in small quantities. A heat release analysis was adapted for fuel-rich operation in addition to the investigations already described. The results of the heat release analysis of the experiments are compared with simulations performed by collaborators and the results of the simulations are used to draw conclusions about the chemical kinetics during auto-ignition with different additives. These investigations are shown in Chapter 6.

Since for lean HCCI operation ozone is a very potent ignition-promoting additive [10,11], experiments are discussed in Chapter 7 in which DME was gradually replaced with ozone as an additive in order to determine its effectiveness in fuel-rich operation as well. The goal here is to use ozone to significantly reduce the amount of hydrocarbon additives or even to replace them completely, as this could be a great advantage from an economic point of view, since hydrocarbon additives are significantly more expensive than methane. For this purpose, the experimental setup was extended to include an ozone generator, which enriches a stream of pure oxygen with ozone. A reaction path analysis performed by collaborators provides information on the mode of action during auto-ignition with ozone.

The utilization of $CO_2$ from carbon capture processes in downstream processes is increasingly sought after, due to the high cost and difficulty of storing $CO_2$. One attractive possibility is converting it to syngas via dry reforming with methane. Studies were carried out to investigate whether and how such a process can be carried out in an engine. However, due to the significant increase in the heat capacity of the mixture caused by the addition of $CO_2$, which makes auto-ignition more challenging, spark ignited operation using pure oxygen was chosen as the operating strategy instead of HCCI operation. In addition to converting $CO_2$, this strategy offers the benefit of producing a product that is not diluted with atmospheric nitrogen, unlike HCCI operation with air. These studies are discussed in Chapter 8.

# 2 Theoretical background

## 2.1 Production of syngas

Synthesis gas or syngas is a term commonly used for a mixture of hydrogen and carbon monoxide. Usually it also contains methane, carbon dioxide, nitrogen, and traces of other gases. Syngas is an important base chemical that is used for the synthesis of ammonia, methanol, DME, ethanol and a many other hydrocarbons. Also, most of the worldwide available hydrogen is produced by separation from syngas. There are many ways to produce syngas from various gaseous or liquid educts like natural gas, alcohols, and hydrocarbons. Syngas is also made by gasification of solid carbon sources like coal with steam. The composition of the syngas depends on the production process.

The most-used industrial process for syngas production is the steam reforming of natural gas also called steam methane reforming (SMR). Further common practices are partial oxidation (POX) and autothermal reforming (ATR). Dry reforming (DR) of methane with $CO_2$ as a reforming agent is also gaining interest.

### 2.1.1 Steam reforming

Reforming methane with steam is usually carried out on a nickel or cobalt catalyst at temperatures in the range of 500 to 1100°C. Since natural gas contains sulfur in small amounts a desulfurization is a necessary pretreatment to avoid poisoning and deactivation of the catalyst. Eq. (1) describes the reaction of SMR. The reaction is highly endothermic and requires heat supply.

$$CH_4 + H_2O \leftrightarrow CO + 3H_2, \quad \Delta H^0{}_{298} = 206\frac{kJ}{mol} \tag{1}$$

$$CO + H_2O \leftrightarrow H_2 + CO_2, \quad \Delta H^0{}_{298} = -41\frac{kJ}{mol} \tag{2}$$

While the reaction suggests a stoichiometric steam to carbon (S/C) ratio of 1, in real processes typically ratios of 2.5-3 are applied since lower ratios result in coking and thus in the deactivation of the catalyst by carbon deposition [12].

If the desired product of the process is not just syngas but only hydrogen a water gas shift (WGS) reaction is carried out after the SMR process to convert the CO with $H_2O$ to further hydrogen and to $CO_2$ (eq. (2)).

### 2.1.2 Partial oxidation

POX of methane is an alternative route to syngas. It can be done with and without a catalyst. Without catalyst the temperatures need to be high enough to avoid excessive soot formation. A special burner design is used to control the temperature levels. When using a catalyst, the process is also called catalytic partial oxidation (CPO). In CPO a premixed methane/oxygen mixture is fed to a catalytic reactor without using a burner [13]. POX provides $H_2$/CO ratios of ~2 (with NG as an educt) that are favorable for Fischer-Tropsch (FT) and methanol synthesis [14]. Eq. (3) shows the chemical reaction of POX.

$$CH_4 + 0.5O_2 \leftrightarrow CO + 2H_2, \; \Delta H^0{}_{298} = -71\frac{kJ}{mol} \tag{3}$$

It is exothermic and does not require heat supply like SMR or DR.

### 2.1.3 Dry reforming

The reformation of methane with $CO_2$ as a reforming agent (eq. (4)) is also called dry reforming.

$$CH_4 + CO_2 \leftrightarrow 2CO + 2H_2, \quad \Delta H^0{}_{298} = 260 \frac{kJ}{mol} \tag{4}$$

Since $CO_2$ gained increased focus as a greenhouse-active gas in the last years it also became more interesting as input for the production of syngas. The reaction is highly endothermic and yields a syngas with a $H_2$/CO ratio of 1. It is often used in secondary reforming processes to reduce the $H_2$/CO ratio of a steam reforming process [15]. However, the reaction of $CH_4$ and $CO_2$ is very susceptible to carbon deposition. Therefore, the choice of operating parameters and catalysts is limited.

### 2.1.4 Autothermal reforming

ATR is a combination of methane reforming with POX. It combines the two processes to avoid the need for an additional heat supply to the reactor since the exothermicity of the POX reaction is used to supply the heat that is needed for the endothermic reforming reaction. The most common form of ATR is the combination of steam reforming with partial oxidation. Far less common is the combination of dry reforming with POX. Since for ATR there is no need for large heat transfer surfaces, ATR reactors can be more compact than SMR reactors. This reduces the investment costs and in addition, the lower $H_2$/CO ratio compared to SMR makes the process more suitable for FT synthesis.

## 2.2 Internal combustion engine

The technology of combustion engines has been developed for over a century. Internal combustion engines are machines that can convert fuel to mechanical work with a high power density. This compactness makes them ideal for use in mobile applications. For this reason, most engines worldwide are used for transportation. But there are also stationary applications such as combined heat and power plants (CHP). Internal combustion engines have a very good scalability and can be as tiny as a power supply of a remote-controlled toy car and as big as needed for propulsion of a huge ship.

There are different types of internal combustion engines that can be distinguished by the type of combustion strategy, the way pressure is converted into rotational movement of the crank shaft, the kind of fuel they use, the strategy they use to exchange the charge, configuration of the cylinders and by other characteristics. Regarding the conversion of pressure into rotational movement by far the most important type of engine is the reciprocating piston engine. There are other less common topologies like for example the rotary piston engine.

The most significant strategy for exchange of the cylinder charge is four-stroke engine operation. Figure 1 shows a p-V-diagram of a four-stroke SI engine.

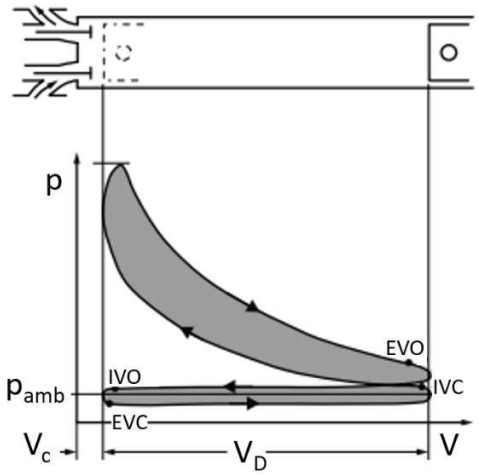


Figure 1: p-V-diagram for a four-stroke SI engine, adapted from [16].

In a four-stroke engine the increase in cylinder volume by the moving piston and the resulting decreasing pressure draws in the fresh charge. Then the intake valve closes (IVC) and the piston compresses the mixture. The mixture is ignited near TDC and during the expansion stroke work is transferred to the piston. The exhaust valve opens (EVO) and the exhaust is pushed out by the piston. Before TDC the intake valve opens (IVO) and briefly after TDC the exhaust valve closes (EVC). This "positive valve overlap" helps to flush the combustion chamber. The next cycle then starts.

### 2.2.1 Basic combustion strategies

There are two types of combustion processes that are widely used for internal combustion engines. The first type is spark ignition operation, which is used in a type of engine referred to as Otto engine. It is using a spark plug to ignite a mixture of air and relatively auto-ignition resistant fuels like gasoline. The second type is compression ignition (CI), which is used in Diesel engines. This strategy uses more reactive fuels that auto-ignite when injected into compressed air. In the following those two strategies and additionally one newer strategy that is recently investigated, homogeneous charge compression ignition (HCCI) will be explained.

#### 2.2.1.1 Spark ignition

In SI operation a premixed stoichiometric or somewhat lean charge of air and fuel is ignited by a spark plug. Traditionally the fuel is mixed with the air by using a carburetor but today most applications use fuel injectors in the intake manifold or even direct injection into the combustion chamber. Figure 2 shows a schematic of the combustion chamber in a spark ignition engine.

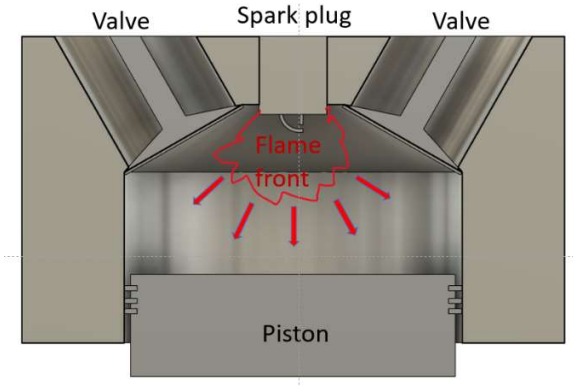


Figure 2: Schematic of a spark ignition engine with flame propagation.

From the spark igniting the mixture, a turbulent flame propagates through the combustion chamber until it is quenched near the walls. The speed of the flame propagation depends on equivalence ratio, the fuel, and on the motion of the cylinder charge. Turbulence drastically increases the speed of the flame propagation, which is the reason why higher engine speeds do not lead to early flame quenching at a constant ignition timing. From the spark plug, the flame spreads until it is quenched near the cylinder walls. Due to this fact, the combustion chambers of spark-ignited engines are usually designed with an angled combustion chamber roof to promote uniform flame spread in all directions. Most SI engines use stoichiometric combustion because in this case a three-way catalyst can be used to drastically reduce pollutant emissions and also because the highest power density can be reached. In other engines, especially in heavy-duty gas engines however, lean mixtures are used. The overall lower combustion temperatures reduce $NO_x$ formation and lean mixtures offer a higher thermal efficiency.

The most common way of load control in an SI engine is a quantitative approach by controlling the charge mass. The fuel and air are mixed in the intake and the amount of mixture aspirated to the cylinder is subsequently controlled by a throttle that induces a pressure drop on the cylinder side during intake. By opening or closing the throttle the engine's load can be increased or decreased. In direct injection engines the power can also be controlled qualitatively by varying the amount of injected fuel.

When an SI engine operates at the auto-ignition limit, it means that the air-fuel mixture is on the verge of spontaneously igniting due to high temperatures and pressures in the combustion chamber. At this operating condition, the pressure increase caused by the initial ignition at the spark plug can lead to auto-ignition at other hotspots within the cylinder before the flame front has reached them. This can lead to two opposing flame fronts that cause oscillating cylinder pressures and very high pressure rise rates. This phenomenon is known as knocking and can cause severe damage to an engine. For this reason, an important criterion for a fuel used in an SI engine is a high octane number. The octane number characterizes a fuels resistance to auto ignition. It is defined as the volume fraction of iso-octane in a mixture of iso-octane and n-heptane that has the same knock resistance as the tested fuel at constant, predefined operating conditions. Higher octane numbers allow for elevated compression ratios or early spark timings and can help to improve overall performance.

The operating limits when varying the equivalence ratio in spark ignition operation depend on factors like charge temperature, the kind of spark plug, compression ratio, spark timing and charge motion among others. The limits for lean and rich operation both result from decreasing flame speeds leading to quenching of the flame and misfires.

#### 2.2.1.2 Compression ignition

In a compression ignition engine, the charge is compressed to temperatures high enough to ignite the fuel-air mixture. The most representative form of CI engine is the Diesel engine. In a Diesel engine the fuel ignites continuously during the injection into compressed air and forms a jet with zones of different composition and temperatures. Since the fuel is mixing with the surrounding air during injection, a traditional CI engine is always

operated globally lean to ensure complete combustion. Nevertheless, in the simultaneous mixing and combustion locally fuel rich zones are formed in which soot is produced. Soot formation is one of the key problems and limitations of CI combustion. Figure 3 shows a schematic of a stabilized diesel jet.

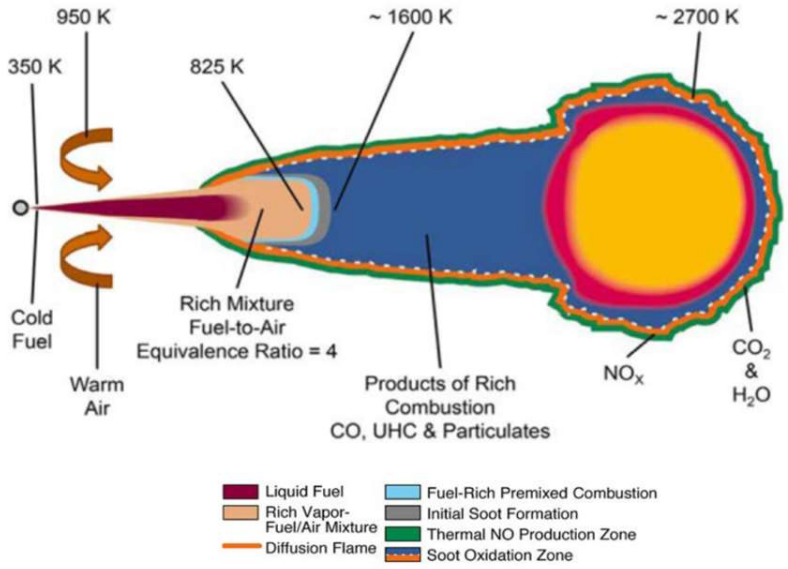


Figure 3: Schematic of a combustion jet in a diesel engine [17]

The jet travels a short distance while it heats up, evaporates, and mixes with air. At first a fuel-rich zone is formed, and a fuel-rich premixed combustion occurs which leads to initial formation of soot. The jet moves further into the combustion chamber and mixes with more air which initially causes it to form more products of incomplete combustion. The equivalence ratios are lowest at the outer edges of the jet. There (green zone) the mixture is leanest, and most $NO_x$ is formed. A diffusion flame (orange) surrounds the spray and oxidizes part of the soot and other products of incomplete combustion. Since it takes high temperatures and oxygen to oxidize a higher fraction of the soot more $NO_x$ is formed if more soot is oxidized. This is a common trade-off in CI combustion since the emission of both pollutants is undesirable.

An advantage of CI engines over SI engines is that elevating the compression ratio is not limited by the fuel characteristics. The most important limitation for compression ratio in CI engines is heat loss, which increases with higher surface to volume ratios in the top dead center (TDC) at higher compression ratios. Typical values for compression ratios in CI engines are in the range of 12 to 24. Another advantage of CI engines is their qualitative load control. The engine load is controlled by the amount of fuel injected into the cylinder. In general CI engines have higher efficiencies because of these two advantages. However, since they must withstand higher pressures, they need to be designed mechanically stronger which increases the manufacturing costs.

In CI engines the fuel is injected at high pressures > 1000 bar. Higher pressure leads to better atomization of the spray and thus it improves combustion. The pressure is elevated by a pump, and in modern CI engines it is distributed from a rail to all injectors. In CI combustion it is important for a fuel to have a high tendency to auto ignite. The measure used for this characteristic is the cetane number. Similar to the octane number it is the fraction of cetane in a cetane and 1-methylnaphthalin mixture that has the same ignition characteristics as the fuel that is tested. Generally, a higher cetane number reduces pollutant emissions since the fuel ignites early and there is sufficient time to oxidize a major part of the pollutants before the reaction is quenched due to decompression. In

the end the cetane number that can be used is depending on the type of engine. A wide variety of fuels can be used in CI engines ranging from heated heavy fuel oil that is used in marine applications to gaseous fuels like dimethylether (DME). However, in most applications light fuel oils are used.

#### 2.2.1.3 Homogeneous Charge Compression Ignition

Of several alternative combustion process concepts, homogenous charge compression ignition (HCCI) is most relevant here. HCCI combines advantages of SI- and CI combustion. In HCCI a premixed charge is ignited by temperature increase due to compression. This makes it possible to operate on very lean mixtures and mixtures diluted by exhaust gas recirculation that would normally not allow for stable operation in SI mode. In HCCI operation the mixture ignites (theoretically) homogeneously and does not form a high temperature flame region. Lean burn, exhaust gas recirculation and low flame temperatures all reduce the emission of $NO_x$. There is no soot particulate formation like in CI operation since the combustion is premixed and no locally fuel rich zones can form. No throttling is needed because the engine is mostly controlled by dilution of the charge. Combining those features results in high thermal efficiencies with low emissions which may be an attractive alternative to conventional engine combustion. However, the kinetically controlled nature of the auto-ignition makes combustion control very difficult in HCCI. Ignition is almost exclusively depending on fuel reactivity and temperature. Other effects like stratification and turbulence have shown minor influence on HCCI combustion [18,19]. Changes or stratification in temperature or fuel-composition or small changes in the residual gas content can change the combustion phasing drastically. This is particularly noticeable at full load or in transient operation. Due to these difficulties, the HCCI process is not widely used in series production engines to this day. For stationary applications however these difficulties are not too challenging because there is almost no transient and only limited part load operation.

Figure 4 shows the soot and $NO_x$ formation for traditional diesel and spark ignition operation and HCCI operation depending on in cylinder temperature and equivalence ratio.

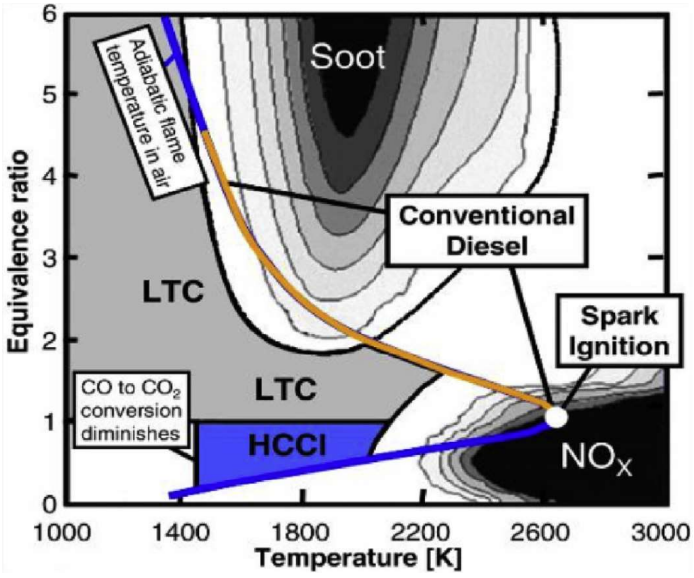


Figure 4: Operating regimes of traditional spark-ignited (SI) engine, diesel engine and HCCI combustion engine [20].

The advantage of HCCI combustion and general low temperature combustion (LTC) above traditional SI and CI operation in terms of pollutant emission can be seen. For CI operation (yellow line) there is always a conflict between soot and $NO_x$ formation because if one is avoided more of the other is emitted. For Spark ignition operation there is always $NO_x$ formation because of high temperatures in the flame front. HCCI operation enables the simultaneous avoidance of both pollutants. However, the disadvantage of low combustion temperatures is that

oxidation of the part of the mixture that is pushed into crevices near TDC is much less complete than for higher temperatures. This leads to increased emissions of CO and unburned hydrocarbons.

There are several strategies that can be used to control the combustion phasing in HCCI operation indirectly. The most common approach is to vary the amount of residual gas in the cylinder. One way to achieve this is by varying the valve timings so part of the residual gas is recompressed or rebreathed to the cylinder, depending on the strategy. The amount of hot residual gas is used to control in cylinder temperatures and associated reactivity of the charge. This becomes problematic in low-load regions where the residual gas temperatures are not sufficient to ensure auto-ignition. Another approach is to vary the intake temperature by preheating the mixture. This is not very practical in mobile applications but for stationary engines this can be convenient. Dual-fuel operation is another strategy that can be used. It uses two fuels of different auto-ignition behavior and controls combustion phasing by changing the mixture. If the fraction of the more reactive fuel is increased combustion phasing will advance and vice versa. However, this approach requires a second fuel tank and an additional injection system. Also, an engine with variable compression ratio can be used to control the combustion phasing via compression. The problem with this approach is that variable compression ratios are very difficult to implement. [21]

### 2.2.2 Pressure based metrics

This section describes some basic measures for the characterization of the combustion process in internal combustion engines that were used for processing of the results presented later in this work. The measures are based on in-cylinder pressure traces and thermodynamic calculations.

#### 2.2.2.1 Indicated mean effective pressure

The work transferred to the piston can be calculated as

$$W = \oint p \, dV \tag{5}$$

with the in-cylinder pressure p and the actual cylinder volume V which is a function of the crank angle. By dividing the work by the displacement volume, the indicated mean effective pressure (IMEP) can be calculated.

$$IMEP = \frac{W}{V_D} \tag{6}$$

It is a volume specific work and can, for example, be used to evaluate operating conditions or to compare engines of different sizes.

#### 2.2.2.2 Cycle-to-cycle variability

Engine combustion is subject to cycle-to-cycle variability. These variations can be attributed to the stochastic behavior of turbulent flows and combustion itself. The cylinder pressure of 10 consecutive cycles in SI operation is shown in Figure 5.

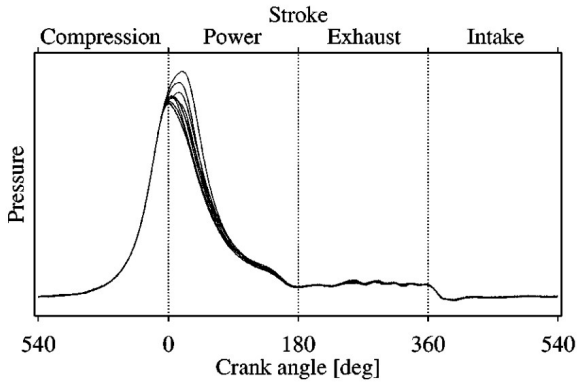


Figure 5: Variability in cylinder pressure from cycle to cycle. Pressure traces from ten consecutive cycles of a four-stroke Otto engine. [22]

A significant difference in cylinder pressure traces for ten consecutive cycles can be seen. This has a distinct influence on IMEP and other combustion characteristics. If those variations in cylinder pressure are too large, engine operation may become unstable.

A widely used metric for this is the coefficient of variation (CoV) of the IMEP, which is the standard deviation σ of the IMEP of many consecutive cycles divided by their arithmetic mean $\overline{\text{IMEP}}$.

$$\text{CoV} = \frac{\sigma_{IMEP}}{\overline{\text{IMEP}}} \tag{7}$$

If the CoV exceeds about 10% in mobile applications it results in drivability problems [23] (p. 417). In modern engines the CoV is usually much lower (< 2%). In stationary applications, however, higher CoV might be acceptable since there is no high requirement for smooth running.

#### 2.2.2.3 Heat release analysis

Heat release analysis (HRA) uses measured pressure traces and thermodynamic calculations to draw conclusions about the reaction in the combustion chamber.

The reaction for the complete combustion of methane as a fuel is:

$$CH_4 + 2\,O_2 \leftrightarrow CO_2 + 2\,H_2O, \quad \Delta H^0{}_{298} = -802\frac{kJ}{mol} \tag{8}$$

with all components in gaseous form. When one mole of methane is converted with two moles of $O_2$ the released reaction enthalpy at ambient temperature is 802 kJ. This reaction enthalpy is also called the lower heating value (LHV). There are several reasons why this energy is not completely converted into mechanical work. Those are incomplete combustion, thermodynamic limitations of the process, heat losses and mechanical losses due to friction.

In production engines a combustion efficiency $\eta_{comb}$ of > 98% is typical. If the combustion efficiency is then multiplied with the reaction enthalpy and the fuel mass $m_f$ this yields the theoretically released heat by chemical reaction $Q_{ch}$.

The first law of thermodynamics for an open system for the combustion chamber can be written as

$$\delta Q_{ch} = dU_s + \delta W + \delta Q_{ht} + \sum h_i \, dm_i \tag{9}$$

while $dU_s$ ist the change in sensible energy, $\delta W$ is the piston work, and $\delta Q_{ht}$ is the heat loss to the cylinder walls [23] (p.386). The term $h_i dm_i$ represents the mass losses due to crevices. Since they are usually small, they are neglected in the following. If eq. (9) is represented as a function of the crank angle and combined with the ideal gas law this yields eq. (10) with the crank angle θ and the heat capacity ratio γ of the mixture.

$$\frac{dQ_{ch}}{d\theta} = \frac{\gamma}{\gamma - 1} p \frac{dV}{d\theta} + \frac{1}{\gamma - 1} V \frac{dp}{d\theta} + \frac{dQ_{ht}}{d\theta} \tag{10}$$

The heat capacity ratio γ is a function of the composition and the temperature in the combustion chamber. Both change during combustion. There are several ways to calculate γ. A comparison of different methods can be found in [24]. A method that can be used for traditional combustion engines is a simple approach that calculates γ as a linear function of the cylinder temperature (eq. (11)) [25].

$$\gamma(x_i, T) = \frac{c_p}{c_v} = a - b * T(\theta) \tag{11}$$

In this case a and b are values that are tabulated for different engine types, fuel types and equivalence ratios.

Figure 6 shows a typical cumulative heat release trace for engine combustion.

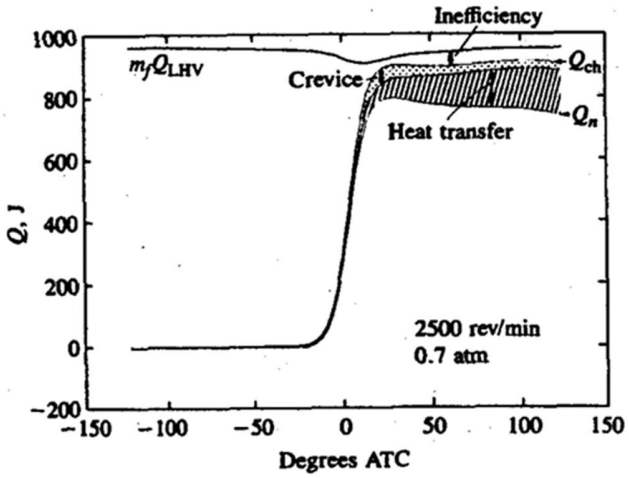


Figure 6: Results of heat-release analysis showing the effects of heat transfer, crevices, and combustion inefficiency [23] (p. 388).

The heat that would be theoretically released by complete combustion $m_f Q_{LHV}$ can be seen at the top. Because of combustion inefficiency $Q_{ch}$ is lower. The trace of $Q_{ch}$ versus crank angle shows the typical S shape for heat release. The crevice losses and the losses due to heat transfer are so small before and at the beginning of combustion that they cannot be seen. When combustion increases pressure and temperature these losses also increase. Mass is pushed into crevices due to high pressure and the high temperatures increase heat loss. After subtraction of the losses the lowest trace of the net heat release $Q_n$ remains. This is the actual heat release that can be seen from the pressure trace without compensating for the other losses.

It is especially useful to look at the actual heat release rates since they give insight about how fast reaction occurs depending on the crank angle. Figure 7 shows as an example some heat release rates of different operating points in an HCCI engine operated on lean n-heptane mixtures with ozone addition.

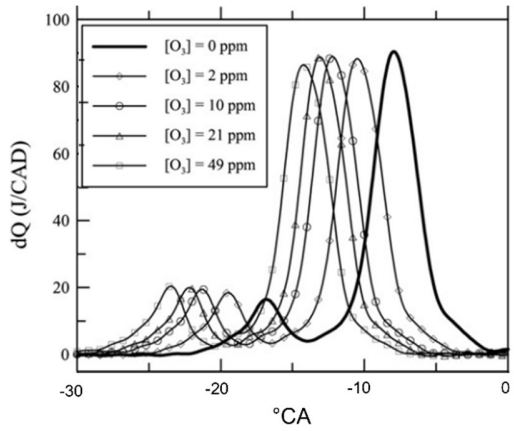


Figure 7: Heat release rates of n-heptane HCCI operation with different amounts of ozone [10].

The heat release rates show the two-stage auto-ignition of the n-heptane with a lower early low temperature combustion peak followed by a short negative temperature coefficient (NTC) region and the higher second main combustion peak. With increasing ozone fraction the whole combustion shifts to early crank angles. Also, a slight increase in the low temperature combustion peak can be seen for increasing ozone fractions. This example shows how HRA can find even slight changes in combustion.

## 2.3 Combined heat and power production

The conversion of heat to mechanical work in heat engines is limited so usually there is a significant amount of residual thermal energy from heat engines. Cogeneration or also combined heat and power (CHP) production is an approach to use this energy for other purposes instead of separately producing it in a second process. This increases overall efficiency and reduces resource costs. There are different options to realize such a process. Using combustion engines is one of them. Figure 8 shows a simple schematic of the energy flow for an ICE with generator.

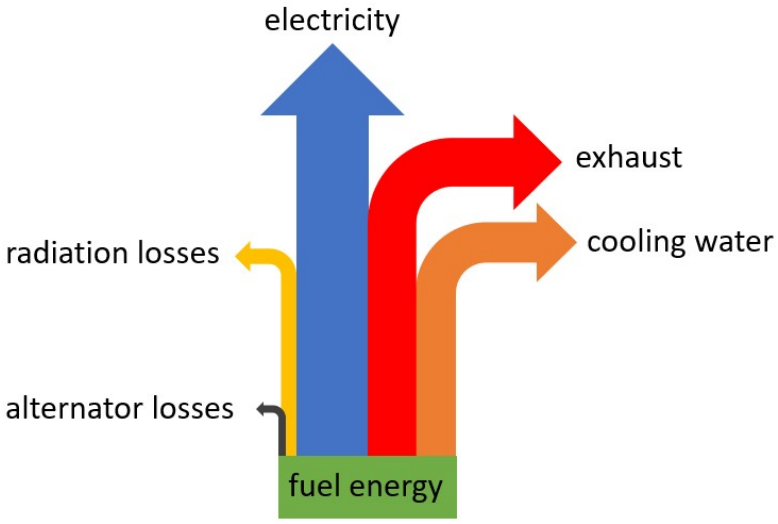


Figure 8: Simple Sankey diagram of an ICE with generator.

While about 43% of the fuel energy can be converted to electricity, about the same amount of energy is distributed to exhaust gas and cooling water heat. The cooling water usually has a temperature of around 80°C, which is quite sufficient for building heating, which often requires a temperature level of at least 60°C. The exhaust heat has temperatures above 400°C and can be used for purposes that require heat at a higher temperature level than that of the cooling water, although in many cases it is also used for building heating. Often, the heat from both sources is transferred to a single circuit.

Typical areas of application for CHP units are places with a high demand for heat in addition to a demand for electricity. Those can for example be hospitals or large swimming pools. A schematic of an ICE based CHP unit is shown in Figure 9.

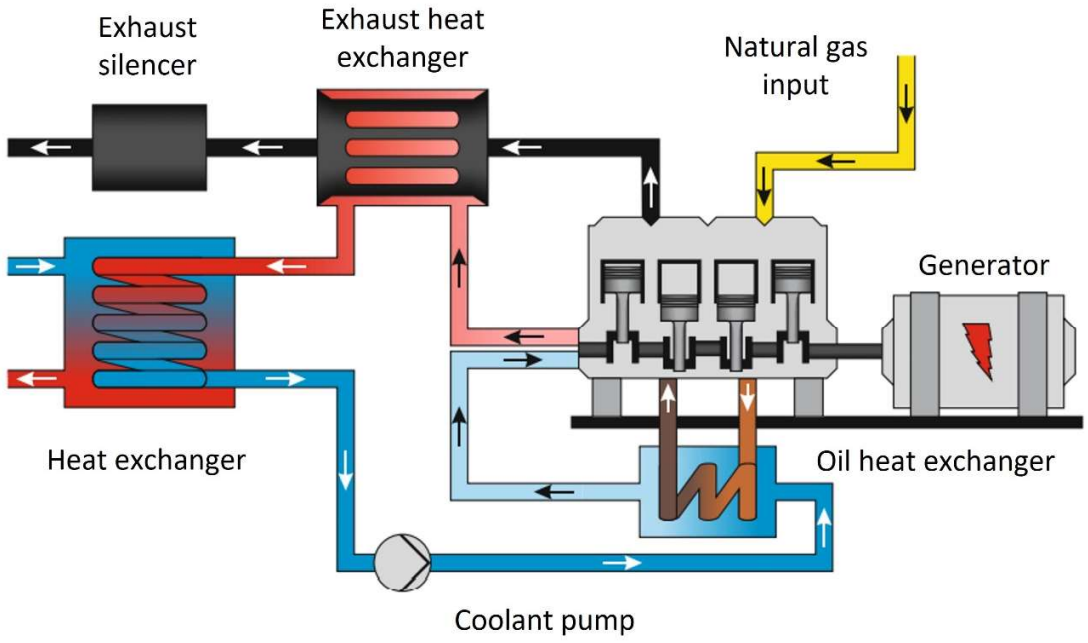


Figure 9: Schematic of a CHP unit [9]

The natural gas operated engine powers a generator to produce electricity. After the hot cooling water exits the engine, it passes the exhaust heat exchanger to also capture part of the higher temperature exhaust heat. Afterwards the hot water enters another heat exchanger where the heat is transferred to an external water circuit and can be used for other purposes.

CHP systems benefit from decentralized applications since power and heat can be provided without necessity of expensive infrastructure for distribution. Next to conventional power plants and combustion engines also micro turbines or solid oxide fuel cells (SOFC) are popular for use in cogeneration systems. Such systems can be realized in sizes that fit the demand of residential buildings.

## 2.4 Polygeneration

The idea of cogeneration systems can be extended by not only using the energy outputs of the system but also the material outputs. Such processes are called polygeneration processes. Polygeneration is the combined production of several useful outputs in one system with the goal to achieve maximum thermodynamic efficiency. Combining the output of several products in a single process aims to reduce the overall residues. Polygeneration processes can provide multiple energy vectors and other products at the same time.

One of the advantages of polygeneration processes is their capability to combine fossil and renewable energy sources. Possible energy sources are e.g., coal, fossil fuels or natural gas but also solar, wind or geothermal. Figure 10 shows possible pathways of polygeneration processes.

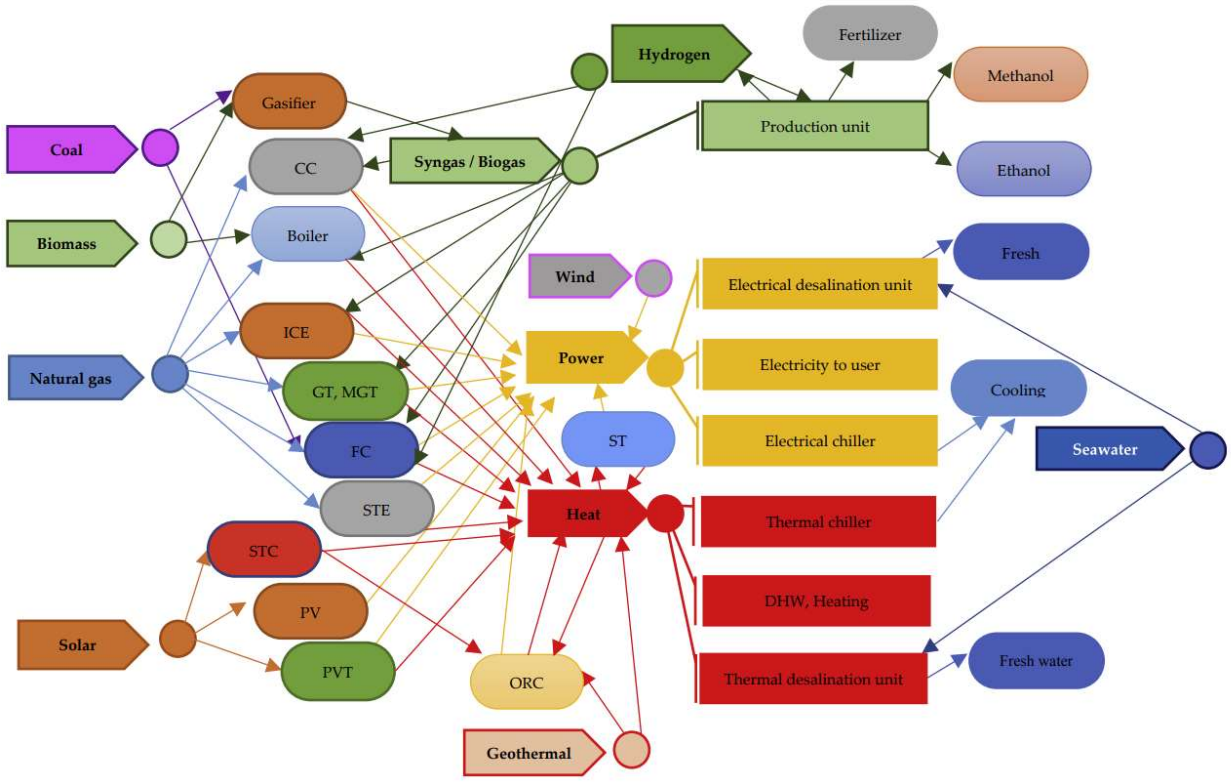


Figure 10: Possible pathways of polygeneration processes [26]

The number of combinations is rather unlimited. Combinations include, for example, the simultaneous generation of power, heat and drinking water from renewable energy sources, which is especially interesting for smaller islands. Other approaches combine for example a steel plant with the production of methanol as byproduct [27]. Common products next to power, heat and cooling can be potable water and syngas, which is further converted to hydrogen, methanol, ethanol, or other fuels.

Polygeneration systems often have many variables and need to be adjusted and optimized carefully. Therefore, different techniques and tools are used to analyze and optimize such systems. Those incorporate energy analysis to estimate energy savings the system can provide compared to a conventional one, pinch analysis to make optimum use of the different heat flows in the system, exergy analysis to quantify irreversibilities in the system, and economic analyses to evaluate the costs. If a system is optimized for efficiency and costs the processes are usually coupled in a fixed way afterwards so every process can run at its optimum. However, as stated before, high efficiency is not the most important factor if there is no demand for the outputs. For this reason, the economy of many polygeneration systems struggles with fluctuation in demand.

Subsequently an example for a polygeneration process that uses an ICE is shown. Figure 11 shows the polygeneration concept which was proposed by Schröder et al. [28].

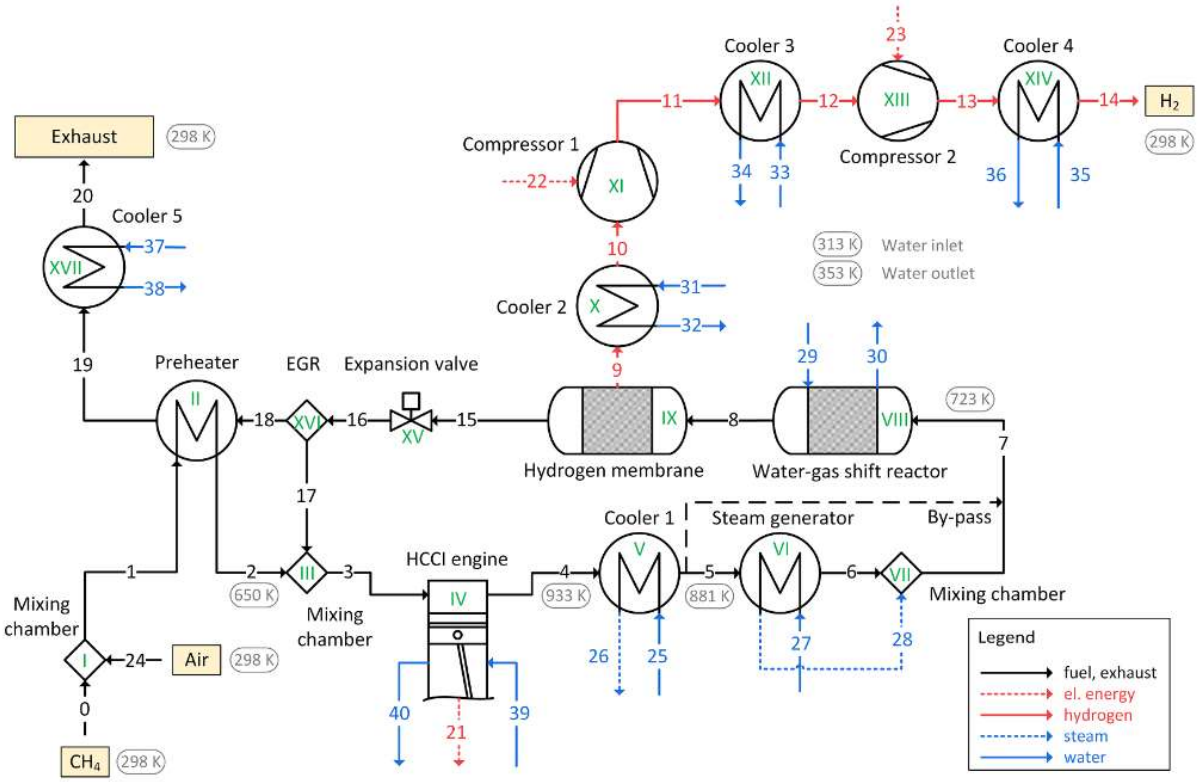


Figure 11: Polygeneration process concept with an HCCI engine as a prime mover. [28]

It uses an ICE operated on fuel-rich mixtures to produce power, heat, and syngas at the same time. The syngas is further converted and separated to yield hydrogen. A fuel rich mixture of methane or natural gas and air is preheated using exhaust gas recuperation (II). It is mixed with a part of the exhaust gas (III) and fed to the engine (2). The hot exhaust is used to increase the temperature of the mixture and thus it's reactivity to allow for auto-ignition of the methane-based cylinder charge. In the engine (IV) power, heat, and syngas are produced via partial oxidation of methane. The exhaust is cooled 723 K (7) and mixed with steam in preparation for the water-gas shift reaction (VIII) that converts most of the CO in the stream with steam to $H_2$ and $CO_2$. The hydrogen is separated by a membrane (IX) and compressed for storage (14).

Besides the relatively inexpensive reactor a concept, using an ICE as reactor has the potential advantage of flexibility. In times of power demand an engine can be operated conventionally to produce maximum power output while in times of power excess it can be operated fuel-rich to generate syngas at reduced power output. Such a process could provide a great solution to overcome the problems polygeneration processes face with fluctuating demand.

# 3 Materials and methods

This chapter describes the devices and procedures that were used to conduct the experiments in detail. Some of the aspects covered in this chapter will be repeated in condensed form in later chapters for the respective experiments. However, here a more comprehensive overview shall be given.

## 3.1 Lab environment

The experiment's infrastructure includes external cooling water supply, air ventilation, a chimney exclusively for the exhaust, compressed air, and nitrogen. Figure 12 shows the lab environment.

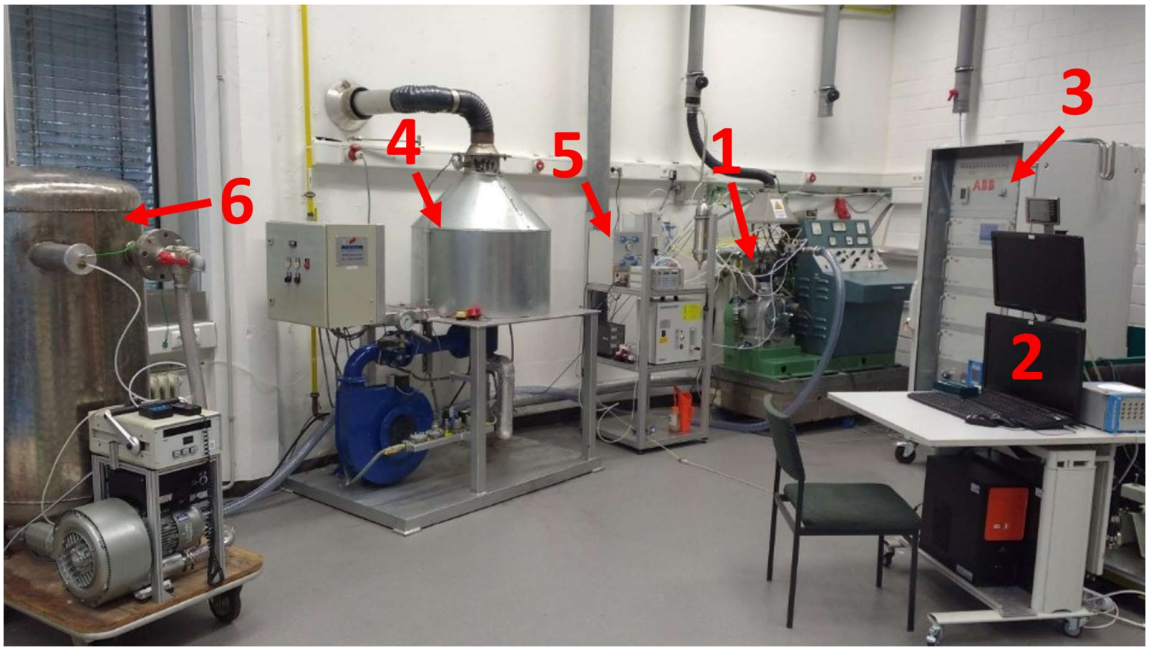


Figure 12: Lab environment

It consists of the engine with electrical control panel (1), two computers (2) for control of the indication system and the MFC's, the exhaust gas analyzer (3), the afterburner (4), a liquid injection system (5) and the plenum with compressor and MFM (6) to supply and control the air for the intake mixture.

The control panel of the engine is used to start and stop the motoring of the engine. Originally it was also used to switch the spark plug on and off, to switch between different modes of engine operation and to monitor the engine. A program in the software "LabVIEW" that runs on one of the computers controls the MFC's and monitors temperatures and pressures. The software for the indication system "Combi" runs on the second computer.

Figure 13 shows a simplified flow diagram of the experiment.

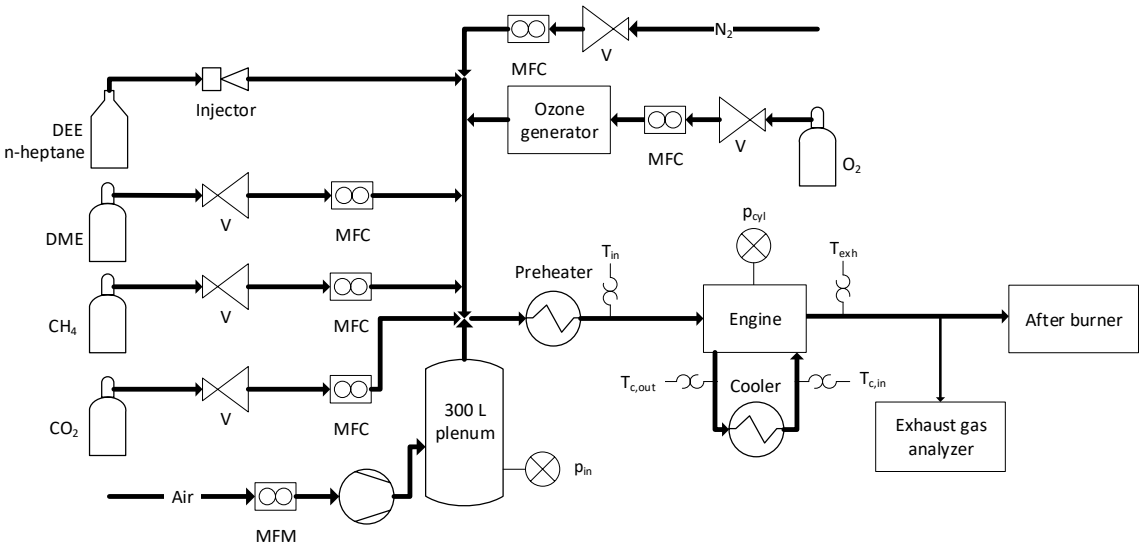


Figure 13: Simplified flow diagram of the experiment

The air is supplied to the plenum by a compressor. It passes the mass flow meter (MFM) before entering the compressor. The compressor is just used to compensate for the pressure loss in the intake manifold. The pressure is held within 0-10 mbar above ambient pressure by adjusting the compressor power manually. The plenum has about 300 Liters volume and is big enough to compensate pressure fluctuations in the intake that might affect accuracy of the MFM or MFC's. While nitrogen is supplied by a house internal pipe DME, $CH_4$, $O_2$, and $CO_2$ are supplied from gas cylinders. The pressure of all gases is adjusted by valves to the specified inlet pressure of the respective MFC, and the gas flow is controlled by the MFC. The oxygen passes the ozone generator which can be activated on demand to enrich the oxygen with ozone. Liquid fuel additives DEE and n-heptane are stored in a pressurized fuel tank and supplied via an injector with 4 bars pressure. All materials are mixed prior to the preheater. The mixture is preheated to temperatures in the range of $T_{in}$ = 50 to 190°C depending on the experiment. The engine has an evaporation cooler which is cooled with a house internal cooling system. The temperatures of the internal and external cooling water circuits are monitored. After leaving the exhaust valve the temperature of the exhaust is measured and a small part of the exhaust is bypassed to the exhaust gas analyzer while most of the exhaust is burned in the afterburner.

Some important experimental parameters are summarized in Table 1.

Table 1: Engine parameters

| | |
|---|---|
| Cylinders | 1 |
| Displacement | 332 cm³ |
| Bore / stroke | 65 mm / 100 mm |
| Engine speed | 600 $min^{-1}$ |
| Intake conditions | p = 1 bar, T = 50 - 190°C |
| Compression ratio | 4 - 20 |
| Fuels | $CH_4$, $CO_2$, Additives (DME, DEE, n-heptane, $O_3$) |
| Mixture formation | Liquid/gaseous port fuel injection |
| Inlet valve timings | -335°CA aTDC until -135°CA aTDC |
| Exhaust valve timings | 150°CA aTDC until 360°CA aTDC |

## 3.2 Engine

### 3.2.1 Basic engine configuration

The engine used in this work is a BASF Octane number research engine that was manufactured in 1957 by the company “Hermann RUF Mannheim”. It was designed specifically to conduct octane number measurements with the “research octane number” (RON) method and the “Motor octane number” (MON) method. These and similar engines are still used today because the standard for octane number testing is unchanged. Figure 14 shows a CAD model of the engine’s cylinder head.

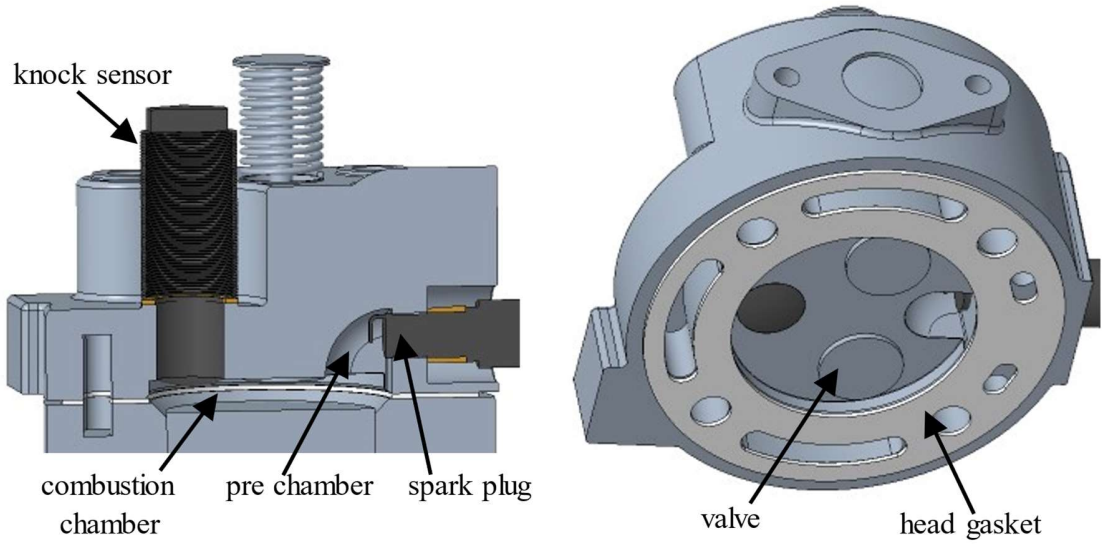


Figure 14: CAD model of the cylinder head. Left side cross section, right side view from below.

The engine has a single cylinder with 332 cm³ displacement and two valves. Characteristic is the so-called “L-head” design which is named after the combustion chamber geometry that has a pre chamber in which the spark plug is mounted. The combustion starts at the spark plug in the pre chamber and propagates into the main part of the combustion chamber. This increases the knock tendency of the engine which is desired in this specific case. A knock sensor is integrated into the cylinder head to enable knock detection. The piston is flat as it also is in most modern SI engines. Another characteristic feature is the adjustable compression ratio of the engine. By turning a crank, the compression ratio is adjusted via a worm drive which raises or lowers the cylinder head and liner relative to the piston. A schematic of this mechanic is shown in Figure 15.

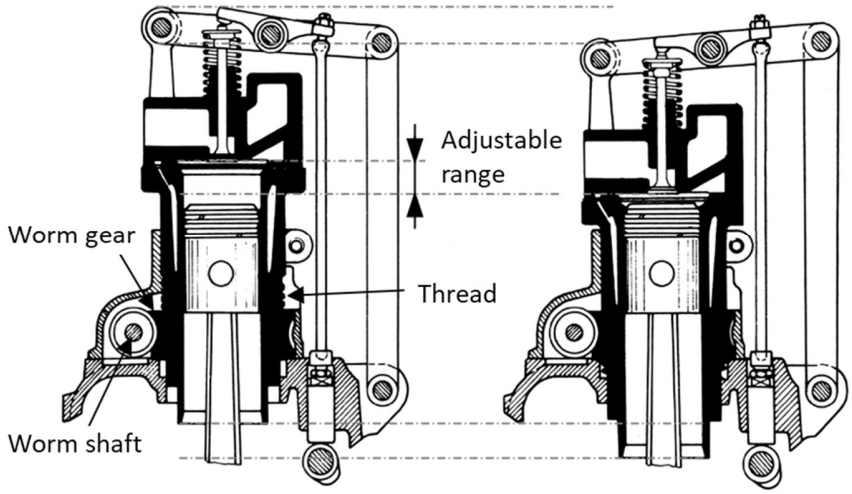


Figure 15: Worm drive for adjusting compression ratio of the BASF engine [29]

This way the engine's compression ratio can be varied between 4 and 10. The valve lift is held constant. The engine is cooled via evaporation cooling. Distilled water is evaporated at 100°C in the engine and then condensed in an external heat exchanger. An external motor drives the engine at either 600 $min^{-1}$ when RON is the selected method or 900 $min^{-1}$ when MON is selected. In the engine's original form, a special carburetor is used to mix the fuels. A preheater heats the mixture up to 165°C.

Ignition is achieved by means of a breaker contact. A rotating cam breaks a circuit which causes the spark coil to send a spark through the spark plug. The breaker contact can also be used to mechanically adjust the ignition timing.

### 3.2.2 Modification of the engine

The engine was modified to run on gaseous fuels in addition to liquid ones. The carburetor was replaced by a port fuel injector (PFI) and gas nozzles. Figure 16 shows an image of the periphery directly in front of the engine's intake.

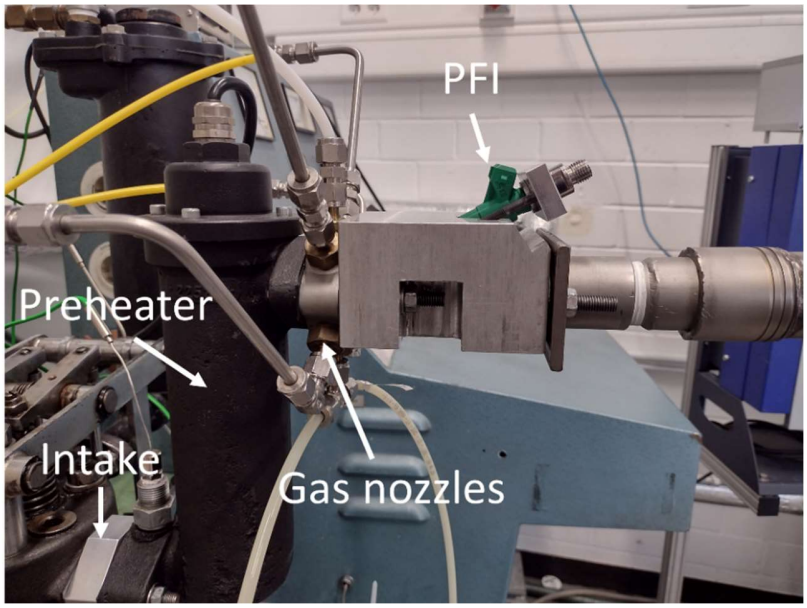


Figure 16: PFI, gas injection, and preheater upstream of the engine intake.

The port fuel injector is mounted in an aluminum block upstream of the preheater. Downstream of the aluminum block follows an intermediate piece in which 6 gas nozzles are mounted. Four of the nozzles inject methane into the air flow. The other nozzles are used to supply optional gases (DME, oxygen, ozone, nitrogen, and/or $CO_2$. The gases mix in the preheater and reach the engine's intake.

For some experiments the engines maximum compression ratio was increased by adding metal inserts into the combustion chamber. The modifications to the combustion chamber are shown in Figure 17.

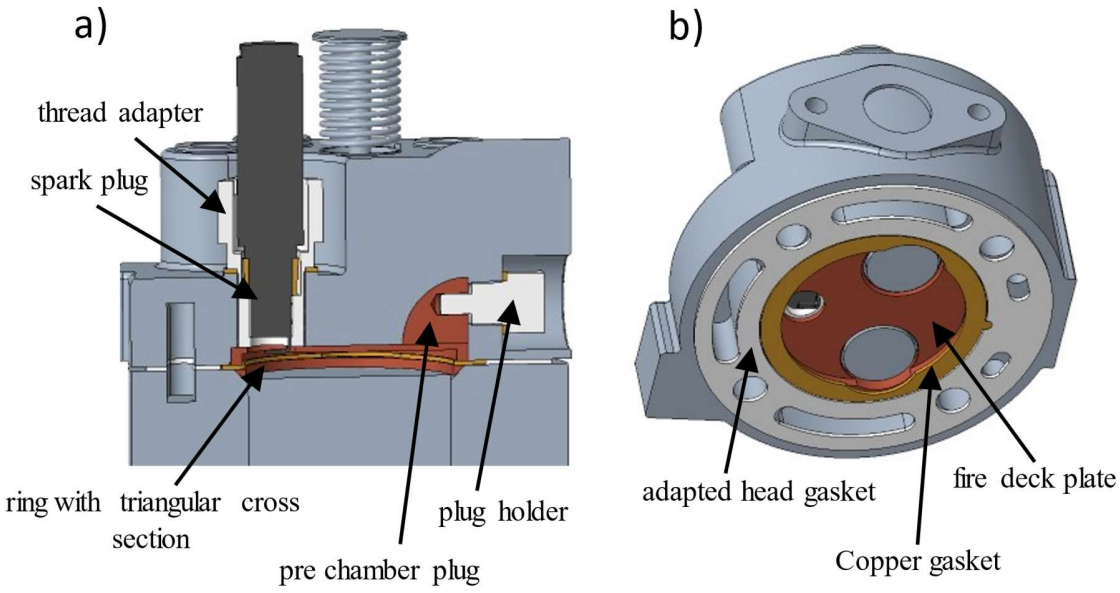


Figure 17: CAD model of the modified cylinder head. Metal inserts in auburn color. a) cross section, b) bottom view.

The knock sensor was removed and replaced by an adapter in which the spark plug was mounted. The pre chamber in which the spark plug was mounted in the engine's original state was filled with a plug held by a pin mounted in

the original spark plug slot. Another metal insert that was added is the fire deck plate. It brings the level of the fire deck to that of the valves which extend into the combustion chamber in the original state. Additionally, it reduces the diameter of the combustion chamber and brings it closer to the piston's diameter. For the section below the head gasket the same purpose is fulfilled by a ring with a triangular cross section which eliminates the chamfer at the top of the piston liner. The addition of those metal inserts increases the adjustable range of the engine's compression ratio from $\varepsilon = 4 – 10$ (12 if turning the crank beyond where the scale is labeled and extrapolating the value for $\varepsilon$) in the original state to $\varepsilon = 4.5 – 21$ in the modified form.

The original ignition system was replaced by a modern spark coil (Type Bosch 0 221 604 006). It is controlled via a TTL signal from the indication system. This allows more convenient variation of the ignition timing with better accuracy and in a wider range than with the original ignition system.

## 3.3 Product analysis

### 3.3.1 Gases

For detection of the exhaust gas composition an online measurement exhaust gas analyzer of the company ABB type "Advance Optima 2020" was used. It uses various sensor modules to detect $CH_4$, $C_2H_4$, CO, $CO_2$, $H_2$ and $O_2$.

The sampled gas is passed through a 5 µm filter mesh to remove most soot particles. Subsequently it is fed to the analyzer through a tube which is heated to 160 °C to prevent condensation of water. Then the flow passes a glass fiber filter and is cooled to 3°C so that most of the water is condensed and removed. Then the flow passes a membrane to ensure that it is water free, and it passes a piston pump and is fed to the sensor modules. Table 2 shows an overview of the analyzer modules.

Table 2: Exhaust measurement technology, range, and accuracy. NDIR: Nondispersive infrared absorption. TC: Thermal conductivity.

| Species | Sensor module | Technology | Calibrated range / % |
|---|---|---|---|
| $CH_4$ | Uras26 | NDIR | 0 – 20 |
| $C_2H_4$ | Uras26 | NDIR | 0 – 5 |
| CO | Uras26 | NDIR | 0 – 30 |
| $CO_2$ | Uras26 | NDIR | 0 – 30 |
| $H_2$ | Caldos27 | TC | 0 – 50 |
| $O_2$ | Magnos206 | Paramagnetic | 0 – 25 |

For the detection of the carbon-containing species $CH_4$, $C_2H_4$, CO, and $CO_2$ infrared photometer modules of the type "Uras26" are used. They use nondispersive infrared absorption at wavelengths in the range of $\lambda = 2.5$ to 8 µm. The linearity deviation is specified as < 1% and the repeatability as < 0.5% of the measurement span.

Hydrogen is detected via a thermal conductivity detector of the type "Caldos27". It is setup to detect the concentration of hydrogen in nitrogen as carrier gas. This is convenient for conventional engine exhaust gas. However, it might lead to increasing errors if a major part of the carrier gas has very different heat conductivity compared to nitrogen. The linearity deviation is specified as < 2% and the repeatability as < 1% of the measurement span.

A magneto-mechanical analyzer of the type “Magnos206” detects oxygen. The linearity deviation is specified as < 0.5% and the repeatability as < 50 ppm $O_2$.

To measure the uncertainty of the exhaust gas analyzer, experimental results were compared to results of a gas chromatograph. It was found that the exhaust gas analyzer overpredicts the CO fraction while the $CO_2$ fraction is underpredicted. This comparison is shown in appendix A.

### 3.3.2 Soot

For the detection of soot in the exhaust gas the “smoke meter” type 415S by AVL is used. A reflectometer measures the blackening of a filter paper that is loaded with a defined volume of exhaust. The blackening of the paper depends mainly on the volume of exhaust and on the soot concentration. For measurement of the Filter Smoke Number (FSN) the volume is defined by ISO DP 10054 to have an effective length (the effective length excludes dead and leakage volume of the sample) of 405 mm and a diameter of 32 mm of the filter paper (330 $cm^3$). For this effective sampling length, the FSN equals the blackening value of the filter paper (PB). The blackening value is defined as

$$PB = \frac{100 - R_R}{10} \tag{12}$$

with the relative brightness of the sample $R_R$

$$R_R = \frac{R_P}{R_F} \cdot 100\% \tag{13}$$

and the reflectometer value of the sample $R_P$ and the reflectometer value of the unblackened paper $R_F$.

## 3.4 Liquid injection system

Liquid additives are injected into the intake via a port fuel injector. The injection system consists of two stainless steel tanks with 400 ccm volume that can be pressurized with compressed air. The pressure was set to 4 bars for all experiments. It is possible to switch between two tanks with different additives. The tanks are connected to a port fuel injector of the type BOSCH 0280156025 via a PTFE tube. The injector is triggered by a TTL-signal from the indication system. By adjusting the pulse duration of the TTL signal, the amount of injected additive can be varied. Figure 18 shows the basic principle of the injection system.

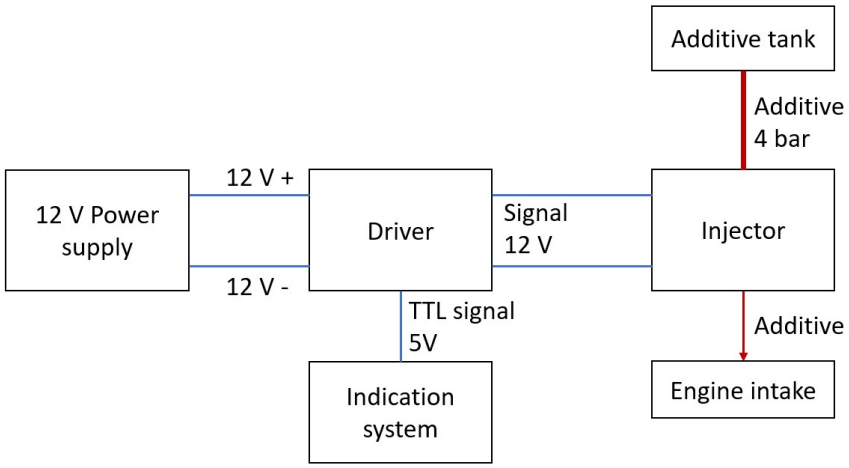


Figure 18: Schematic of the injection system

A custom driver converts the 5 V TTL signal from the indication system to a 12 V signal that drives the injector. To determine the injected amount of additive the volume that was injected in a defined time was measured. Additive was injected into the engine intake with different pulse durations. Afterwards the amount of additive that was needed to refill the tank to its maximum was measured. This process was repeated one time for each pulse duration and the results were averaged. Then a regression line was fitted to the data. This function was then used to predict the injected amount of additive depending on the pulse duration. Figure 19 shows the regression line for the injected mass of DEE versus the pulse duration.

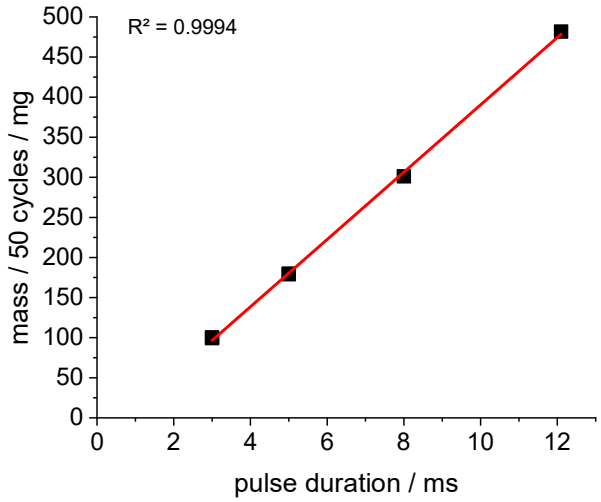


Figure 19: Injected amount of DEE versus pulse duration of the TTL signal.

# 4 The piston engine as a polygeneration reactor

This chapter introduces a method for determining a stable operating range in engines operating in HCCI mode on fuel-rich mixtures. Traditional spark ignition operation is compared to HCCI operation in the fuel-rich regime and the general effect of equivalence ratio in the range of 0.5 to 12 on syngas yield, methane conversion, work and efficiencies is discussed. Furthermore, the effect of compression ratio on syngas production is investigated.

This chapter is a slightly modified part of [30]:

> B. Atakan, S.A. Kaiser, J. Herzler, S. Porras, K. Banke, O. Deutschmann, T. Kasper, M. Fikri, R. Schießl, D. Schröder, C. Rudolph, D. Kaczmarek, H. Gossler, S. Drost, V. Bykov, U. Maas, C. Schulz, Flexible energy conversion and storage via high-temperature gas-phase reactions: The piston engine as a polygeneration reactor, Renewable Sustainable Energy Rev, 133 (2020) 110264, doi:10.1016/j.rser.2020.110264.

Most members of the FOR 1993 contributed to this paper summarizing some of the main aspects and results of the Research Unit. My contribution includes the engine experiments and the writing of the corresponding parts of the manuscript presented in this work.

## 4.1 Methods

The experiments were conducted in a single-cylinder engine that was originally designed for octane number testing of liquid fuels at compressions ratios between 4 and 10. It has 337 $cm^3$ displacement volume and was run here at a speed of 600 rpm. The engine was modified to operate also with gaseous fuels and to reach compression ratios of up to 20. Gaseous and liquid fuels were metered into the (also metered) intake air and the mixture was preheated before it enters the intake. The crank-angle resolved cylinder pressure was recorded, and in the product-gas stream the mole fractions of $O_2$, $CH_4$, $C_2H_4$, CO, and $H_2$ were measured by gas analyzers (ABB) in continuous on-line sampling. The soot content was measured as a filter smoke number by an AVL smoke meter and converted to a mass fraction. The product gases are poisonous and combustible, and since in the laboratory context there is no downstream processing, they were burned. More experimental details can be found in ([8,31]).

## 4.2 Results

### 4.2.1 Operating stability

Given the unusual intake compositions targeted here, the first concern was how HCCI operation could be achieved. Among other considerations, “good” engine operation requires that ignition occurs in every cycle, and that combustion is timed appropriately with respect to the kinematics of compression and expansion – if it is too early, the cylinder pressure increases very quickly, which can damage the engine, and if it is too late, the high-temperature chemistry is frozen before the desired chemical conversion can take place.

As expected, due to the low reactivity of methane, at compression ratios typical for spark-ignition engines (about 9 to 14), autoignition did not occur for any equivalence ratio. Adding a few percent ethane or propane to the methane – to yield a surrogate more representative of pipeline natural gas – did not change this situation. However, as discussed above, with more reactive additives like DME or DEE, HCCI operation is possible within a certain window of additive content in the fuel.

The basic procedure applied here for determining this operating window is a scan, in which the additive flow is systematically increased for a constant methane flow [31]. Two criteria for acceptable operation were chosen. The first criterion is a low coefficient of variation (CoV), a metric of cycle repeatability.

$$\mathrm{CoV} = \frac{\sigma(\mathrm{IMEP_{net}})}{\mathrm{IMEP_{net}}} \tag{14}$$

where $\mathrm{IMEP_{net}}$ is the net indicated mean effective pressure defined as

$$\mathrm{IMEP_{net}} = \mathrm{IMEP} - \mathrm{IMEP_{mot}} \tag{15}$$

That is, at each operating point the indicated mean effective pressure (IMEP) was calculated from the pressure traces of 140 cycles, the $\mathrm{IMEP_{mot}}$ from a motored cycle was then subtracted from each, and the standard deviation $\sigma$ was also estimated from that the resulting $\mathrm{IMEP_{net}}$.

The IMEP is directly linked to the indicated work W per cycle and the swept volume $\Delta$V:

$$W = \mathrm{IMEP} \times \Delta V \tag{16}$$

A CoV value of 10% was chosen as an upper limit for stable operation. The second criterion is the maximum pressure-rise rate ($\mathrm{PRR_{max}}$), a metric for mechanical stress on piston, cylinder, and related components. It was measured with the in-cylinder pressure transducer and an upper limit of 10 bar/°CA was deemed acceptable.

Figure 20 shows a scan for a constant methane flow with the DME flow varied. Across the scan, the overall equivalence ratio slightly changes, from $\phi$ = 2.0 at the lowest to 2.2 at the highest DME fraction. In addition to the CoV and $\mathrm{PRR_{max}}$, IMEP and CA50 are plotted. CA50 is the crank angle at which 50% of the heat release has taken place, a metric of combustion phasing, that is, how the chemical reactions are timed with respect to the kinematics of the engine cycle.

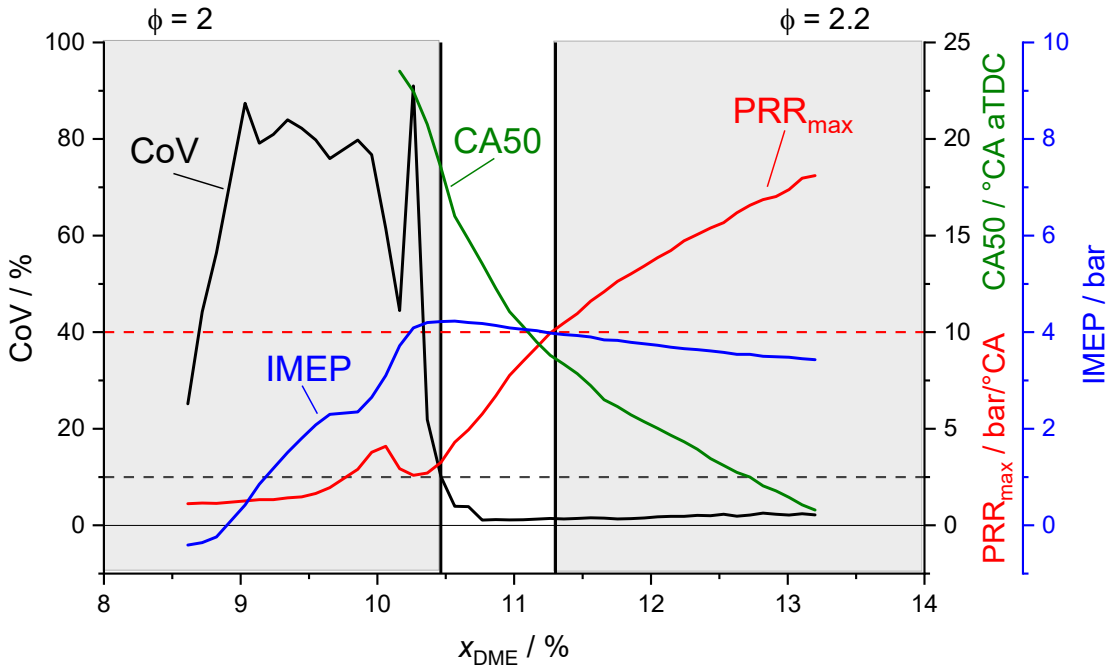


Figure 20: CoV, $PRR_{max}$, CA50, and IMEP for HCCI operation with increasing DME fraction at a constant methane flow, starting from operation without ignition. The white region marks acceptable engine operation. The intake temperature was $T_{in}$ = 423 K and the compression ratio ε = 10.

At low DME mole fractions, the mixture does not ignite, resulting in negative IMEP values. Adding more DME first leads to irregular firing and consequently to a high CoV. With increasing additive concentration, more cycles fire, and the CoV decreases while IMEP and $PRR_{max}$ increase. The non-monotonic behavior in these metrics at $x_{DME}$ = 10 to 10.4% is associated with alternating firing and misfiring cycles due to the residual gas transferring unreacted or reacted mixture, respectively, from one cycle to the next. Increasing the intake additive fraction further induces stable engine operation at 10.5% DME. With more additive, CA50 shifts early. This results in increasing $PRR_{max}$ because the heat is released at a smaller cylinder volume. The maximum IMEP is reached for the latest CA50 with stable engine operation, 16°CA after TDC. In modern engines with a more compact shape of the combustion chamber than this octane-number testing engine, the specific heat losses are lower and (for stoichiometric operation) typical CA50 at maximum IMEP are 3–8°CA after TDC. At 11.3% DME the $PRR_{max}$ reaches the 10 bar/°CA limit. Once the operating window was established, further experiments were performed with the lowest amount of additive that yielded stable operation – here, 10.5% DME.

### 4.2.2 Outputs and efficiencies

Figure 21 shows the species and energetic outputs from the engine as well as efficiencies over a wide range of equivalence ratios, from 0.5 to 12. The figure contains three groups of data points: spark ignition (SI) at lean, stoichiometric, and rich equivalence ratios, rich HCCI (with DME as an additive), and ultra-rich HCCI (with DEE). For $0.5 < \phi < 2.1$ the engine was operated in SI mode without any additive. Figure 21 includes some SI operating points with a CoV exceeding the 10% limit. In HCCI mode, DME was used as additive for $1.5 < \phi < 2.5$, but DEE for higher equivalence ratios, because the mass flow controller for (gaseous) DME did not allow sufficient flow rates, while the liquid DEE could be injected in higher quantities by a commercial port fuel injector.

As Figure 21 a) shows, the highest methane conversions $X_{CH4}$ are achieved with SI for lean to stoichiometric equivalence ratios. For very lean equivalence ratios, operation is unstable and conversion decreases because of

increasing numbers of misfires. The yield Y of syngas is nearly zero. This is the conventional regime of engine operation. For $\phi > 1$, the methane conversion is lower, and a significant amount of syngas is produced, with the maximum in yield in SI mode at $\phi = 1.5$. For higher equivalence ratios, the yield is lower because of frequent misfires.

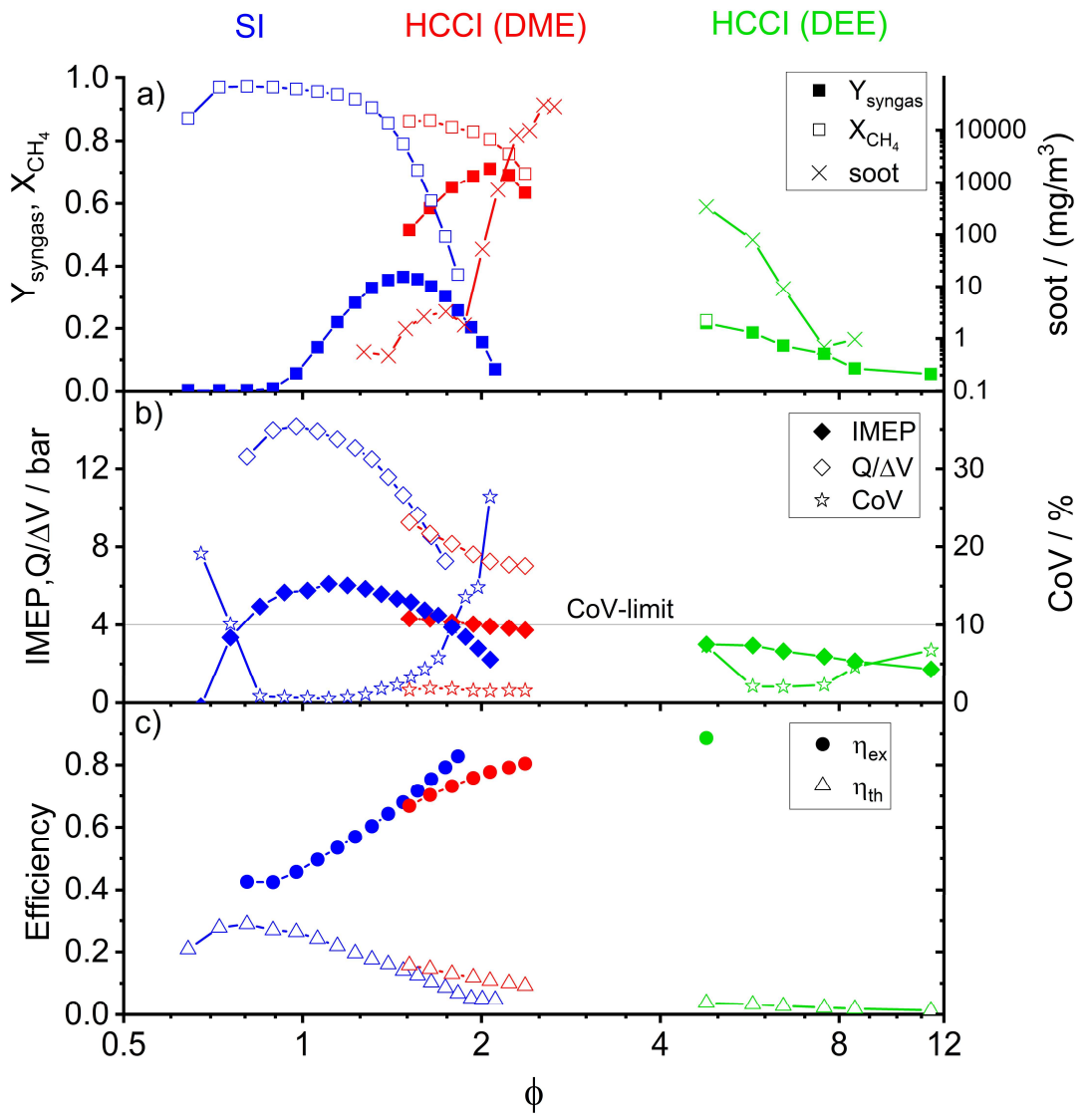


Figure 21: a) Methane conversion ($X_{CH4}$), syngas yield ($Y_{syngas}$), and product-gas soot concentration (note the logarithmic scale), b) displacement-specific work (IMEP) and heat ($-Q/\Delta V$) output of the engine as well as the coefficient of variation of the net IMEP (CoV), c) exergetic ($\eta_{ex}$) and thermal efficiencies ($\eta_{th}$), all as a function of equivalence ratio at $\varepsilon = 10$. Spark-ignition experiments with $T_{in} = 323$ K, HCCI experiments with $T_{in} = 423$ K. Data were not recorded for $2.5 < \phi < 4$ to avoid excessive soot in the instruments. For $\phi > 5$, the methane fraction in the product exceeded the sensor range and therefore Q, $\eta_{ex}$, $Y_{syn}$, and $X_{CH4}$ could not be determined. For very high CoV some of the performance metrics cannot be evaluated reliably and the corresponding data points have been suppressed.

Operating the engine in HCCI mode with additives allowed for stable operation at all equivalence ratios greater than 1.5 (see CoV in Figure 21 b)). Towards stoichiometric conditions, operation is limited by high $PRR_{max}$. The methane conversion is again decreasing with increasing equivalence ratio, but in this case mostly due to a lack of oxygen. For $\phi > 1.5$ it is significantly higher than in SI mode because misfires do not occur with HCCI. In the latter mode, the maximum syngas yield is at about $\phi = 2.1$. Increasing the equivalence ratio further decreases the syngas yield, even though the partial oxidation of methane to syngas is stoichiometric at more fuel-rich conditions ($\phi = 4$ with respect to complete combustion). Like in SI mode (not shown here), the soot concentration in the product gas is very low (< 10 mg/m$^3$) for equivalence ratios below $\phi = 2$ but increases strongly for richer mixtures. In the range of $2.4 < \phi < 4$ no experiments were carried out to prevent damage to the instruments, and generally operation was limited to $\phi < 2.1$. As the equivalence ratio increases beyond $\phi > 4$, decreasing soot concentrations were measured, and beyond $\phi = 7$ soot formation becomes again insignificant. This is likely because due the high heat capacity of these ultra-rich mixtures and the low heat release, the in-cylinder temperatures are too low for soot formation. The ultra-rich regime with $\phi > 4$ is not interesting for syngas production, because the yield is low, but at $\phi = 7$ the product gas contains about 1.5 vol.% ethylene.

Figure 21 b) shows heat and work production of the process. The maximum work and heat outputs are, as expected, at $\phi = 1$. As with the syngas yield (Figure 21 a)), HCCI yields better results at $\phi > 1.5$ than SI because misfiring is avoided. The work output is positive at all investigated equivalence ratios. At $\phi = 11.5$, with 2 bar IMEP it is still about 30% of the maximum at stoichiometric.

In Figure 21 c), the thermal and exergetic efficiencies are shown. The two metrics were calculated as

$$\eta_{th} = \frac{W}{\sum_i m_i \times h_{L,i}} \tag{17}$$

$$\eta_{ex} = 1 - \frac{E_l}{\sum_i m_i \times e_i} \quad with \quad E_l = T_{sur} \times S_{irr} \tag{18}$$

where $h_{L,i}$ is the (specific) lower heating value and $e_i$ is the specific chemical exergy of each hydrocarbon species $i$ at the engine inlet. The exergy loss $E_l$ is the product of the surrounding temperature $T_{sur}$ and the irreversible entropy generation $S_{irr}$. The latter is determined from a first law and second law analysis as described in [8].

While the thermal efficiency counts only work as a useful output, the exergetic efficiency considers all outputs, in this case work, heat, and product gas. With 29%, the thermal efficiency has its maximum at $\phi = 0.8$ and decreases with increasing equivalence ratio. In contrast, the exergetic efficiency has its minimum value of 40% at lean equivalence ratios and increases to over 70% at $\phi > 1.5$. However, when the methane conversion is low, as it is for unstable SI operation with frequent misfires and ultra-rich HCCI, the value of the exergetic efficiency as a figure of merit of the process is limited.

Overall, if syngas is the target chemical output, a good operating strategy would be HCCI at $\phi = 1.9$. The syngas yield would be higher in slightly richer operation, but this is just lean enough to keep engine-out soot concentrations low. The engine runs very stably, the (indicated) work that could be used by other machinery in the plant is still half of its maximum, and the exergetic efficiency is 75%. To put the latter number in context, [2] gives the exergetic efficiency of the commonly used methane steam reforming as 63%. Polygeneration based on solar collectors, providing electricity, heat, cooling, and desalinated water yields exergetic efficiencies up to 32% [32]. Other systems combining power cycles with methanol production or desalinization reach efficiencies up to 60% [33].

### 4.2.3 Elevated compression ratios

For a compression ratio of ε = 10, relatively large quantities of additive (over 20 mass-%) are needed for stable fuel-rich HCCI operation. Higher temperatures towards the end of compression are one way of increasing the mixture reactivity with less additive. This could be achieved by increasing the compression ratio or the intake temperature, but the latter also increases heat losses and potentially the hardware costs, e.g., because more temperature-resistant materials are needed in the engine design. Figure 22 shows the DME mole fraction required for stable engine operation (i.e., at the CoV-limit) for compression ratios from ε = 10 to 19 at intake temperatures of 423 and 323 K and equivalence ratios from ϕ = 1.2 to 2.

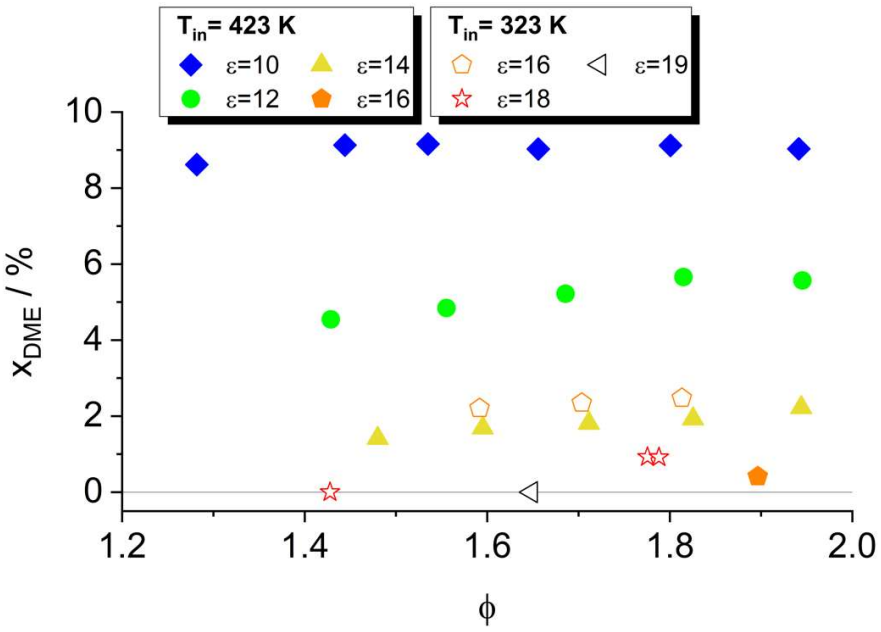


Figure 22: DME mole fraction required for stable HCCI engine operation as a function of equivalence ratio for a range of compression ratios ε and two different intake temperatures $T_{in}$.

Towards high equivalence ratios, excessive sooting above ϕ = 2 limits useful operation at all compression ratios, while high pressure-rise rates determine the limits towards lower equivalence ratios. For higher compression ratios this limit shifts to higher equivalence ratios because the cylinder volume during the reaction is smaller. There is only a weak dependency of the required DME mole fraction on equivalence ratio, but a strong one on compression ratio. For an intake temperature of 423 K, the required DME fraction decreases to less than 2 vol.% at ε = 14. At ε = 16 just 0.5% DME are needed, but only at ϕ = 1.9 stable, low-sooting operation without excessive pressure-rise rates could be established. Lowering the intake temperature to 323 K increases the additive demand but broadens the operating envelope in terms of ϕ. Increasing the compression ratio to 18 and 19 enables acceptable operation without any DME addition at ϕ = 1.42 and 1.64, respectively. However, without additive, the remaining control parameters are intake temperature and equivalence ratio. Adjusting the former is slow, and the latter has little authority – both are known issues in "classic" lean HCCI. It may therefore be desirable to retain combustion control via a small fraction of an effective additive. For this purpose, ozone may be a promising candidate, as work on lean HCCI [10,11,34,35] has shown.

# 5 Partial oxidation of fuel-rich methane/DME mixtures

In this chapter we explore a particular concept of polygeneration using an internal combustion engine as a reactor for partial oxidation to generate synthesis gas in variable combinations with mechanical work and heat. Experiments were performed in a single-cylinder engine operated in homogeneous-charge compression-ignition (HCCI) mode on a mixture of methane and air with dimethyl ether (DME) as a reactivity-enhancing additive. For intake temperature from 100 to 190°C, the range of stable, non-sooting operation with acceptable pressure-rise rates was determined in terms of equivalence ratio and DME mole fraction in the fuel. At 150°C intake temperature, 8.7 to 9.5% DME were needed to stabilize operation at equivalence ratios between about 1.3 and 2.7. Experimental results from fuel-rich conditions with equivalence ratios ranging from 1.65 to 2.34 were compared to simulations with a homogeneous, single-zone engine model. The concept of exergy was used to investigate the thermodynamic performance of the polygeneration engine. The effect of the equivalence ratio on work and heat output, thermal and exergetic efficiency, and selectivity towards useful product species was investigated. In the experiments a work output of up to 160 J ($\phi = 1.65$) per cycle (IMEP = 4.82 bar) and exergetic efficiencies of up to 81.5% ($\phi = 2.34$) were achieved. The simultaneous generation of synthesis gas had a selectivity of up to 72% for hydrogen and 79% for carbon monoxide (both at $\phi = 2.34$).

This chapter is slightly modified from [31]:

> K. Banke, R. Hegner, D. Schröder, C. Schulz, B. Atakan, S.A. Kaiser, Power and syngas production from partial oxidation of fuel-rich methane/DME mixtures in an HCCI engine, Fuel (2019) 97–103, doi:10.1016/j.fuel.2019.01.076.

My own contribution includes setting up and performing the experiments, processing, analyzing, and interpreting data, visualizing experimental results, and writing the introduction, experimental parts and conclusion of the manuscript. Robert Hegner and Dominik Schröder conducted the simulations and wrote the modelling and simulation parts of the manuscript. Sebastian Kaiser and Burak Atakan were involved in the conceptual design of the study and writing the manuscript. Christof Schulz contributed through revision of the manuscript.

## 5.1 Introduction

In initial studies on synthesis-gas generation in engines, Karim et al. [36] used Diesel-fuel pilot injection to achieve ignition. They demonstrated syngas (sum of $H_2$ and CO) production with dry-gas mole fractions of up to 80% at $\phi = 2.4$. Yang et al. operated an HCCI engine at $3.1 < \phi < 9.1$ and achieved syngas mole fractions of ~27%, while Szezich investigated spark ignition (SI) of $CH_4$ resulting in up to 90% syngas [4,37]. While these experiments demonstrated the feasibility of syngas generation in engines, some relied on highly (up to 90%) $O_2$-enriched air to prevent misfires. High pressure-rise rates limited the range of operating conditions and none of the studies discussed how the additional oxygen could be provided. Experiments with air were conducted by McMillian and Lawson, who investigated a fuel-rich natural-gas SI process, but also modeled an HCCI process [5]. With SI, they successfully produced syngas (up to 21% at $\phi = 1.62$). In investigations with the more conventional goal of reducing emissions from vehicle engines, it was shown that in SI multi-cylinder engines operating one engine cylinder fuel-rich and transferring the generated syngas to the other, stoichiometrically operated cylinders can improve combustion characteristics [38]. A recent review discusses a broad range of in-cylinder fuel-reforming processes [39]. A review of polygeneration in piston engines was given by Atakan et al. [30].

In previous work, we theoretically investigated HCCI engine operation over a wide range of equivalence ratios ($0.5 < \phi < 10$), supported by experiments in a rapid compression machine (RCM) [40] with 10 mol% DME as a reactivity-enhancing additive. Besides synthesis gas, up to 1% $C_2H_4$ was formed at $\phi = 7$. A polygeneration concept was developed based on fuel-rich HCCI combustion, including product-gas treatment [41]. This process provides flexible amounts of power and $H_2$ by varying the amount of recirculated product (exhaust) gas. In

experiment and simulation, Wiemann et al. compared fuel-rich SI and HCCI operation to fuel-lean combustion [8]. To achieve autoignition of methane, 5 mol% n-heptane was used as additive. An exergetic efficiency of 45% was achieved at $\phi = 0.72$ and 81% at $\phi = 2.42$. While SI led to misfires at $\phi > 1.5$, HCCI enabled operation up to $\phi = 2.42$, where soot formation became the limiting factor. Because of the potential for stable and efficient fuel-rich operation, we focus on HCCI in the current work. As a reactive additive, DME is used here, representing a class of fuel compounds that can be derived from biomass [42,43]. Expanding on our previous work, we determine the limits of stable HCCI operation with a systematic variation of the additive concentration and intake temperature. Within the stable operating range, we evaluate product yields and exergetic efficiencies of the engine process. Experimental results are compared to those from simulations using a single-zone engine model in terms of work and heat output, thermal and exergetic efficiency, and selectivity towards useful product species.

## 5.2 Methods

### 5.2.1 Engine instrumentation and operation

The experiment is similar to that in Ref. [8]. Thus, only a brief summary is given here (Figure 23). A single-cylinder BASF-type octane-number test engine was modified to run on gaseous fuels. The in-cylinder pressure was recorded as a function of the crank angle (°CA). Except for water, which is condensed at 3°C and removed before analysis, and $N_2$, the major product-stream species ($H_2$, CO, $CH_4$, $CO_2$, $O_2$, $C_2H_4$) were detected with an exhaust-gas analyzer (ABB, Type Advance Optima 2020). Soot was monitored with a filter smoke meter (AVL 415S).

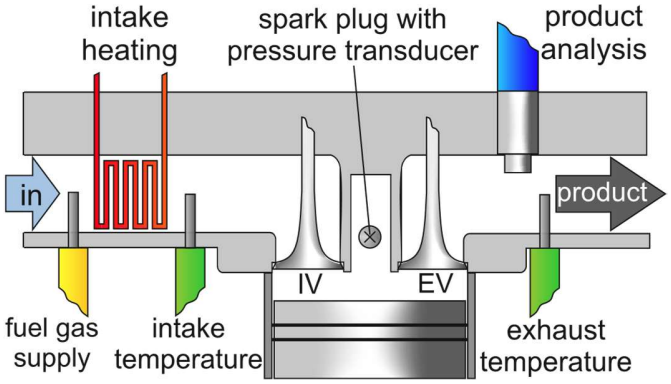


Figure 23: Instrumentation and fuel supply of the single-cylinder engine adapted from [8].

Gaseous $CH_4$ and DME were metered by mass-flow controllers (MFC), electrically heated from 100 to 190°C, and continuously injected into the intake manifold. The overall equivalence ratio $\Phi$ is calculated from eq. (19) with all volume flows at standard conditions.

$$\Phi = 0.21\,\dot{V}_{air,in}/\left(2\,\dot{V}_{CH_4,in} + 3\,\dot{V}_{DME,in}\right) \tag{19}$$

The engine was operated at $1.2<\phi<2.8$ under the conditions listed in Table 3. DME was added to the methane fuel at 5.9–11.2 mol%.

Table 3: Engine properties and operating conditions.

| | |
|---|---|
| Engine type | 4-stroke 2-valve single cylinder |
| Fuel | $CH_4$ + $CH_3OCH_3$ |
| Displacement | 332 $cm^3$ |
| Bore / stroke | 65 / 100 mm |
| Con. rod length | 200 mm |
| Comp. ratio | 10 |
| Engine speed | 600 $min^{-1}$ |
| Intake temperature | 100–190°C |
| Intake pressure | 1 bar |
| Coolant temperature | 100°C |

Before recording data, the engine was run in SI mode on $CH_4$ until the coolant reached 100°C. HCCI was then initiated by adding DME to the mixture. Data recording was started once the measured product-gas composition was stable. For each experiment, the intake flow rates, product-gas mole fractions, temperatures, and 140 cycles of pressure data were recorded. The indicated mean effective pressure (IMEP) and the maximum pressure-rise rate ($PRR_{max}$) were calculated for each cycle and averaged over all cycles. The coefficient of variation (CoV) is usually calculated as the standard deviation of IMEP divided by its mean over a series of cycles. Here, instead of using IMEP, the difference of IMEP of a single cycle and IMEP of a motored cycle was used. This yields a metric that is more closely correlated with combustion instability. The apparent heat release rate was calculated from the averaged pressure trace without taking into account heat losses. From this, the center of combustion (CA50) was determined, i.e., the crank angle at which the cumulative heat release reaches 50% of its eventual total.

### 5.2.2 Engine model

The in-cylinder processes were simulated with spatially-homogeneous time-dependent chemical kinetics considering the compression and expansion strokes, starting at bottom dead center with closed valves. The reactor model in Cantera within Python [44] was used for modeling with a detailed reaction mechanism from Yasunaga et al. (214 species, 1216 reactions) [45,46]. For this mechanism, experiments in shock tubes, RCMs, and flow reactors showed good agreement between simulation and experiment in terms of ignition delay time and product gas species ($CH_4$, DME, $H_2$, $H_2O$, $CO_2$, CO) for DME/$CH_4$ mixtures at $\phi = 2$ [47–50]. The engine model developed here, described in more detail in [8], is based on solving the time-dependent differential equations for conservation of species and energy. It includes wall heat-transfer and residual-gas content and is comparable to the single-zone model by Caton and Zheng [51]. Engine parameters and intake conditions were taken from the experiment.

Heat transfer was estimated using Woschni's formulae (eq. (20) and eq. (21)) for the convective heat transfer coefficient $\alpha$ [52] as a function of temperature $T$ and pressure $p$ in the combustion chamber.

$$\alpha = C\, d^{-0.2} p^{0.8}\, w^{0.8}\, T^{-r} \tag{20}$$

The values of the constants used here are listed in Table 4. In eq. (20), $d$ is the diameter of the cylinder and $w$ is a corrected velocity accounting for turbulence during combustion, calculated as

$$w = C_1\, \tilde{u} + C_2 \frac{V_\mathrm{D}\, T_0}{p_0\, V_0} (p - p_\mathrm{d}) \tag{21}$$

where $V_D$ is the cylinder displacement, $T_0, V_0, p_0$ are the temperature, volume (in SI base units), and pressure at the beginning of compression, $p_d$ is the motored pressure (both in bar) and $\tilde{u}$ is the mean piston speed. The factor $C_2$ was adjusted to match the total heat transfer derived from the energy balance of the experiment at $\phi = 1.65$. This set of constants was then used for all other simulations. Even though in general the Woschni model is known to be inaccurate for predicting heat transfer for HCCI modeling [53–55], here, it yielded total heat losses matching the experimentally determined ones, possibly because $\alpha$ does not vary much across our experiments.

Table 4: Parameters for the heat-transfer estimate according to Woschni [52].

| Woschni-Parameter | Value |
|---|---|
| $C$ | 127.9 |
| $r$ | 0.53 |
| $C_1$ | 2.557 |
| $C_2$ | 0.4354 |

The mass of residual gas remaining in the cylinder $m_{RG}$ was estimated as that of the product gas (temperature, pressure, and composition at bottom-dead center of the expansion stroke) filling the clearance volume of the cylinder (i.e., the volume at top-dead center). This mass is then subsequently adiabatically mixed with the experimentally determined fresh-gas mass $m_{FG}$ with the intake temperature $T_{int}$. This simple "empty-and-fill" model is considered sufficient here since the engine does not have valve overlap and the exhaust valve closes near top-dead center. By this estimate, about 10% (by mass) of gas from the previous cycle remain in the cylinder and mix with the fresh charge of the next cycle. In other words, multiple cycles were simulated transferring 10% of the product gas to the next cycle. For each cycle, the initial temperature for the simulation was the adiabatic mixing temperature of fresh charge and residual gas. The product-gas composition, work and heat output, and exergetic and thermal efficiencies were then averaged over 20 simulated cycles. The total heat transferred to the coolant was calculated by summing over the incremental heat transfer estimated via Woschni's approach at each step of the simulation.

### 5.2.3 Exergy balance and selectivity

Conventionally, the exhaust gas of ICEs mainly contains the products of complete combustion. The product gas in polygeneration in contrast contains useful species and thus remaining chemical and internal energy that is evaluated by calculating the exergy flows entering and leaving the system. Unlike energy, exergy can be destroyed. The corresponding exergy losses, caused by irreversibilities, were used to evaluate how well the fuel exergy is converted to work or conserved in the product gas. The losses in exergy $E_l$ are calculated based on the Gouy-Stodola theorem ($E_l = T_{sur} S_{irr}$) [56] from the ambient temperature $T_{sur}$ (298 K) and the entropy generation $S_{irr}$ over the engine cycle. The corresponding exergetic efficiency $\eta_{ex}$ is determined by eq. (22) under the assumption that exergetically valuable outputs (work, heat, product gas) are used outside the engine and not lost to the environment. The exhaust enthalpy is included among the useful outputs assuming that in the envisioned stationary applications the product gas also provides process heat. The specific chemical exergies of methane $e_{CH_4}$ = 52.3 MJ/kg and DME $e_{DME}$ = 30.9 MJ/kg were taken from [57].

$$\eta_{ex} = 1 - E_l / \left( m_{CH_4} e_{CH_4} + m_{DME} e_{DME} \right) \quad (22)$$

The experimental data were used to calculate the work output, the heat transferred to the cooling water, and the exergetic efficiency using the thermodynamic data available through the Cantera modules together with the first and second laws of thermodynamics, as detailed in [8].

Selectivity is a useful metric to compare chemical conversion in simulation and experiment. However, the present gas analysis cannot determine the fractions of water, nitrogen, and higher hydrocarbons (other than ethylene) in the product gas, thus, the molar product flow $\dot{n}$" cannot be calculated. Some assumptions were made to calculate conversions and selectivities. The first assumption is that the additive's conversion is equal to the methane conversion. Combustion quenching near walls and in particular in crevices results in low temperatures that stop both the conversion of methane and DME. This assumption is supported by preliminary gas chromatography measurements in the product gas that in fact show similar methane and DME conversion. These measurements also showed that at $\Phi = 1.9$ the mole fraction of higher hydrocarbons (except for DME and $C_2H_4$) in the product gas was negligible, which we then assumed to be true for all of the current data evaluation. This may lead to increasing uncertainties for $\Phi > 2$, because soot production increases, which also implies increased formation of acetylene, benzene, and other soot precursors.

The remaining unknown mole fractions in the product stream are that of nitrogen, $x_{N_2}$" , and water, $x_{H_2O}$". These were calculated based on the species balance for hydrogen, eq. (23), and condition that all product mole fractions add to unity eq. (24). Only the hydrogen balance is used here because the oxygen measurement has lower accuracy.

$$\dot{n}'\left(2x_{CH_4}' + 3x_{DME}'\right) = \dot{n}"\left(2x_{CH_4}" + 3x_{DME}" + 2x_{C_2H_4}" + x_{H_2O}"\right) \tag{23}$$

$$1 = \sum_i x_i" = x_{N_2}" + \mathrm{x_{H_2}}" + x_{CH_4}" + \mathrm{x_{C_2H_4}}" + x_{CO_2}" + \mathrm{x_{CO}}" + x_{O_2}" + \mathrm{x_{H_2O}}" + \mathrm{x_{DME}}" \tag{24}$$

The outgoing molar flow $\dot{n}$" can be calculated from the known mass flow $\dot{m}$ through the engine and the mean molar mass of the product flow $M_{mean}$", which is again a function of the mole fractions $x_i$".

$$\dot{n}" = \dot{m}/M_{mean}" \tag{25}$$

For convenience, this system of equations was solved numerically.

Then $\dot{n}$" is used to determine conversions $X_i$, yields $Y_i$, and selectivities $S_i$ as defined in equations (26), (27), and (28) with $\nu_i$ being the number of molecules of species i formed by theoretical total conversion of the fuel towards this species and the incoming and outgoing molar flow of species i, $\dot{n}_i'$ and $\dot{n}_i$ ", respectively.

$$X_i = \frac{\dot{n}_i' - \dot{n}_i"}{\dot{n}_i'} \tag{26}$$

$$Y_i = \frac{\dot{n}_i"}{\dot{n}_i' * (x_{fuel}' * \nu_i)} \tag{27}$$

$$S_i = \frac{Y_i}{X_{fuel}} \tag{28}$$

This procedure results in conversions, yields, and selectivities that include the error of the hydrogen measurement.

## 5.3 Results and discussion

### 5.3.1 Operating envelope and mixture reactivity

Since HCCI combustion is controlled kinetically, engine operation mainly depends on equivalence ratio, fuel composition, and the temperature-pressure history. With $CH_4$ as the base fuel, some DME is needed for autoignition, but too much of it may over-advance combustion phasing, leading to excessive pressure-rise rates that potentially damage the engine. For determining DME concentrations for "acceptable" engine operation, two criteria were set: CoV<5%, and $PRR_{max}$<10 bar/°CA. The dependence of the engine operation on the DME mole fraction was evaluated in an experiment with 8.17 standard liters per minute (slm) $CH_4$. The DME flow was increased stepwise from 0.5–1.0 slm in 0.05-slm increments, corresponding to 5.9–11.2 mol% DME in the fuel. This also led to a change of $\phi$ from 1.66 to 1.84, however, as we will see, $\phi$ has much less influence on the engine operation than the DME concentration. The results for IMEP, CoV, and $PRR_{max}$ are shown in Figure 24 a) as a function of DME mole fraction while Figure 24 b) shows the combustion phasing as CA50 in °CA after top dead center. For negative IMEP, CA50 was not considered meaningful and is suppressed in the plot.

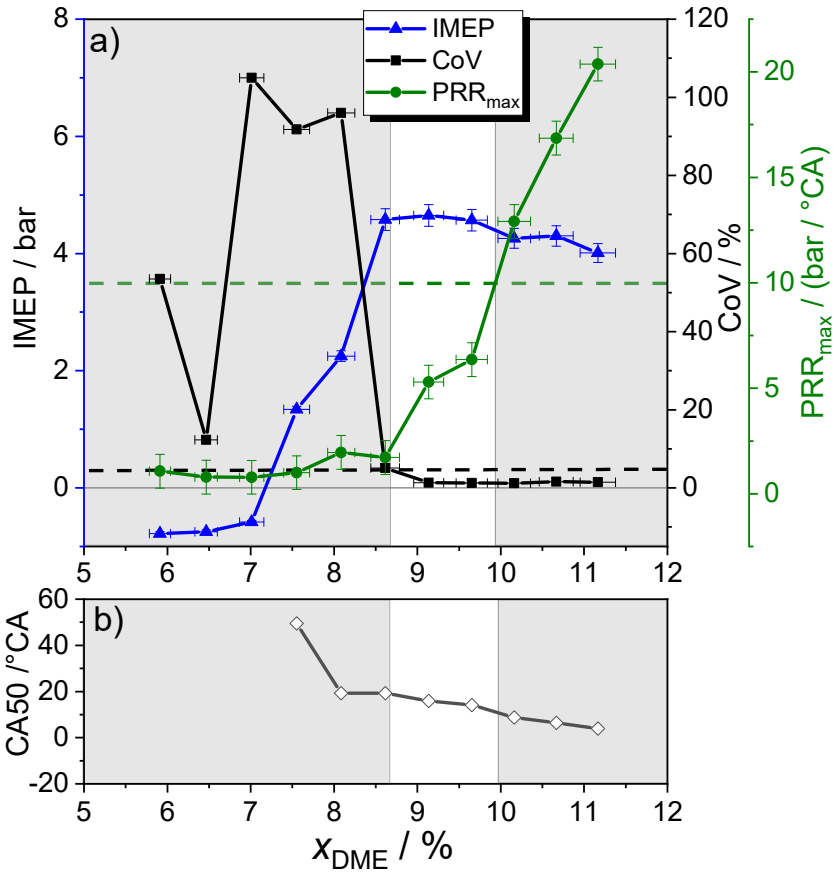


Figure 24: a) IMEP, CoV, and $PRR_{max}$, and b) CA50, all for varying $x_{DME}$ at a constant methane flow of 8.17 slm and an intake temperature of 150°C. The white region in the graph marks acceptable engine operation, dashed lines mark the limits for acceptable CoV and $PRR_{max}$.

Error bars are calculated from the specification of the MFCs, the pressure sensor, and the air-flow meter. At low DME concentrations, no ignition occurs, resulting in a negative IMEP. Increasing $x_{DME}$ to ~7% leads to sporadically firing cycles and high CoV. Further increase in $x_{DME}$ results in a higher number of firing cycles and increasing IMEP. The $x_{DME}$ at the exact operating limits was determined by interpolation. The lower limit (CoV = 5%) is reached at $x_{DME}$ = 8.6%. At $x_{DME}$ = 9.1%, the first data point within the limits for acceptable engine operation was recorded. Increasing $x_{DME}$ even further leads to higher pressure-rise rates, because ignition shifts to earlier crank angles. At about $x_{DME}$ = 9.8%, the pressure-rise rate exceeds the limit of 10 bar/°CA. As expected, adding more DME advances the combustion phasing, with stable operation concurring with a CA50 around 15°CA.

For further investigation, this operability scan was abbreviated and performed for different $CH_4$ flows just until a CoV < 5% could be established before recording was started. Using higher $x_{DME}$ was not beneficial, because it led to lower IMEP and higher $PRR_{max}$. This results in the choice of the lowest $x_{DME}$ (in this example 9.1%) within the operating limits. This scan in the DME mole fraction was performed for methane flows from 6.17 to 11.67 slm in 0.5 slm increments and four intake temperatures (100, 130, 150, and 190°C, see Figure 25).

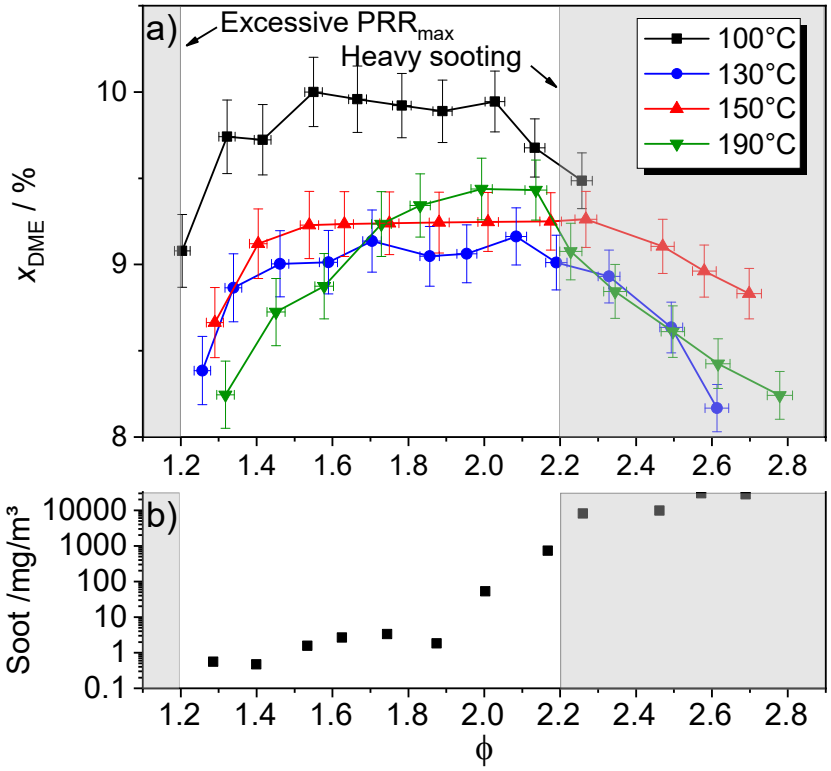


Figure 25: a) DME mole fraction $x_{DME}$ required for stable engine operation at different intake temperatures as a function of equivalence ratio ϕ. b) Soot concentration in the product stream for 150°C intake temperature.

The lower limit of the investigated equivalence ratios is given by excessive PRR. At this limit, adding sufficient amounts of additive to fulfil the CoV criterion resulted in exceeding the PRR limit. The upper limit is given by excessive soot formation at high equivalence ratios. The required amount of DME is highest for the lowest intake temperature, 100°C, which is expected because the mixture reactivity is lowest here. At higher temperatures, no systematic correlation between required $x_{DME}$ and intake temperature was found. Considering error bars, for intake temperatures higher than 100°C and at equivalence ratios around 2, the required DME mole fraction does not significantly depend on temperature. At all temperatures, less DME is needed both at low and at high ϕ. The decrease for low ϕ is steep and results from the increasing sensitivity of the PRR to $x_{DME}$ and increasing energy content closer to stoichiometric conditions. Somewhat counter-intuitive is the decrease of the required $x_{DME}$ for

increasing ϕ above 2, discussed in more detail below. Finally, since for an intake temperature of 150°C the required $x_{DME}$ is nearly constant at ~9.3% in the range of ϕ = 1.6 to 2.3, this range and intake temperature were selected for further analysis. A slightly higher $x_{DME}$ of 9.5% was chosen to ensure operation within the stability limits.

Figure 26 a) shows experimental traces of the cylinder pressure for operation at three different equivalence ratios. Dashed lines represent experimental data and solid lines the simulation results. Additionally, the simulated conversion of $CH_4$ and DME as a function of the crank angle is shown. Figure 26 b) shows the temperature from the simulation.

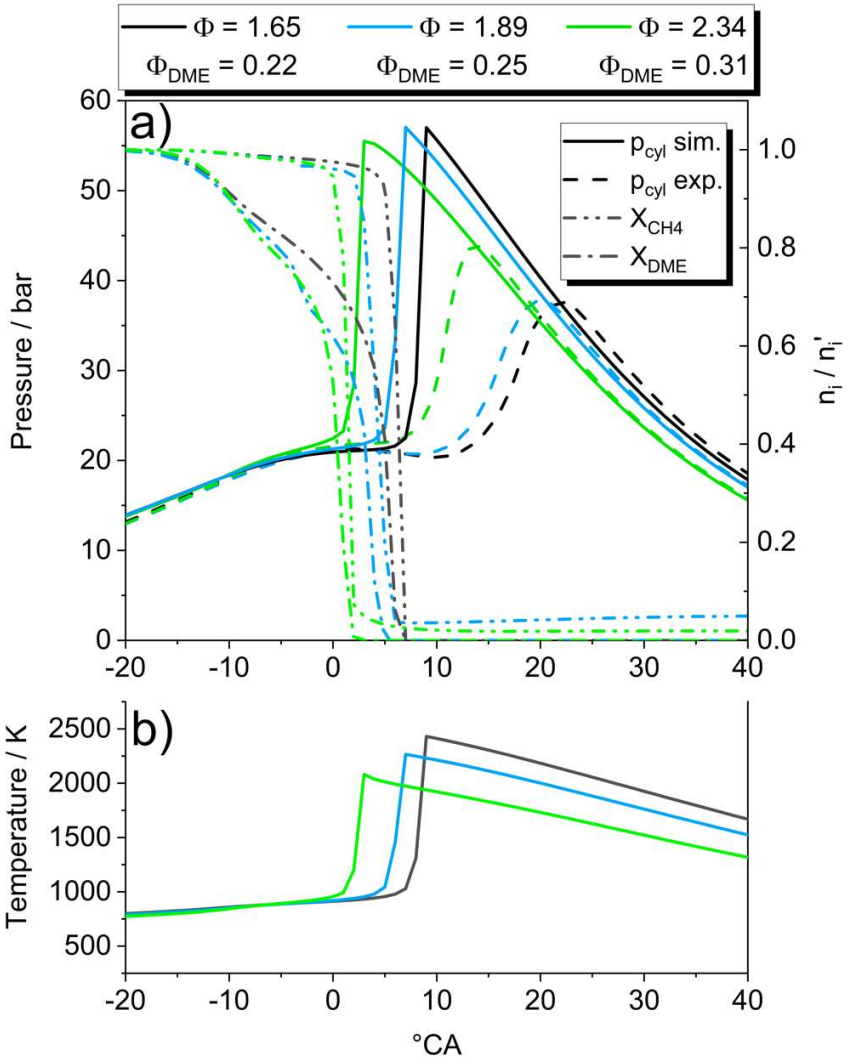


Figure 26: a) Pressure traces from experiment and simulation as well as simulated $CH_4$ and DME conversion. b) Temperature traces from the simulation. All at 150°C intake temperature, $x_{DME}$ of 9.5%, and for three equivalence ratios.

The most noticeable feature is the early-shift in combustion phasing with increasing ϕ, in experiment and simulation. One might expect the contrary, because ϕ > 1 generally suggests lower mixture reactivity. A possible explanation is that the overall equivalence ratio is indeed further from ϕ = 1, but the equivalence ratio $\Phi_{DME}$ based on the additive DME alone is closer to stoichiometric. The simulation results in Figure 26 a) show that significant $CH_4$ conversion starts when already about half of the DME is converted. If $CH_4$ is considered inert at the start of combustion, which is a reasonable approximation compared to DME [58], $\Phi_{DME}$ is very lean for all cases, as the

values in the legend show. Increasing this equivalence ratio enhances reactivity. This explanation is supported by the simulations showing that the DME conversion shifts towards earlier crank angles with increasing ϕ (Figure 26 a)), suggesting an increased reactivity. In the experiments, the lower heat-release rate of richer mixtures is compensated by the heat release taking place at smaller cylinder volumes, leading to increased peak pressures. In the simulations, ignition takes place closer to TDC, where the change in volume per degree CA is small and cannot compensate the reduced heat release rate, resulting in decreasing peak pressures for richer mixtures. As expected, the maximum temperatures (Figure 26 b)) decrease with increasing equivalence ratio due to lower heat release. At ϕ = 2.34, the peak temperature is 2050 K, and Figure 25 b) shows increased soot formation. This is consistent with previous findings that soot formation is especially strong at temperatures between 1500 and 2000 K and equivalence ratios above ϕ = 2 [59].

Another unexpected result is that the pressure traces obtained from the simulation predict much earlier ignition than the experimental data (in addition to the overly fast combustion that is due to the single-zone model not capturing thermal stratification [60]). This may be due to differences between the initial conditions in experiment and simulation. In the simulation, the temperature of the fresh charge in the cylinder (to which the residual gas is then added) is assumed to be the same as the intake temperature. The actual temperature in the experiment is likely to be lower due to heat loss to the walls before the intake valve closes, reducing both the fresh-gas and residual product-gas temperatures. Temporally inaccurate modeling of heat transfer may also induce differences in the pressure traces between simulation and experiment. Since HCCI ignition is highly sensitive to temperature, higher temperatures in the simulation would lead to earlier ignition. To evaluate the impact of this uncertainty, the mixing temperature (the temperature at the start of compression) and the residual gas content were varied in the simulation. As shown in Figure 27, at ϕ = 1.65, reducing the mixing temperature by ΔT = 8 and 15 K delays ignition by 4° and 11° crank angle, respectively. The pressure traces at these two reduced temperatures roughly bracket the experimental trace. Similar results are found for other equivalence ratios.

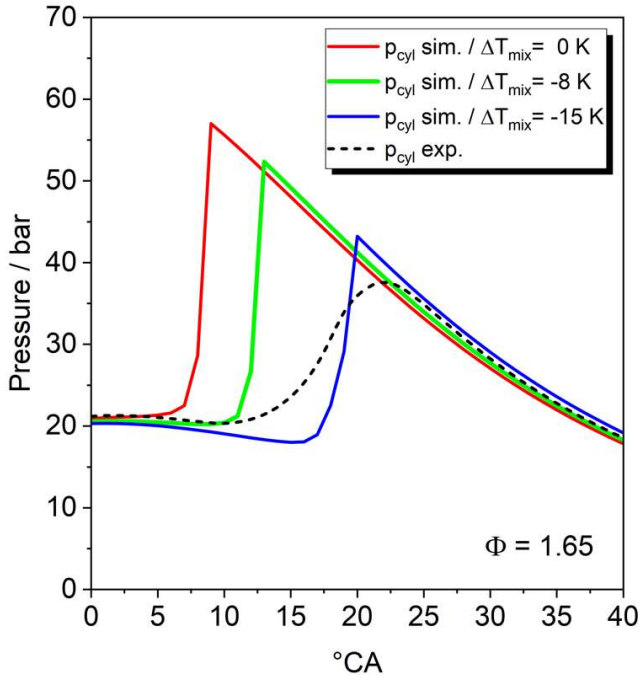


Figure 27: Pressure traces from experiment and simulation with a variation of the initial temperature $T_{mix}$ at the start of compression.

At ϕ = 1.65, increasing the residual gas content in the simulation by 50% advances the peak pressure by only 2°CA, while there is no significant change for ϕ = 2.34. This low sensitivity may be due to the fact that intake and

product-gas temperatures are similar, differing only by 141 K and 56 K for $\phi = 1.65$ and 2.34, respectively. From this sensitivity study we conclude that the systematic difference in combustion phasing between experiment and simulation is likely due to inaccuracies in the simulation's starting temperature that are well within the uncertainty of estimating that temperature and could be accounted for by an adjustment of about 10 K.

Increasing the residual gas mass by 50% in the simulation changes the synthesis gas mole fractions insignificantly, but the $CH_4$ conversion decreases. For example, at $\phi = 2.34$ the $H_2$ and CO mole fractions decrease by 2.6% and 1.7% respectively while the $CH_4$ slip increases by 61%.

### 5.3.2 Fuel conversion and product-gas composition

Simulated and measured $CH_4$ conversion is compared in Figure 28. The experimental uncertainties for the conversion and selectivities were calculated from the specifications of the gas analyzer.

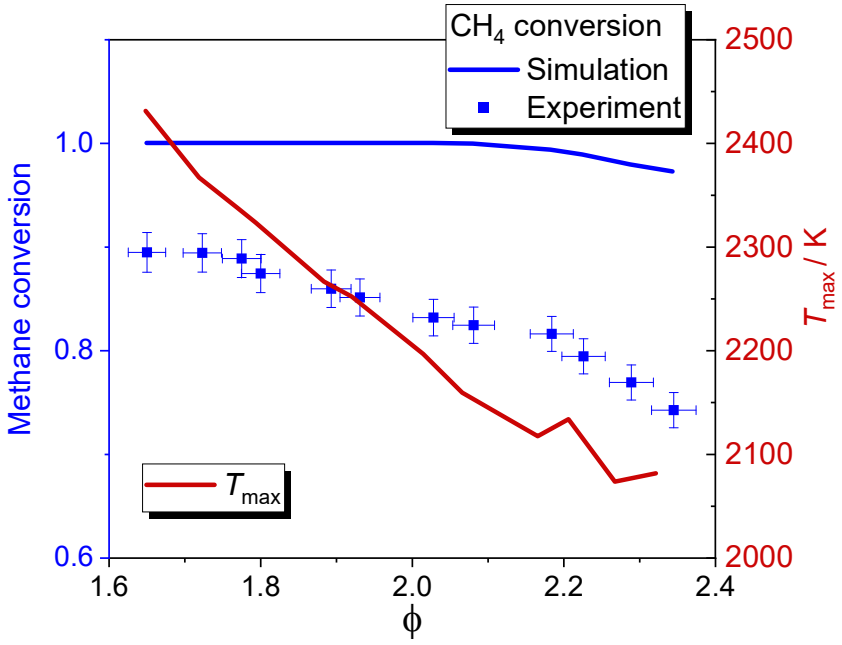


Figure 28: Methane conversion and maximum (simulated) temperatures as a function of equivalence ratio. Symbols: experiment, lines: simulation.

The methane conversion decreases with increasing $\phi$ in both experiment and simulation. This effect can be attributed to the lower maximum temperatures and lower oxygen content at fuel-rich conditions, both impeding fuel conversion. Maximum simulated temperatures at $\phi = 1.65$ are about 2430 K, but at $\phi = 2.34$ only 2080 K. It is a well-known problem that HCCI single-zone models tend to over-estimate the fuel conversion [8,60,61], in this case by about 9 percent points at $\phi = 1.65$ and increasing with $\phi$, because in the engine, the lower temperatures near the cylinder walls and higher temperatures in the core gas lead to reduced fuel conversion in the wall-near regions. Single-zone models however, consist of only one zone of comparably hot gas, where most of the fuel is converted.

We discuss the selectivity in this work since we can qualitatively compare results from experiment and model despite the difference in fuel conversion. The results for the product species $H_2$, CO, $CO_2$, and $C_2H_4$ are shown in Figure 29.

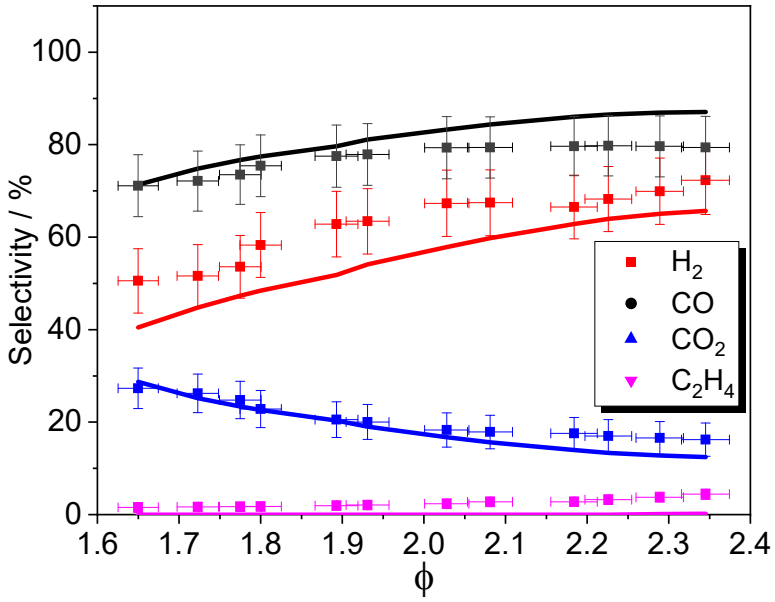


Figure 29: Selectivities of product-gas species. Symbols: experiment, lines: simulation.

Generally, the selectivity of the potentially valuable species $H_2$, CO, and $C_2H_4$ is increasing with increasing $\phi$. While the selectivities of CO, $CO_2$, and $C_2H_4$ add up to 100% in the simulation, a sum of 117 – 122% was obtained from the measurement. This indicates that the experimentally-obtained carbon balance is inaccurate, probably due to uncertainties in the product-gas analysis and mass-flow controllers. Here, we account for the carbon excess of about 17 – 22% by dividing the selectivities of the carbon-containing species by their corresponding sum at each equivalence ratio. Experimentally, as $\phi$ increases from 1.65 to 2.34, $H_2$ selectivity increases from 50 to 72%, CO from 71 to 79%, and ethylene from 1.5 to 4%, while the $CO_2$ selectivity decreases from 27 to 16%. The decreasing $O_2$ content and the consequently lower maximum temperature can explain these trends. The formation of $H_2O$ and $CO_2$ from $H_2$ and CO at high $\phi$ is limited by the low $O_2$ concentration, thus a significant fraction of CO and $H_2$ is not converted and remains in the product gas. The H/C ratio in the product gas varies between 1.1 and 1.4. Experiment and simulation are in good agreement with a mean deviation of 10% for CO, $H_2$, and $CO_2$, which is within the experimental uncertainty. The $C_2H_4$ selectivity shows the highest deviation between simulation and experiment, with almost no $C_2H_4$ formed in the simulation. A possible explanation is that $C_2H_4$ mostly forms in colder regions of the cylinder, like crevices and boundary layers that are not included in single-zone models. Again, the use of a multi-zone model could improve the agreement between model and experiment with respect to hydrocarbon species [61,62]. The selectivity seems to be an appropriate means to compare experimental and modeling results with deviating fuel conversion.

### 5.3.3 Work and heat output

Polygeneration processes are designed to not only provide base chemicals but also work and heat. The latter two outputs are shown in Figure 30 as a function of $\phi$. As expected, these outputs decrease with increasing equivalence ratios, ranging between 314 and 245 J per cycle for heat and 160 and 135 J for work. The decrease is a result of the decreasing maximum temperatures with increasing $\phi$, which reduces heat transfer to the coolant, but also fuel conversion and reaction enthalpies (less $CO_2$ and $H_2O$ formed). This consequently reduces the work output of the engine in favor of the generation of valuable product species. Simulation and experiment are in very good agreement for the heat output, while the work output of the engine is slightly over-predicted. The deviation can be explained by the higher fuel conversion and the fact that the gas exchange strokes are not included in the model. Experimental data suggest that the gas exchange strokes reduce the work output by about 11 J.

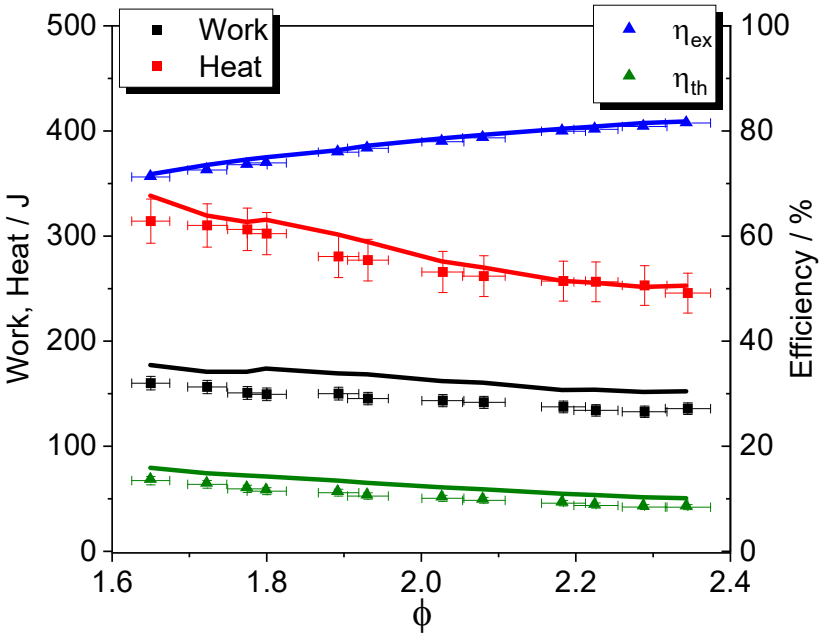


Figure 30: Work and heat output per cycle and exergetic and thermal efficiencies. Symbols: experiment, lines: simulation.

### 5.3.4 Efficiencies

In order to assess polygeneration in the engine on a thermodynamic basis, at least two efficiency metrics are available: thermal and exergetic efficiency. Both are shown in Figure 30. The thermal efficiency is comparably low and decreases from 13 to 8% in the range of investigated equivalence ratios. However, the thermal efficiency alone is not a suitable parameter to assess polygeneration processes, since the heat output and energy content of the chemical products are neglected. The exergetic efficiency, which includes all three forms of available energy, increases from 71 to 82% as $\phi$ increases from 1.65 to 2.34, exceeding those for common syngas-production processes like methane steam reforming, which has an exergetic efficiency of ~63% [2]. In addition, the resulting efficiencies are also exceeding those for other polygeneration processes: Polygeneration based on solar collectors, providing electricity, heat, cooling, and desalinated water yield exergetic efficiencies up to 32% [32]. Other systems combining power cycles with methanol production or desalinization reach efficiencies up to 60% [33,63]. For both metrics (thermal and exergetic efficiencies), simulation and experiments are in very good agreement. Compared to our previous work with n-heptane as additive [8], the exergetic efficiency slightly increases with DME, by about 1 percent point. This is consistent with the fact that heat losses with DME as an additive are about 8% lower than with n-heptane, while the work output is only 3% higher. This may be due to differences in combustion phasing with the two additives. Nearly the same mass fractions of both n-heptane and DME are needed for HCCI.

## 5.4 Conclusions

An IC engine operating in HCCI mode at fuel-rich equivalence ratios with methane/DME as reactants was considered as a device for a polygeneration process that simultaneously produces synthesis gas, work, and heat. Experiments were compared with simulations based on a homogeneous engine model. Work, heat, selectivities, and thermal as well as exergetic efficiencies were evaluated.

A method to experimentally identify stable operating points was introduced. For an intake temperature of 150°C, the mole fraction of DME that was needed for stable operation was mostly constant at 9.3% in a range from

$\Phi$ = 1.6 to 2.3, however, significant soot production starts at $\Phi$ = 2. Below this limit the soot concentration in the product gas was less than 10 mg/m³. Within the envelope of stable engine operation increasing the equivalence ratio shifted the combustion phasing towards earlier crank angles. Results from the simulation suggest that this is because during ignition, initially methane is almost inert and the equivalence ratio of DME alone shifts closer to stoichiometric conditions for increasing overall $\Phi$.

The trends observed in the experiments were well reproduced by the simulations. However, the combustion phasing differs, probably because of the high sensitivity to uncertainty in the experimental temperature at the start of compression. Adjusting the starting temperature by about 10 K brings the simulated phasing in line with the experiments. In the experiment, $C_2H_4$ is measured with selectivities up to 5%, while the single-zone model predicts almost no output of that species, likely because in the experiment it is formed at low temperatures in crevices and near the wall. The thermal efficiency, work, and heat output were decreasing with increasing equivalence ratios, while selectivities towards CO and $CO_2$ as well as the exergetic efficiency were increasing.

The results show that the engine can be used for polygeneration in a flexible manner. When less work (likely to be converted to electricity) is required, the work output can be reduced by 20% by increasing the equivalence ratio, while the exergetic efficiency increases from 71 to 82%, exceeding efficiencies of other polygeneration processes. Simultaneously, the fuel is converted to synthesis gas by partial oxidation, with selectivities of up to 72% for $H_2$ and 79% for CO. The resulting H/C ratios range from 1.1 to 1.4 and could be increased to the desired value, which is usually 2, by the water-gas shift reaction [41]. A complete shift from the production of chemicals to that of power would be possible by operating the engine on a stoichiometric mixture.

In conclusion, polygeneration in internal combustion engines may provide an advantage in terms of exergetic efficiency and flexibility, and DME is a promising additive for methane. Since the amount of DME needed is not negligible, further autoignition-supporting additives should be evaluated. Based on the results presented here, future work will also include the development of a multi-zone model to further improve the simulations, and improvements in the product-gas analysis to close the carbon balance more accurately. Also, we expect an increase of the ethylene yields by increasing the equivalence ratios to even higher values, beyond the upper sooting limit.

# 6 Evaluation of additives for fuel-rich HCCI operation: DME, DEE and n-heptane

In the work reported in this chapter, the effects of methoxymethane (dimethyl ether, DME), ethoxyethane (diethyl ether, DEE), and n-heptane as additives in compression-ignition of fuel-rich methane/air mixtures were investigated in experiment and simulation. The experiments were performed in a single-cylinder octane-number test engine at a compression ratio of 10. Engine operating stability, auto-ignition behavior, and syngas production were examined. The simulations used a single zone model with detailed chemical kinetics. The method for pressure trace analysis was adapted to the very fuel-rich conditions examined in this study. The choice of additive does not significantly influence syngas production, but a distinct influence on auto-ignition was found. The most effective additive in terms of mass fraction was DEE which produced stable operation at around 20% by weight. While the use of DME and n-heptane resulted in similar heat release traces, DEE yielded more early heat release and less of a negative temperature coefficient (NTC) behavior. The widest stable operating range in terms of additive fraction was found for DME. A reaction path analysis showed that the effect on ignition is similar for all three additives: they react early in the compression stroke and lead to H-abstraction from $CH_4$. Comparing heat release rates and calculated cylinder temperatures indicated that not only the additive's reactivity but also its heat capacity contributes to auto-ignition behavior.

This chapter is slightly modified from [64]:

> K. Banke, D. Freund, B. Atakan, S.A. Kaiser, Evaluation of fuel additives for HCCI engines operated on fuel-rich methane/air mixtures: DME, DEE, and n-heptane, Applications in Energy and Combustion Science, 13 (2023) 100112, doi:10.1016/j.jaecs.2023.100112.

My contributions included planning, setting up and performing the experiments, the processing, analysis, interpretation, and visualization of the experimental data, and writing the introduction, data processing and experimental parts of the manuscript. Dominik Freund conducted the simulations, reaction kinetic calculations and wrote the corresponding parts of the manuscript. Burak Atakan and Sebastian Kaiser were involved in the conceptual design, in developing the adapted heat release analysis and in writing and revising the manuscript.

## 6.1 Introduction

In our previous work we showed that fuel-rich engine operation can be extended to higher equivalence ratios by using HCCI instead of spark ignition [8]. Methane is relatively inert and requires high temperatures for auto-ignition. These can be achieved by high compression ratios or intake flow preheating, but the increase in overall process temperatures also increases heat losses and costs for more temperature-materials. Thus, it may be advantageous to decrease the required auto-ignition temperatures by adding small fractions of ethers or *n*-heptane.

Another, related aspect is that HCCI operation is controlled kinetically, making process control one of the main challenges. Therefore, it is important to investigate possible control parameters. This has extensively been done for lean mixtures (i.e., for "conventional" power-oriented HCCI) [65], but investigations for fuel-rich mixtures are lacking. There are several approaches to control combustion phasing in HCCI engines, e.g., via internal or external exhaust gas recirculation (EGR), the intake temperature, the compression ratio, fuel additives, and fuel reforming. A detailed summary of common approaches is given in a review on reactivity controlled compression ignition (RCCI) by Reitz [66]. The current work investigates HCCI process control for fuel-rich operation on $CH_4$ via fuel additives that are injected in the intake.

The additives investigated in this work are dimethyl ether (DME), diethyl ether (DEE), and *n*-heptane. Some of their relevant properties, and those of methane, are listed in Table 5.

Table 5: Selected properties of fuel and additives at 1 bar and 25°C.

| Fuel | Formula | Molar mass / g/mol | Cetane number | Isobaric heat capacity / J/(mol*K) |
|---|---|---|---|---|
| Methane | $CH_4$ | 16.043 | - | 35.6 |
| Dimethyl ether | $CH_3OCH_3$ | 46.069 | 55 [67,68] | 65.71 |
| Diethyl ether | $C_2H_5OC_2H_5$ | 74.123 | 140 [69] | 115.89 |
| *n*-heptane | $C_7H_{16}$ | 100.21 | 53 [70] | 166.89 |

*n*-Heptane, the primary reference fuel (PRF) with octane number zero, is often used as a "chemical" diesel surrogate, because it has ignition characteristics similar to diesel fuel. DME is considered as an alternative. A difference between it and the other two additives is that it is gaseous at ambient conditions. It has good auto-ignition characteristics (cetane number 55) [67]. It is especially interesting as a fuel for HCCI engines because it shows strong low-temperature ignition reactions [71]. DEE has the very high cetane number of 140 [69], indicating that it is very reactive in the high-temperature high-pressure environment that the cetane-number test employs. It also reacts fast at relatively low temperatures [72]. Shock-tube experiments showed that DEE is more reactive than DME in lean and stoichiometric mixtures, consistent with its higher cetane number [73], while in batch reactor simulations, DME was found to be more reactive than *n*-heptane [74]. Both DME and DEE can be produced from biomass which make them potentially renewable fuels.

For lean HCCI combustion, DME addition to natural gas was investigated in CFD simulations with detailed chemical kinetics (86 species and 360 reactions) by Kong [58]. He found that the ignition is mainly controlled by DME oxidation and that a major part of the DME reacts prior to methane conversion. This is consistent with our own findings for fuel-rich conditions [31].

The conversion of fuel-rich methane/air mixtures with 10 mol% DME as an additive in HCCI conditions was investigated by Hegner et al. in simulations and experiments in a rapid compression machine (RCM) [40]. Equivalence ratios of up to $\Phi = 10$ where investigated. The simulations implemented a single-zone engine model and predicted maximum $H_2$ mole fractions of 25% in the product gas at $\Phi = 4$, while the RCM experiments showed maximum $H_2$ mole fractions of 20% at $\Phi = 6$. It was also shown that DME considerably reduces the intake temperature required for auto-ignition. The influence of DME and *n*-heptane on $CH_4$ conversion was investigated in shock tubes and flow reactors by Sen et al. [47]. The results were compared to simulations using different reaction mechanisms. They found that both additives reduce the required reaction temperatures and generally any additive can be used for this purpose if it produces additional OH radicals.

Syngas production from natural gas via fuel-rich HCCI operation was also investigated in simulations by Morsy [75]. He performed parameter studies in initial temperature, engine speed, equivalence ratio, oxygen enrichment, and initial pressure using a single zone model and the GRI-3 mechanism. He suggests an engine speed of 500 rpm, 1 atm initial pressure, and an oxygen / nitrogen ratio of 0.3 / 0.7 at $\Phi = 3$ as optimum operating conditions for maximum syngas fractions, resulting in about 45% $H_2$ in the product.

All of the additives used in this work have a distinct negative temperature coefficient (NTC) behavior [76–78], i.e., there is a temperature range in which reactivity *decreases* with increasing temperature. Deng et al. investigated non-premixed DME/air flames experimentally and confirmed the importance of the NTC behavior of DME for low-temperature combustion processes [76]. Tran et al. investigated the low-temperature DEE combustion in a jet-stirred reactor and found that DEE starts to react at 425 K and has not one, but two NTC ranges [77]. They observed that this dual-NTC range manifests itself in the CO and formaldehyde ($CH_2O$) mole fraction plotted as a function of temperature. Gauthier et al. investigated the auto-ignition characteristics of *n*-heptane using shock tube experiments and confirmed a strong NTC behavior for HCCI-relevant conditions ($\Phi = 2$, $p = 15 – 25$ bar, $T = 850 – 1280$ K) [79].

The aim of this work is to investigate and compare the effects of three additives on fuel-rich auto-ignition in HCCI. The most suitable additive is determined by comparing the additives in terms of mole, mass, and energy fraction in the fuel-air-mixture, the timing and intensity of the heat release, and the operating stability.

## 6.2 Methods

### 6.2.1 Experiment

The hardware used for the experiments is mostly that used in our previous experiments [8,31]. A schematic of flows and instrumentation is shown in Figure 31.

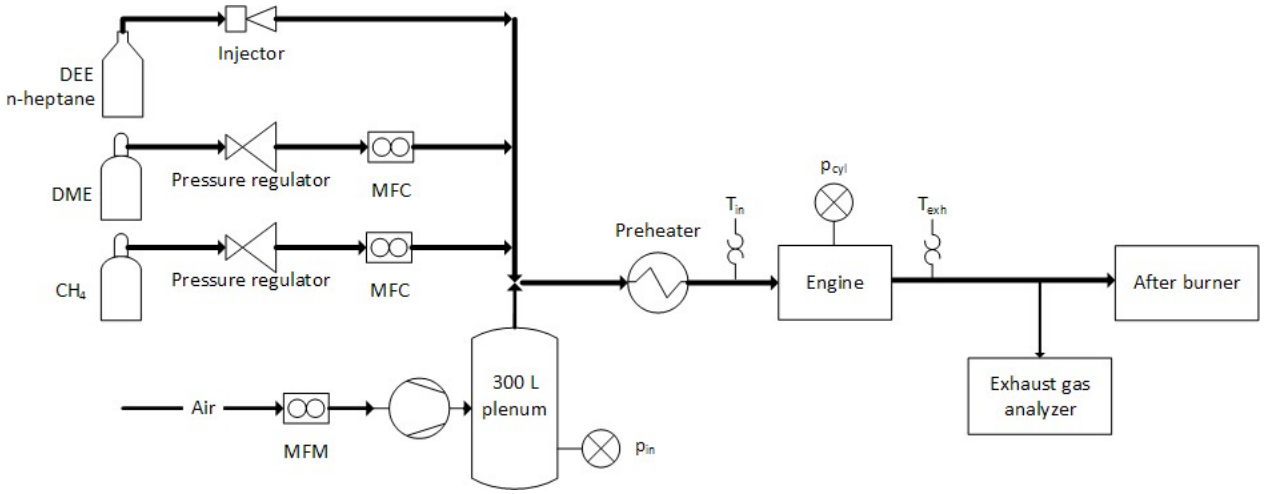


Figure 31: Schematic of the instrumentation.

The methane and DME flows were controlled with mass flow controllers (MFC), while the flow of air was measured using a mass flow meter (MFM). The liquid additives DEE and *n*-heptane were injected by a commercial port-fuel injector. The mixture was preheated up to 150°C. The crank-angle resolved in-cylinder pressure was measured with a piezoelectric pressure transducer integrated into the spark plug. Except for $H_2O$, which was condensed at 3°C and removed before analysis, and $N_2$, the major product gas species ($H_2$, CO, $CO_2$, $CH_4$, $C_2H_4$, $O_2$) were detected using a commercial exhaust gas analyzer (ABB, Type optima advance 2020). Table 6 lists key parameters of the experiment.

Table 6: Engine properties and operation conditions.

| Description | Symbol | Value | Unit |
|---|---|---|---|
| Rotational speed | $rpm$ | 595 | 1/min |
| Compression ratio | $\varepsilon$ | 10 | - |
| Bore | $d$ | 65 | mm |
| Stroke | $s$ | 100 | mm |
| Displacement | $D$ | 332 | cm³ |
| Fuel/air equivalence ratio | $\Phi$ | 1.6-2.4 | - |
| Intake temperature | $T_{in}$ | 150 | °C |
| Intake pressure | $p_{in}$ | 1 | bar |
| Coolant temperature | $T_C$ | 100 | °C |

A BASF octane number research engine was used for the experiments. The engine was operated in SI-mode at stochiometric conditions with a compression ratio of ε = 10 until a coolant temperature of 100°C was reached. Then the spark plug was switched off and additive was added to achieve ignition. Engine operation was considered "stable" when the coefficient of variation (CoV) of the indicated mean effective pressure (IMEP) was below 10%, and "acceptable" when at the same time the maximum pressure rise rate ($PRR_{max}$) was below 10 bar/°CA. A CoV of less than 5% is typically targeted for mobile applications, but a higher value seems acceptable for stationary applications where noise is less of an issue. Lim et al. even suggest 20% for a similar application [6]. At each operating point 140 consecutive cycles were recorded. The IMEP was calculated for each cycle individually and afterwards averaged over the 140 consecutive cycles. The CoV is usually calculated by dividing the standard deviation of the IMEP over the recorded cycles by their mean IMEP. Here, instead of the IMEP, the difference of fired and motored IMEP was used. This is a more convenient metric that is also correlated more closely with combustion instability. Equivalence ratios from 1.6 to 2.4 where investigated here, because previous experiments already had shown that this range includes the maximum syngas yield for DME as an additive, as well as the soot limit at approximately Φ = 2 [31].

### 6.2.2 Yields and conversion

The equivalence ratio Φ is defined as the ratio of the fuel mass $m_{fuel}$ (the sum of methane and additive masses) to the mass of air $m_{air}$ divided by the ratio of the fuel mass to the mass of air that would be needed for stoichiometric conversion of the fuel to $CO_2$ and water, as given in eq.(1). The equivalence ratio of just methane ($\Phi_{CH4}$) or just the additive ($\Phi_{add}$, here, $\Phi_{DME}$, $\Phi_{DEE}$, or $\Phi_{C7H16}$) are defined correspondingly by replacing $m_{fuel}$ with the methane or additive mass in the numerator and using the stoichiometric air demand of that species in the denominator.

$$\Phi = \frac{m_{fuel}/m_{air}}{(m_{fuel}/m_{air})_{st}} \tag{29}$$

The mass fractions $y_{add}$ are defined as the mass of additive divided by the mass of all fuel species (methane and additive). The mole fractions $x_{add}$ are defined as the number of additive molecules divided by the number of fuel molecules. To calculate the product yields, the outgoing molar flow rate $\dot{n}_{out}$ needs to be known. Since our gas analysis cannot detect all species in the product gas, some assumptions had to be made to calculate $\dot{n}_{out}$[31].

Essentially, the fraction of water in the product gas was calculated from the hydrogen balance and then the $N_2$ fraction was calculated from the condition that all product species mole fractions add to unity. The mean molar mass of the product and the known mass flow rate $\dot{m}$ through the engine were used to calculate $\dot{n}_{out}$. With $\dot{n}_{out}$ , the yields $Y_i$ can be calculated via eq. (30). Here, $\nu_i$ is the stoichiometric coefficient of species i, calculated for the conversion of one mole of fuel.

$$Y_i = \frac{\dot{n}_{i,out}}{\dot{n}_{in}(x_{fuel,in}\,\nu_i)} \tag{30}$$

Conversions are calculated with eq. (31).

$$X_i = \frac{\dot{n}_{i,\,in} - \dot{n}_{i,out}}{\dot{n}_{i,\,in}} \tag{31}$$

### 6.2.3 Heat release analysis

The heat release analysis was performed according to Heywood [23] (p.509-514). Eq. (32) can be derived from the first law of thermodynamics for a closed system using the ideal-gas law. Blowby and crevice losses are neglected.

$$\frac{dQ_{ch}}{d\theta} = \frac{\gamma}{\gamma - 1} p \frac{dV}{d\theta} + \frac{1}{\gamma - 1} V \frac{dp}{d\theta} + \frac{dQ_{ht}}{d\theta} \tag{32}$$

$Q_{ch}$ is the energy released by chemical reaction, $\gamma\ is$ the specific heat capacity ratio, $Q_{ht}$ is the heat transferred from the cylinder charge to the walls, and $\theta$ is the crank angle of the engine. The expression $\frac{dQ_{ch}}{d\theta}$ is also referred to as heat release rate (HRR). In the case of stoichiometric or lean combustion, $Q_{ch}$ is often simply calculated as the mass of fuel multiplied with magnitude of the specific enthalpy change in complete stochiometric combustion ("lower heating value", LHV) and the "combustion efficiency" ($\eta_{comb}$), which is then often estimated to be between about 96 and 98% (eq. (33)).

$$Q_{ch} = m_{fuel,in} \cdot LHV \cdot \eta_{comb} \tag{33}$$

However, for very fuel-rich mixtures combustion is far from complete and reference to the case of complete combustion is not useful. Instead, LHV and combustion efficiency were replaced by the difference in internal energy $\Delta u_{eq}$ between the supplied fuel/additive/air mixture and the internal energy of that mixture in chemical equilibrium at the initial temperature and pressure, which is the maximum chemical energy that can be transferred as heat (eq. (34)).

$$\Delta u_{eq} = u(T_{in}, p_{in})|_{eq} - u(T_{in}, p_{in})|_{in} \tag{34}$$

This leads to a modified expression for the heat release $Q_{ch}$(eq. (35)).

$$Q_{ch} = m_{fuel,in} \cdot \Delta u_{eq} \tag{35}$$

Eq. (34) was evaluated in Python with the module Cantera [80]. First, the fuel-additive-air mixture was equilibrated at intake conditions (150°C and 1 bar). Then, the elevated temperature and pressure of the reacted mixture were reset to intake conditions. $\Delta u_{eq}$ is the difference in internal energy in the two states, and this difference is far from the LHV for very rich mixtures. For instance, at an equivalence ratio of 1.88 and DME as the additive (with $\Phi_{CH4}$ = 1.6 and $\Phi_{DME}$ = 0.23), $\Delta u_{eq}$ is 50.5% lower than the LHV.

The specific heat capacity ratio $\gamma$ in eq. (32) is often calculated as a function of temperature using parameter fitting, e.g. the linear approach suggested by Cheung and Heywood [25]. Since fitting parameters for very fuel-rich operating conditions cannot be found in the literature, $\gamma$ was instead calculated using a two-zone model with a reacted and an unreacted zone, as for example in [34]. The experimentally measured intake and exhaust compositions and the spatially averaged in-cylinder temperature were used to calculate the crank-angle dependent heat capacities of each zone. The in-cylinder temperature was calculated via the ideal-gas law from the trapped charge mass and the pressure trace. In a first step, only $\gamma_{unr}(\theta)$ of the unreacted zone (with intake composition) was used to calculate the cumulative heat release. In a second step, the normalized cumulative heat release (the so-called mass burn function, MBF) was used to calculate $\gamma$ as a weighted average of the values in the unreacted and the reacted zone (with exhaust composition) (eq. (36)).

$$\gamma(\theta) = \gamma_{unr}(\theta) \cdot \big(1 - MBF(\theta)\big) + \gamma_{reac}(\theta) \cdot MBF(\theta) \tag{36}$$

The heat transfer to the cylinder walls was estimated using the semi-empirical correlation from Woschni [52]. The result was then scaled to match the difference between the integrated net heat release rate and $Q_{ch}$ [81]. The pressure traces used for heat release analysis were averaged over 140 cycles. The resulting heat release rates were first smoothed with a third-order Butterworth low-pass filter with a cutoff frequency of 0.03 times the Nyquist frequency of the data acquisition ($f_{nyq}$ = 18 kHz) and then with locally weighted scatterplot smoothing (LOWESS) with a normalized distance of d = 0.05.

### 6.2.4 Simulation of the engine

To gain insight into the auto-ignition characteristics of each additive at fuel-rich conditions the engine was simulated with a zero-dimensional single-zone model. Cantera was used in the framework of python for describing the thermodynamics and reaction kinetics [80]. The model includes an inlet and an outlet valve and describes four strokes. The cylinder volume *V* is given by the piston movement according to Heywood [23] (p. 45).

Consistent with the experiments, the heat transfer coefficient of the inner wall was calculated via the Woschni correlation [52], which is a reasonable approach for HCCI engines when some of the parameters are adjusted to match the experimental results [55]. A description of the implementation of the Woschni equations in our engine model can be found in [8]. Metrics like syngas fractions, combustion stability, and work output are influenced significantly by combustion phasing, as will be shown in the results section. For this reason, the combustion phasing in the simulation was matched to the experimental one. CA50 – the crank angle at which 50% of the overall heat has been released – was taken as the metric for combustion phasing. In contrast to the experiment in the engine model the heat release rate can be calculated explicitly by evaluating the volumetric molar net production rate $\dot{\omega}_\iota$ of each species $i$ (in $\frac{kmol}{m^3 s}$) at each timestep. Subsequently, the heat release rate $\frac{dQ_{ch}}{d\theta}$ was determined according to eq. (37).

$$\frac{dQ_{ch}}{d\theta} = V(\theta) \cdot \sum_i \big(du^o_{f,i}(T_{ref}) \cdot \dot{\omega}_\iota(\theta)\big) \tag{37}$$

In this expression $du^o_{f,i}$ denotes the standard internal energy of formation of each species $i$ at the reference temperature $T_{ref}$. The volumetric net production rate was calculated by Cantera using a reaction mechanism that includes a set of species with their properties, and elementary reactions. The reaction mechanisms used here are PolyMech 2.0 for DME [82], the mechanism of Serinyel et al. for DEE [83], and that of Stagni et al. for *n*-heptane [84]. Fitting the simulation to the experiment was done in two steps: first, adjusting the compression ratio in the model to best match the pressure trace of the experiment (in which the uncertainty of mechanically setting the compression ratio is ±0.5), and second, adjusting the Woschni parameters for the DME case so that CA50 of simulation and experiment agree within ±1 °CA.

## 6.3 Results and discussion

This section starts with the method used to determine the stable engine operating range. Stable operation is important not only in itself, but also because only then does analysis of product gas composition and heat release rates yield useful results. Next, syngas production (yields and conversions) is investigated to evaluate the chemical output of the process. Furthermore, heat release analysis was conducted to investigate auto-ignition. The crank angle resolved species traces from the single zone model serve to gain a more detailed understanding of the effects and reactions during auto-ignition and to possibly explain the different behavior of the additives that was found in the heat release analysis.

### 6.3.1 Operating stability limits

The basic experiment for determining operating stability performed here is a scan, in which for a constant methane flow the additive flow is systematically increased, as described in chapter 4.2.1.

To investigate the operating limits for the additives for different equivalence ratios, operability scans were performed for methane equivalence ratios from $\Phi_{CH4}$ = 1.2 to about 1.8 (6 to 9 slm methane). With DME the additive flow increment was 0.006 in $\Phi_{add}$, with DEE about 0.004, and with *n*-heptane about 0.005. Figure 32 shows the mass fraction $y_{add}$ of each additive, CA50, and the energy fraction $e_{add}$ versus the methane equivalence ratio $\Phi_{CH4}$ at the CoV limit and at the $PRR_{max}$ limit. The energy fraction of the additive is calculated according to eq. (38) with the mass fractions $y$ and the lower heating value LHV.

$$e_{add} = \frac{y_{add} \cdot LHV_{add}}{y_{add} \cdot LHV_{add} + y_{CH_4} \cdot LHV_{CH_4}} \tag{38}$$

Values for $y_{add}$, CA50, and $e_{add}$ at the limits were calculated via linear interpolation between the nearest two experimentally recorded operating points.

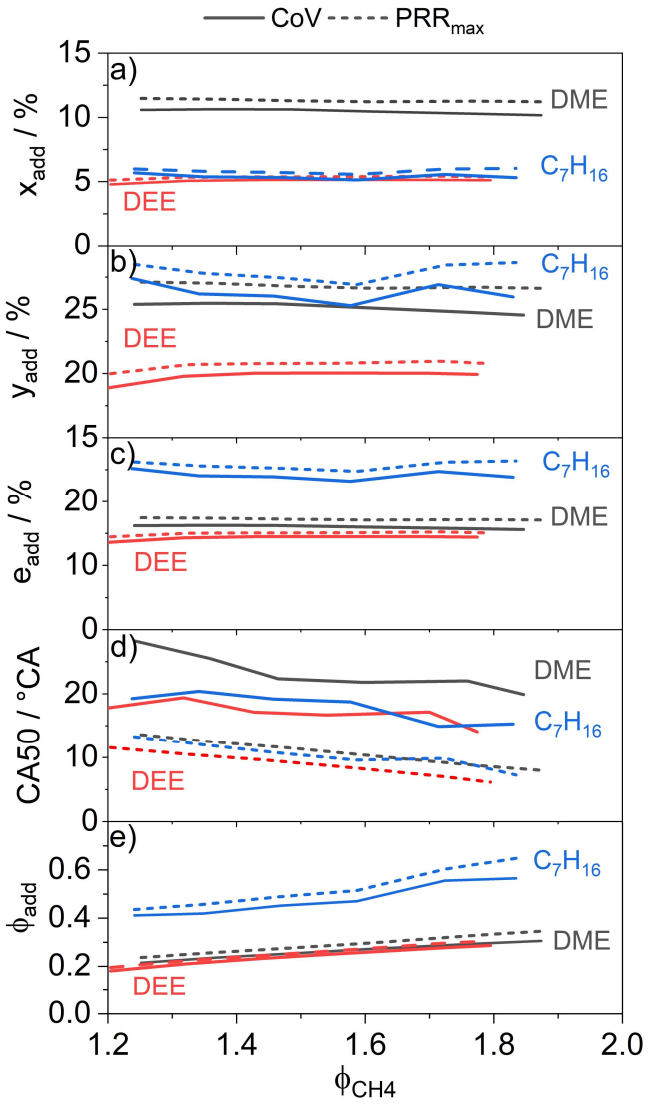


Figure 32: Characteristics of the lower (given by the CoV) and upper (given by $PRR_{max}$) operating limits as a function of the methane equivalence ratio. A) Mole fractions of additive in the fuel, b) mass fractions of additive in the fuel, c) energy fraction of the additive, d) combustion phasing, and e) additive equivalence ratio.

As Figure 32 b) shows, in terms of mass fraction, the additive demand of the engine at both the upper and the lower operating limit is mostly independent of $\Phi_{CH4}$. Results for *n*-heptane and DME are very similar. The needed mass fraction of DEE is about 5%-points lower and the range between CoV limit and $PRR_{max}$ limit is narrower than for the other additives. In terms of mole fractions, shown in Figure 32a), the demand for DEE and *n*-heptane is very similar. About twice as much DME is needed for stable operation. One might assume that the two ethers yield similar results since they are both partially oxygenated molecules and chemically closer to each other than they are to *n*-heptane. It seems likely that more DME is needed in terms of mole fractions because it provides less reaction enthalpy and it has fewer atoms, providing fewer potential radicals per mole. However, concerning the added reaction enthalpy, Figure 32 c) shows the energy fraction of the additives at the operating limits. It is markedly higher with *n*-heptane than with DME or DEE. This suggests that the contribution of the additive to the overall heat release is not solely important for auto-ignition.

All else equal, the combustion phasing shown in Figure 32 d) can be interpreted as a measure of overall mixture reactivity. With all additives, at both lower and upper operating limit, CA50 shifts to earlier crank angles with

increasing methane equivalence ratio. This is counter-intuitive, because in combustible mixtures, the reactivity is generally maximum near stoichiometric conditions and *decreases* as the mixture becomes richer. We already found this effect for DME in our previous work [31]. If methane is considered inert at the start of combustion, which is a reasonable assumption when compared to the reactive additives, the equivalence ratio of the additive seems to be more important for auto-ignition than the overall equivalence ratio. It is shifting closer to stoichiometric with increasing overall Φ increasing the mixtures reactivity. The current results indicate that this conclusion is not limited to DME but is more general.

The fact that the additive fraction is mostly constant over the equivalence ratio, as seen in Figure 32 a) and b) is then somewhat coincidental. A higher additive equivalence ratio is needed for increasing methane equivalence ratio to compensate the increase of mixture heat capacity. With increasing heat capacity, the same heat release increases the cylinder pressure less. More additive needs to be added to compensate for this thermodynamic effect.

Comparing the different additives, the CoV-limit for DME is at much later CA50 than for the other ones. DME seems to enable very late stable combustion. This also means that the operating range is widest with this additive. A caveat is that this may also partly stem from mixture inhomogeneity (“stratification”), since DME is supplied gaseous while the other additives are injected as liquids.

### 6.3.2 Heat release rates

Figure 33 shows the experimental heat release rates at crank angles from -50° to 10° aTDC for increasing additive fractions at constant methane equivalence ratio. The heat release at these early crank angles is associated with the ignition process and may give insight into the ignition characteristics in the different cases.

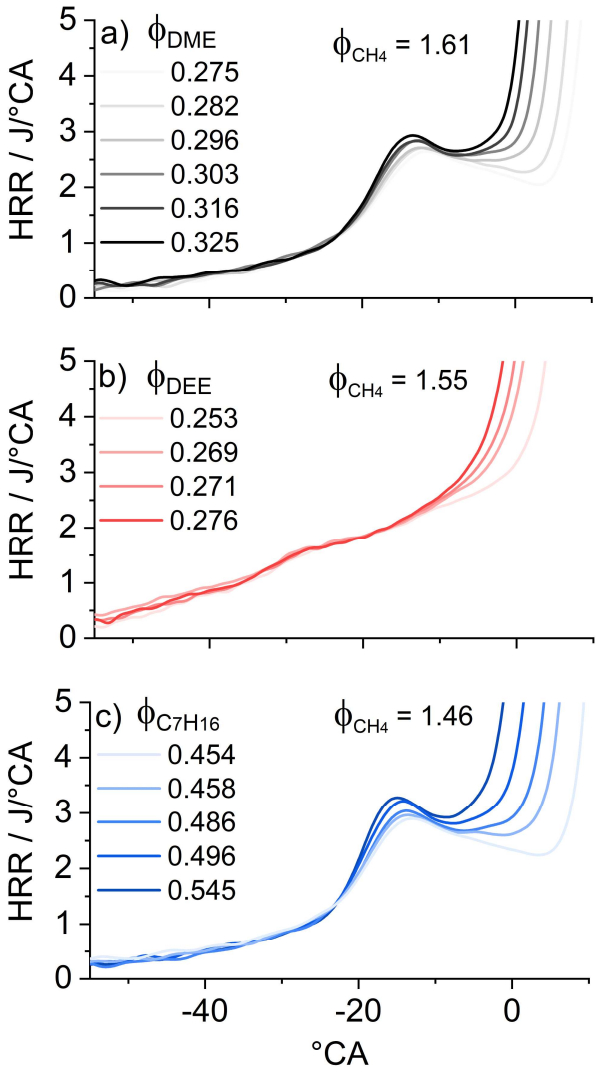


Figure 33: Heat release rates during ignition for variations of the additive flow at constant methane flows (i.e., almost constant $\Phi_{CH4}$). A) For DME as additive, b) DEE, and c) *n*-heptane. A lower methane equivalence ratio was chosen for *n*-heptane to not exceed the soot limit at about $\Phi = 2$ and to limit the differences in heat capacity between experiments. In each case, the lowest additive equivalence ratios shown here were the closest within the CoV-limit.

For all additives, as expected, higher $\Phi_{add}$ increases the early heat release and accelerates the main combustion. The traces with DME and *n*-heptane show a very distinct low temperature heat release (LTHR) followed by an NTC region near -10°CA. With increasing temperature, the heat release rate first decreases before it increases again with further temperature increase. This is qualitatively similar to results for lean HCCI operation on DME/methane mixtures [85]. DEE however does not show a such strong NTC behavior. Instead, there is more heat release at very early crank angles around -40°CA compared to the other additives and no peak in the LTHR. To explain this, the cylinder pressures during ignition must be considered. At -30°CA a pressure of about 10 bar is reached. At TDC the pressure is around 20 bar. Burke et al. [86] showed that 80/20 $CH_4$/DME-mixtures at $\Phi$ = 2 maintain their temperature-dependent NTC behavior up to at least 25 bar. For *n*-heptane Gauthier et al. [79] observed NTC behavior up to 45 bar. However, for DEE Werler et al. [87] showed that the NTC behavior of DEE starts to decrease with increasing pressure significantly at about 5.5 bar. Since the pressure in the cylinder during LTHR and ignition is between about 6 to 20 bar, less NTC behavior is expected for DEE than for the other additives.

From among the cases in Figure 33, Figure 34 a) shows the experimental heat release for cases with similar CA50 of around 15°CA (solid lines) compared to those from the simulation with the corresponding CA50 (±1°CA) (dashed lines). Figure 34 b) shows the resulting in-cylinder temperature in the experiment and simulation, as well as simulated motored temperatures – that is, with the chemistry "switched off", the temperature increase then being solely due to compression. The temperatures in the experiment are calculated from charge mass, cylinder pressure, and the gas composition via the ideal-gas law. The gas composition is calculated using a MBF-weighted two-zone model equivalent to the one used for γ in eq. (36).

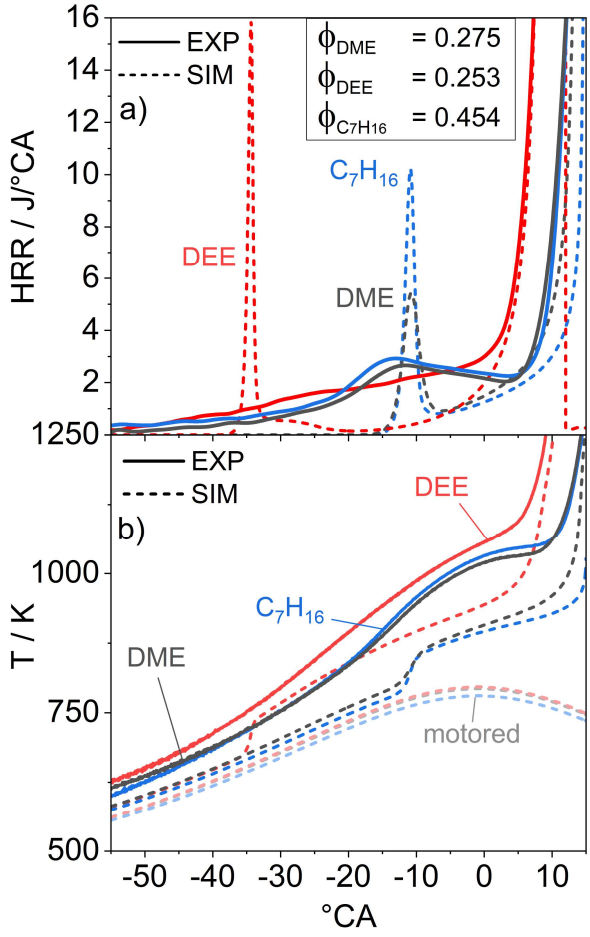


Figure 34: a) Heat release rates in experiment and simulation for those experimental conditions in Figure 33 that have the most similar CA50 (17°CA,11°CA, and 17°CA). b) Temperature traces in experiment and simulation at the CoV limit. The motored temperatures are simulated.

The heat release rates show distinct similarities and differences between experiment and simulation. The heat release rate in the experiment increases gradually from about -50°CA whereas in the simulation only short time intervals with high heat release rates occur. The steep peaks in heat release rates in the simulation are a well-known feature of single-zone models of HCCI combustion, which in experimental reality is not homogeneous in mixture reactivity, in particular due to spatial inhomogeneity in temperature induced by wall heat transfer [88,89]. Apart from their thus exaggerated shape, the timings of the peaks in the simulation coincide with those in the experiment quite accurately for DME and *n*-heptane. In the experiment, DEE does not yield a clear LTHR peak, but in agreement with the experiment the simulation clearly predicts more heat release at earlier crank angles compared to DME and *n*-heptane.

The DME and *n*-heptane traces are qualitatively similar, but *n*-heptane releases more heat in experiment and simulation. This is expected because the energy fraction of *n*-heptane is higher as discussed above. The overall heat release of DEE before TDC seems to be less concentrated than that of the other additives. This may be the explanation for the early stability limit of DEE shown in Figure 32 d). While the NTC behavior creates a time delay before the main combustion in the DME and *n*-heptane cases, this effect is less pronounced for DEE. It reacts earlier, and the simulation confirms this. However, the simulation predicts a stronger NTC behavior which indicates that the in-cylinder temperatures in the experiment might be higher, which is supported by Figure 34 b), showing generally higher calculated experimental temperatures.

In Figure 34 b) the *n*-heptane case shows lower compression-induced (motored) temperature increase because of this mixture's higher heat capacity. However, because of the greater heat release in the reactive cases, the temperature increases to similar the levels as those of the DME and DEE traces before ignition. This suggests that for *n*-heptane the higher energy fraction is needed to compensate for this additive's higher heat capacity. We conclude that heat capacity is not negligible in the choice of the additive, with high values being a disadvantage.

For DEE the motored temperature is very similar to the DME case. DEE's heat capacity is higher but in this specific case the overall equivalence ratio is lower with $\Phi = 1.8$ for the DEE experiment and $\Phi = 1.9$ for the DME experiment, and thus the molar heat capacities of the two mixtures are nearly identical. The simulated temperature in the DEE traces increases early. In the experiment this is less distinct, but still visible at crank angles from -20 to 0°CA. This temperature increase corresponds to the increased heat release rate at about -30°CA seen in Figure 34 for DEE and seems to accelerate the ignition process such that stable operation can be achieved at lower additive energy fraction. The simulated temperature traces show the same trends, but the overall temperature levels are lower and – as discussed above – gradients are locally steeper.

### 6.3.3 Syngas production

The most important chemical output of the engine with this set of operating parameters, especially the equivalence ratio, is syngas ($H_2$/CO), mostly produced by the partial oxidation of methane. In our previous work, syngas production with *n*-heptane and DME was investigated [8,31]. There, we first investigated operating points with a constant *n*-heptane mole fraction of 5% [8]. The combustion phasing (CA50) was then very early and the $PRR_{max}$ exceeded the limit of 10 bar/°CA set in the present work. Later, the additive fraction was used as parameter to control combustion phasing which was adjusted to meet the CoV limit [31]. To better compare syngas production with the different additives, the influence of the combustion phasing needs to be clarified first.

In a first experiment CA50 was varied by increasing $x_{DME}$ from the CoV limit at 10.7% to 12% ($\Phi_{DME} = 0.279$ and 0.317 respectively) while simultaneously decreasing the methane flow to keep the overall equivalence ratio $\Phi$ constant. The results in terms of syngas production are shown in Figure 35.

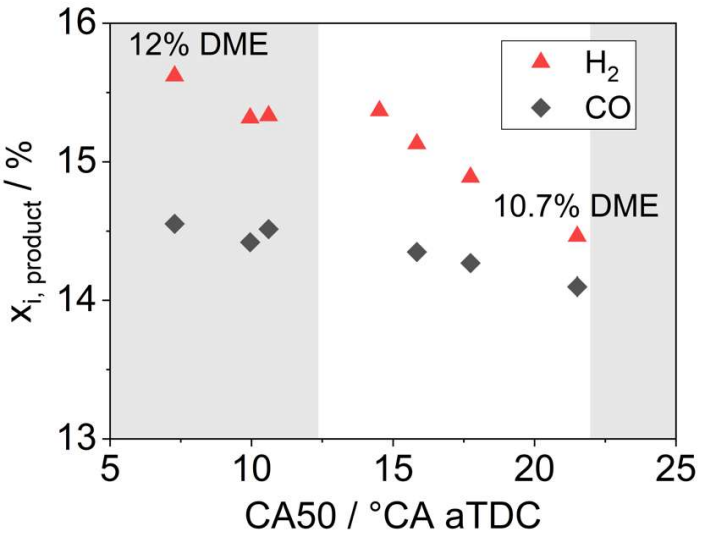


Figure 35: $H_2$ and CO mole fractions in the product gas for a variation of CA50 at constant $\Phi = 1.9$. The white region marks acceptable engine operation.

The pressure rise rate exceeds the limit if CA50 is reached at crank angles before 11° after TDC. The corresponding area in the graph is marked gray. The lowest $H_2$ and CO mole fractions are observed for the lowest DME fraction (i.e., at the stability limit) with CA50 = 22°CA. With earlier conversion, both $H_2$ and CO fractions increase nearly monotonically to maxima that are 1 and 0.5%-points, respectively, higher than the minima.

To exclude this influence of combustion phasing on the syngas fraction in the product gas we investigated the additive dependence of the syngas production at a constant CA50 of 15°CA. Figure 36 shows the methane conversion and the yields of $H_2$, CO, and $CO_2$.

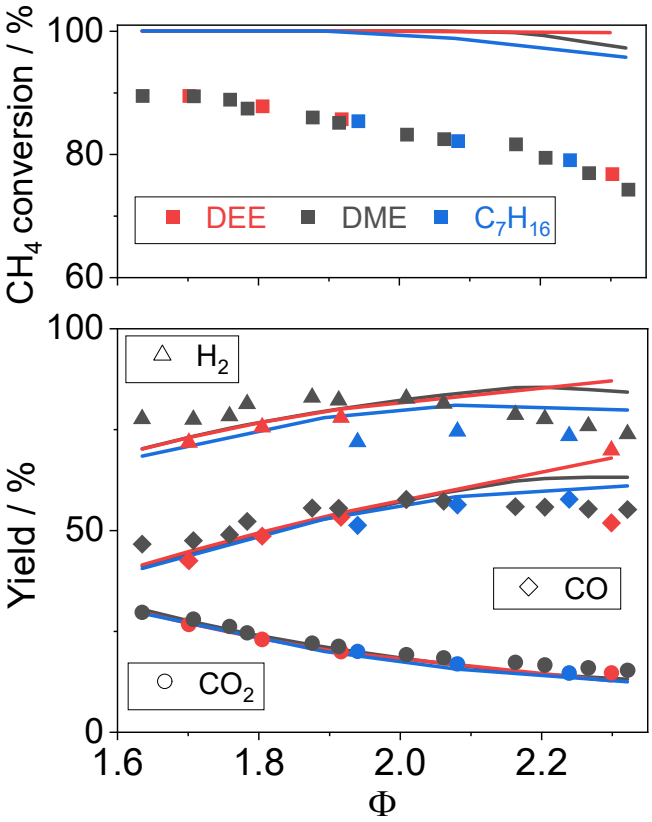


Figure 36: Methane conversion, $H_2$, CO, and $CO_2$ yields for different additives at constant CA50 = 15°CA. Symbols: experiment, lines: simulation.

Overall, we find that the choice of additive does not significantly influence any of the investigated conversion metrics. Generally, methane conversion decreases with increasing equivalence ratio, which can be attributed to the increasing lack of oxygen. The single-zone model does not capture effects like wall and crevice quenching. Thus, the methane conversion in the simulation is nearly complete for most conditions, while it is always less than 90% in the experiment. At equivalence ratios below 2 the simulated conversion is complete, slightly decreasing to 96% at $\Phi = 2.3$. In the experiment the maximum $H_2$ yield is found at around $\Phi = 1.9$ and the maximum CO yield at around $\Phi = 2.1$. At higher equivalence ratios the yields decrease, because of the decreasing methane conversion, which is probably because of lower process temperatures, while at lower equivalence ratios the complete combustion towards $CO_2$ and $H_2O$ becomes more important. The simulation most accurately captures the experimental trends when the methane conversion is high, at $\Phi < 2$. In addition to $H_2$, CO, and $CO_2$, traces of other species such as $C_2H_4$ are also produced, but these are only present in very small fractions (< 0.2 mol-% $C_2H_4$) in the investigated parameter range. In the current work that focusses on syngas production they are not relevant.

### 6.3.4 Temporal evolution of species concentrations

In HCCI combustion, the low temperature chemistry is very important, because it influences the auto-ignition characteristics. The heat release rates shown in Figure 34 indicated significant conversion at early crank angles, prior to ignition. To analyze the corresponding reactions, Figure 37 shows the mole fractions of fuel, additive, and some selected intermediate species for the three investigated additives.

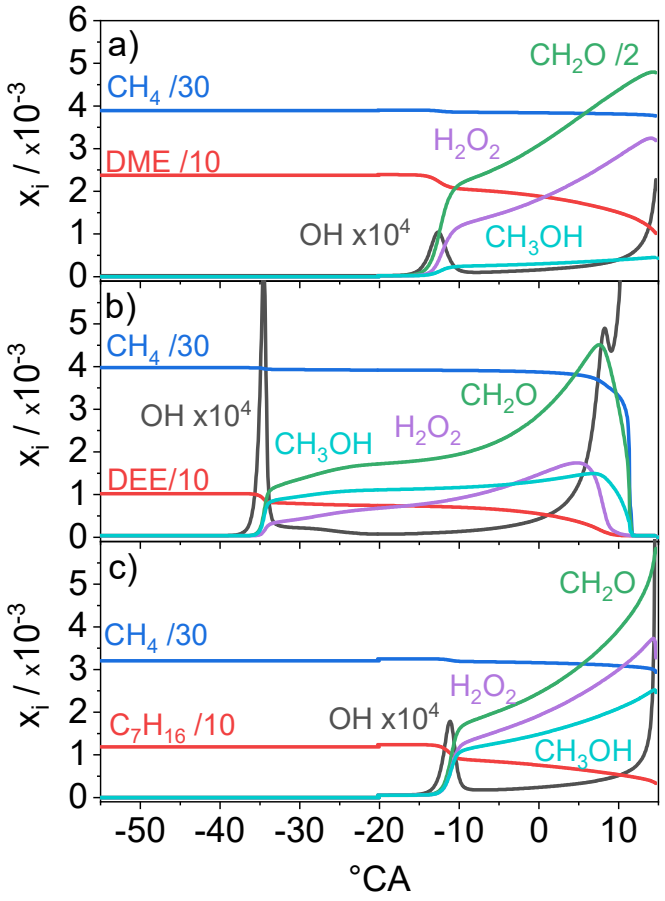


Figure 37: Species mole fractions as a function of crank angle for a) DME (16.9 mol%), $\Phi_{DME} = 0.659$, b) DEE (7.7 mol%, $\Phi_{DEE} = 0.36$), and c) *n*-heptane (11 mol%, $\Phi_{C7H16} = 0.774$). The conditions in the simulations are the same as for Figure 34.

The first reactions occur when the additives are partially converted. DEE reacts early at -40°CA at a temperature of 648 K and a pressure of 5.7 bar. In comparison, DME and *n*-heptane need higher temperatures and pressures of 781 K and 13.3 bar and 768 K and 13.1 bar, respectively, and thus react later at -16°CA. These reactions are mainly H abstraction from the additives which then lead to additional OH radicals, seen as peaks in Figure 37. These peaks coincide with the LTHR peaks from Figure 34. The H abstraction of DME yields $CH_3OCH_2$ and water, and the subsequent dissociation of $CH_3OCH_2$ provides further OH radicals and significant amounts of formaldehyde ($CH_2O$), as described by Kaczmarek et al. [82]. For DEE the most important reactions at low temperatures are

$$C_2H_5OC_2H_5 + OH = C_2H_5OC_2H_4s + H_2O \quad (39)$$

$$C_2H_5OC_2H_5 + OH = C_2H_5OC_2H_4p + H_2O \quad (40)$$

which is in accordance with the findings of Tang et al [90]. The most important reaction of *n*-heptane is the H abstraction reaction

$$n - C_7H_{16} + OH = n - C_7H_{15} + H_2O. \quad (41)$$

The dissociation of n-$C_7H_{15}$ leads to additional OH radicals. With further compression and thus increasing temperature the reaction speed decreases due to the NTC behavior of each additive as discussed in Section 1.2. For DEE, a second, minor NTC region is visible in the OH trace showing a local minimum at 9°CA, shortly before ignition.

In general, the oxidation of methane, initiated mainly by the OH radicals formed by the additives, leads to an increase in $CH_2O$, $H_2O_2$, and $CH_3OH$ concentrations. When the temperature and intermediate concentrations are high enough the ignition is induced by the dissociation of $H_2O_2$. The intermediate formation is similar for each additive since it is mainly dependent on methane oxidation kinetics. The only significant difference is the higher $CH_2O$ and lower methanol ($CH_3OH$) mole fractions when DME is used. The higher $CH_2O$ mole fractions can be explained by the DME low-temperature oxidation kinetics as discussed above. In the DME case methanol is mainly formed by

$$CH_3O + CH_3OCH_3 = CH_3OH + CH_3OCH_2. \quad (42)$$

This pathway competes with the H abstraction of DME that yields $CH_3OCH_2$ as well. The methanol-forming pathway is less favored. Similar competing pathways do not occur for DEE or *n*-heptane. For DEE, methanol is formed by interactions with $CH_3O$ and DEE, hydrogen, or formaldehyde:

$$CH_3O + CH_2O = CH_3OH + HCO \quad (43)$$

$$CH_3O + H_2 = CH_3OH + H \quad (44)$$

$$CH_3O + C_2H_5OC_2H_5 = C_2H_5OC_2H_4\ s/p + CH_3OH \quad (45)$$

The *n*-heptane oxidation shows a behavior analogous to DEE, except that interactions of $CH_3O$ with formaldehyde are not significant. The important reactions yielding methanol are eq. (44) and:

$$CH_3O + n-C_7H_{16} = CH_3O + n-C_7H_{15} \quad (46)$$

To conclude, all three additives initiate methane oxidation by OH radical formation and subsequent H abstraction of methane. Although there are differences in the amount of intermediate species that are formed before ignition, the most important pathways are similar and dominated by the methane kinetics.

## 6.4 Conclusions

The influence of DME, DEE and n-heptane as additives in fuel-rich HCCI combustion of methane was investigated in engine experiments and single-zone modeling. The additive fractions were varied for methane equivalence ratios between 1.2 and 1.9 to determine the stable operating ranges. The widest operating range in $\Phi_{add}$ and $x_{add}$ was achieved with DME as the additive. The choice of additive does not significantly influence the product composition, but it has a distinct influence on auto-ignition. In the engine context, not only the low temperature chemistry but also the additive's heat capacity determines the ignition-promoting effect and the stable operating range. In terms of mass and energy fraction, significantly more n-heptane than DME needs to be added to achieve similar results, because n-heptane's heat capacity is higher, lowering the temperature at the end of compression. At comparable mixture heat capacities, lower amounts of DEE than of DME lead to stable operation. Analysis of the heat release rates showed that DME and n-heptane behave similar before ignition. DEE, however, shows considerably less NTC behavior and more early heat release which may be the reason for its early $PRR_{max}$-limit.

A comparison of the reaction pathways and intermediate species formation for the three additives revealed important similarities and some minor differences. DME, DEE, and n-heptane have in common that they react early in the compression stroke and thereby lead to OH radical formation that initiates methane conversion by H-abstraction. The main intermediate species – $CH_2O$, $H_2O_2$, $CH_3OH$ – are the same, and besides the earlier reaction of DEE, the only significant difference are the two times higher $CH_2O$ and lower $CH_3OH$ concentrations when DME is used.

With respect to additive demand DEE is the most favorable additive. DEE needs to be used with the lowest additive mole fraction, mass fraction, and energy fraction. Compared to DME and n-heptane, DEE also leads to the earliest heat release, it has the second-lowest heat capacity after DME, and a weak NTC behavior. If the operating range is more important, DME may be preferred because with it the engine operates acceptably over a wider range of CA50.

# 7 Ozone as an ignition-promoter for fuel-rich HCCI operation

As shown in previous chapters, fuel-rich combustion of methane in a homogeneous charge compression ignition (HCCI) engine can be used as a polygeneration process producing work, heat, and useful chemicals like syngas. Due to the inertness of methane, additives like dimethyl ether (DME) are needed to achieve ignition at moderate inlet temperatures and to control combustion phasing. Because significant concentrations of DME are needed at 150 °C a considerable part of the fuel energy comes from DME, but this may be reduced with an additive like ozone. Here, a combined experimental and modelling study on the ignition of fuel-rich partial oxidation at $\Phi = 1.9$ of methane/air mixtures with ozone and DME as additives in an HCCI engine is conducted. Experimental results show that ozone is a suitable additive for fuel-rich HCCI reducing the amount of DME needed from 11.0% to 5.3% by adding only 75 ppm ozone. Since ozone does not survive until the end of the compression stroke, the reaction paths are analyzed in a single-zone model. The modelling shows that different ignition precursors or buffer molecules are formed, depending on the additives. If only DME is added, hydrogen peroxide ($H_2O_2$) and formaldehyde ($CH_2O$) are the most important intermediates, leading to OH formation and ignition around top dead center. With ozone addition, methyl hydroperoxide ($CH_3OOH$) becomes very important earlier in the compression stroke under these fuel-rich conditions. It is then later converted to $CH_2O$ and $H_2O_2$. Thus, ozone is a very effective additive not only for fuel-lean, but also for fuel-rich combustion. However, the mechanism differs between both regimes. Due to the reduction of expensive additives, ozone could help improving the economics of a polygeneration process with fuel-rich operated HCCI engines.

This chapter is slightly modified from [91]:

> D. Schröder, K. Banke, S.A. Kaiser, B. Atakan, The kinetics of methane ignition in fuel-rich HCCI engines: DME replacement by ozone, Proc Combust Inst, 38 (2020) 5567–5574, doi:10.1016/j.proci.2020.05.046.

The first author of this publication is Dominik Schröder. He performed simulations and reaction path analysis and the corresponding analysis and visualization of the data. He wrote the chapters “Buffer intermediates and reaction-path analysis” and “Simulation”, the conclusions and part of the introduction. My contributions include planning, setting up and performing the experiments, the processing, analysis, interpretation, and visualization of the experimental data, and writing the first paragraph of the introduction, the chapters “Experiment” and “Effect of ozone on combustion phasing”. Burak Atakan and Sebastian Kaiser were involved in the conceptual design and in writing and revising the manuscript.

## 7.1 Introduction

In the previous chapters it was shown that the partial oxidation of methane in an ICE can reach exergetic efficiencies of 81.5% if operated in homogeneous-charge compression-ignition (HCCI) mode. Since methane is relatively difficult to ignite, more reactive additives like n-heptane [8] or dimethylether (DME) [31] were used to achieve and control ignition at moderate compression ratios. However, it was found that for these experimental conditions a relatively high fraction of the fuel energy (about 15-20%) was then provided by the valuable additives. This runs counter the idea of using methane, i.e., natural gas, as an inexpensive and easily available base fuel, motivating the search for a more suitable additive. On-site produced ozone could be a possible solution. In *lean* HCCI combustion, following the pioneering work of Flynn [92], several researchers investigated ozone as an ignition-promoting additive [11,34,35,93–98]. Work at the University of Orleans (France) investigated various aspects of ozone addition in lean HCCI combustion. It was found that only 50 ppm of ozone in n-heptane HCCI combustion at $\Phi = 0.3$ shifted combustion phasing by 10°CA [10]. Enhanced reactivity was also found for ozone addition to other fuels, like iso-octane [35] and several alcohols [11]. Given these encouraging results in lean HCCI it seemed obvious to ask whether ozone may also promote ignition in fuel-*rich* methane HCCI. Thus, we conducted

experiments with different ozone fractions in fuel-rich methane/DME/air mixtures at $\Phi = 1.9$ (Some DME was needed because the experiments were performed at the rather low compression ratio of 10 [31]).

It is well known from literature on the oxidation in fuel-lean mixtures that ozone decomposes already at temperatures below 300°C to $O_2$ and O radicals. That means that in an engine's compression stroke, ozone itself probably does not survive long enough to still be present when the auto-ignition temperatures of methane are reached. Masurier et al. [99] showed that typical intermediate species in fuel-lean methane/propane/air mixtures are formaldehyde ($CH_2O$), hydrogen peroxide ($H_2O_2$), hydroperoxyl radicals ($HO_2$), and hydroxyl radicals (OH), and that those species are formed earlier when 10 ppm of ozone were added. Basevich et al. [100] investigated the auto-ignition of fuel-lean methane/air mixtures and the occurrence of a blue-luminescent preflame zone in which partial oxidation takes place before ignition. According to their work methyl hydroperoxide ($CH_3OOH$) and $H_2O_2$ are formed simultaneously. Subsequently they decompose and yield OH that accelerates the oxidation. In a plug-flow reactor, Kaczmarek et al. [101] showed that for methane/n-heptane/air/argon mixtures the reaction of methane with OH radicals is the most important reaction for methane consumption in fuel-rich mixtures ($\Phi = 2 – 20$). They also demonstrated for that methane/air mixtures at $\Phi = 8$ OH is formed along different paths depending on temperature: below 800 K this occurs mainly by the decomposition of $CH_3OOH$, while above 800 K $H_2O_2$ is the main precursor. Wang et al. [102] investigated the reforming of an iso-octane/n-heptane mixture in an HCCI engine at $\Phi = 1.4$ via simulations. They found that $CH_3OOH$, $H_2O_2$, and 1-hydroperoxyl propionaldehyde ($C_3H_6O_3$) were formed at temperatures below 740 K and were therefore regarded as important intermediates in low-temperature reactions. They subsequently used these species individually as additives in their engine model and found that each of them decreases the ignition delay time.

To summarize the relevant previous work, it is established that ozone strongly accelerates lean HCCI auto-ignition, but there appears to be a number of important intermediate species in the oxidation of alkanes that may be directly or indirectly influenced by the interaction of ozone and the various fuels. The objective of this work is to establish if ozone is an effective ignition promoter also in fuel-rich HCCI of methane, and – since we found that this is the case – to understand the ignition kinetics and the importance of different intermediate species.

## 7.2 Methods

### 7.2.1 Experiment

The experiments are performed in a four-stroke single-cylinder octane-number test engine modified to also operate with gaseous fuels. The experimental setup is basically identical to that used in our previous work [31] and therefore mainly the parts associated with ozone addition are described here. Ozone is produced via corona discharge in two different ozone generators (Innotec OGuA 5000 for fractions up to 250 ppm, Ozone Solutions TG-40 for up to 1700 ppm). The generators are fed with 2 slm pure oxygen. In addition, 7.6 slm $N_2$ are fed to the engine's intake to keep the $O_2/N_2$ ratio of air. The gases are mixed and then preheated to 150 °C just upstream of the intake. The cylinder pressure traces for each operating point were recorded and then averaged over 140 consecutive cycles. Table 7 shows the engine properties and operation conditions and Figure 38 illustrates a schematic of the instrumentation.

Table 7: Engine properties and operation conditions.

| Description | Symbol | Value | Unit |
|---|---|---|---|
| Rotational speed | $rpm$ | 595 | 1/min |
| Compression ratio | $\varepsilon$ | 10 | - |
| Bore | $d$ | 65 | mm |
| Stroke | $s$ | 100 | mm |
| Displacement | $D$ | 332 | cm³ |
| Fuel/air equivalence ratio | $\Phi$ | 1.9 | - |
| Intake temperature | $T_{in}$ | 150 | °C |
| Intake pressure | $p_{in}$ | 1 | bar |
| Coolant temperature | $T_C$ | 100 | °C |

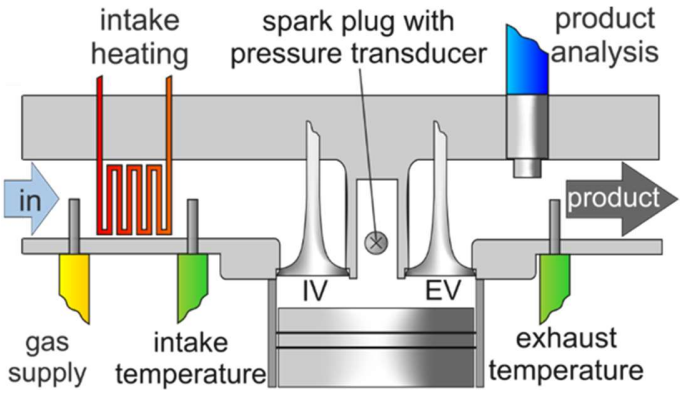


Figure 38: Schematic of the instrumentation (see also [31]).

### 7.2.2 Simulation

The model consists of a zero-dimensional single-zone reactor representing the reaction volume inside the cylinder including one inlet and one outlet valve for gas exchange. The engine is modeled in Python using the library Cantera [80] for describing the thermodynamics and reaction kinetics. We chose the engine parameters according to those of the engine experiments as shown in Table 7 with the piston movement given by the piston velocity equation of Heywood [23]. The crank angle convention in this paper assigns 0 °CA to compression TDC, i.e., crank angles before compression TDC are negative.

For the thermodynamics and reaction kinetics two reaction mechanisms are combined: the mechanism of Burke et al. [86] that includes 116 species and 710 reactions for methane/DME mixtures is expanded with the ozone mechanism of Zhao et al. [103]. For each timestep of 0.2 °CA, with the reactor volume changing due to the piston movement, Cantera solves the species and energy conservation equations. The heat transfer through the walls is modeled by the Woschni correlation [52] as in our previous work [31]. Since the gas-exchange strokes are now included, these strokes lead to an additional heat transfer through the walls during gas-exchange. The Woschni parameters were adjusted to reflect this. The residual gas leads to small changes in the simulation results for each work cycle. In stable operating conditions the results converge within three work cycles. For the analysis we simulate 10 cycles after convergence and average the results.

Since the aim of this work is to investigate ignition, the start of combustion in the experiment should be matched by the model. Here, CA20 (the crank angle at which 20% of the heat release has taken place) was chosen as a metric for ignition timing. Eq. (47) defines the heat release rate (HRR) in the engine model, which is then accumulated and peak-normalized to calculate CA20.

$$HRR(t) = V(t) \cdot R \cdot T(t) \cdot \sum_i \left( \frac{dh_{f,i}^o}{R \cdot T(t)} \cdot \dot{\omega}_i \right) \tag{47}$$

The HRR is dependent on the volume $V$ and temperature $T$ of the mixture, the ideal gas constant $R$, and the net production rates of each species $\dot{\omega}_i$ and their corresponding standard enthalpies of formation $dh_{f,i}^o$. The model is adjusted to match the experiment in two steps. First, we adjust the model compression ratio to 10.35, which is within the experimental uncertainty, such that the motored pressure trace from the model matches the experimental one. Then, for a DME/ozone mixture with 5.3 mol% DME and 75 ppm ozone we adjust the Woschni parameters and the initial temperature at the inlet such that CA20 matches that in the experiment. Figure 39 shows the sensitivity of the model's CA20 and temperature at TDC on the initial temperature.

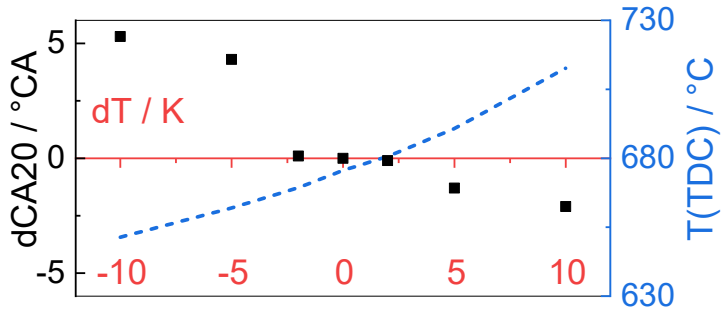


Figure 39: Change of CA20 (*dCA20*) and temperature at top dead center (TDC) as a function of the change in initial temperature (dT), illustrating the sensitivity of the combustion phasing on the initial temperature.

Temperature changes of ±10 K result in CA20 changes of -2.1 and 5.3 °CA, while the temperature at TDC changes by +37 K and -24 K, respectively. The in-cylinder temperature after intake valve closing cannot be measured and the model is not suitable to accurately account for the temperature change during the intake stroke, so there is a small initial temperature uncertainty. Reflecting these uncertainties, we thus adjusted the main parameters affecting the TDC temperature to match CA20 in experiment and simulation.

## 7.3 Results and discussion

### 7.3.1 Effect of ozone on combustion phasing

Figure 40 compares the cylinder pressure traces in experiment and simulation for three different ozone fractions (34, 47, 75 ppm) in the intake mixture at a constant DME fraction of 5.3% of the fuel and a constant $\Phi = 1.9$.

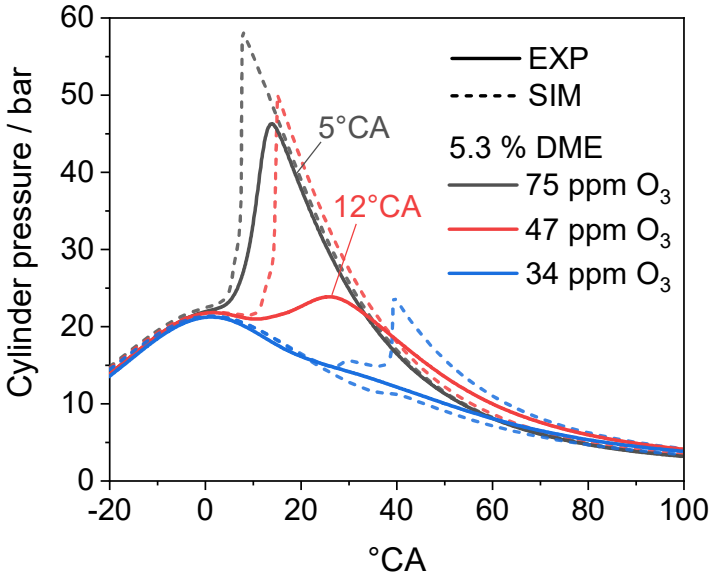


Figure 40: Cylinder pressure (bar) as a function of °CA for a constant DME mole fraction of 5.3% (in methane/DME) and changing ozone mole fractions of 75, 47 and 37 ppm (in methane/DME/air). Solid lines show experimental results, dashed lines show model results. Labels mark CA20 (not for unstable operation with 34 ppm).

In the model the Woschni parameters and the intake temperature were adjusted to match experimental and simulated CA20 for 75 ppm ozone to within 1°CA. For 47 ppm CA20 matched when the intake temperature was further increased by 2 K. We conclude that the model predicts the net effect of ozone addition on combustion phasing sufficiently well. With 34 ppm ozone, combustion becomes unstable in both experiment and simulation; in the experiment the coefficient of variation of the indicated mean effective pressure is 73%. The averaged experimental pressure trace shown in Figure 40 contains many misfires, while for the model two different cycles are shown, also demonstrating the strong cycle-to-cycle variations influenced by the residual gas from each previous cycle.

The more ozone is added, the earlier ignition occurs, resulting in higher maximum pressure and temperature in the cylinder. This can be seen in experiment and model. The model results show higher maximum pressures at earlier crank angles and higher pressure rise rates, typical for single-zone models [104]. Our previous work showed that this results in slight overprediction of the engine's work output, but has no significant influence on the product-gas composition [31]. This indicates that the model is suitable for analyzing the ignition and reaction kinetics in HCCI engines. The main result here is that in both experiment and model small amounts of ozone influence the ignition also for fuel-rich HCCI, as already known for lean HCCI [11–21]. The combustion can thus be controlled by adjusting the ozone content.

The efficacy of DME substitution by ozone was quantified systematically at $\Phi = 1.9$. DME was substituted by ozone while keeping CA50 at about 15 °CA. Without ozone, 11% DME in methane were needed for stable ignition. The DME-content of the fuel needed for stable operation in experiment and simulation could be systematically reduced by ozone addition. The results are shown in Figure 41.

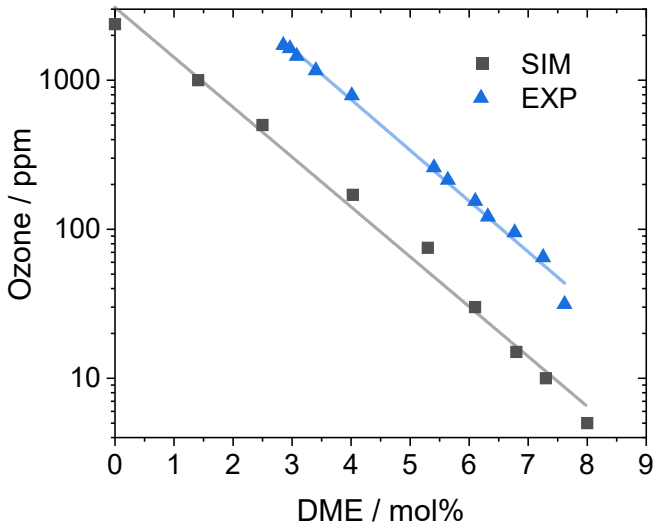


Figure 41: Ozone mole fraction in ppm (of methane/DME/air mixture) as a function of DME mole fraction (in mol% of methane/DME mixture) needed for a constant CA50. Blue triangles show experimental results, grey squares show model results.

The trends in experiment and simulation agree well: small amounts of ozone substitute large amounts of DME, but the effect exponentially decreases with increasing $O_3$ fraction. The simulation predicts a stronger effect of ozone addition in that more DME may be substituted by smaller amounts of ozone in the model compared to the experiment while holding the combustion phasing constant. The fuel energy (lower heating value) provided by DME to the overall fuel energy ($CH_4$ + DME) is 17% for the case with 11% DME without $O_3$. By adding just 64 ppm $O_3$, the energy contribution of DME is reduced to 12%, while the ozone generator needs less than 1% of this energy.

### 7.3.2 Buffer intermediates and reaction-path analysis

To understand the mechanism of this DME substitution by ozone, we first investigate the mole fractions of the major intermediates before ignition, then reaction-path analyses at certain important crank angles are carried out to gain further mechanistic insight. For this we start with pure ozone addition to methane, which was not studied experimentally, because at the relatively low compression ratio (10) of the current study the necessary ozone concentrations exceeded the capacity of our ozone generator. Then, further cases both with only DME addition and with both additives will be compared.

Figure 42 shows the mole fractions for 2380 ppm $O_3$ as single additive (corresponding to the simulated 0% DME case in Figure 41).

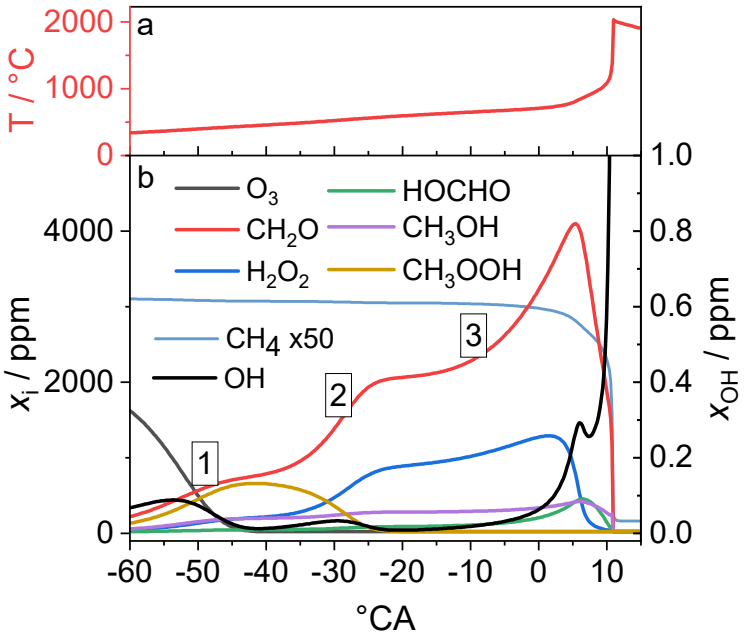


Figure 42: (a) Temperature and (b) mole fractions of the most important intermediates, OH radicals and methane as a function of crank angle.

Significant decomposition of ozone into oxygen molecules and oxygen radicals starts at -100°CA and a temperature of 220°C. At -60°CA around 30% of the initial ozone amount is consumed. At this time the formation of reactive intermediates begins, but larger amounts are not present. At -40°CA ozone is completely decomposed and thus it is not a reactant at ignition. The mole fractions of the intermediates O and OH at that CA are negligibly small. The effect of ozone on ignition must therefore be an indirect effect of the oxygen radicals generated from ozone decomposition. The main intermediate species that are formed and subsequently consumed again between the start of the ozone decomposition and the ignition of the mixture are in decreasing order of their maximum mole fractions: formaldehyde ($CH_2O$), hydrogen peroxide ($H_2O_2$), methyl hydroperoxide ($CH_3OOH$), formic acid (HOCHO), and methanol ($CH_3OH$). $CH_3OOH$ is the only intermediate species that is formed in larger quantities and does not remain in the mixture until ignition. The $CH_2O$ and $H_2O_2$ mole fractions increase in three distinct steps until the temperature is high enough for ignition (about 1050 K in this case). The three steps are at -50°CA, -30°CA, and -11°CA as labeled in Figure 42. Reaction-path analyses were carried out for these crank angles. They are illustrated in Figure 43.

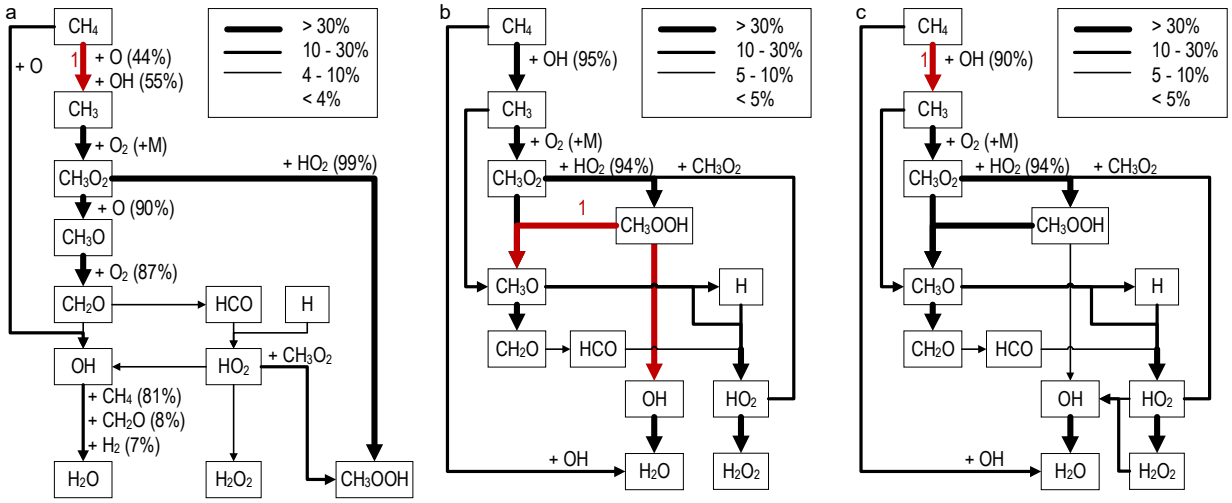


Figure 43: Reaction paths for the most important species containing H-atoms. Red arrows illustrate the highest mole flows (kmol/m³s). The mole flows are divided by the highest mole flow (indicated by 1) and the ratio is illustrated by the line thickness. a) step 1 (-50°CA, T = 390 °C, p = 5.1 bar); b) step 2 (-30°CA, T = 515 °C, p = 10.3 bar); c) step 3 (-11°CA, T = 643 °C, p = 19.4 bar)

*Step 1: ozone decomposition*

Figure 43 a) illustrates the most important reaction pathways for H-atoms at -50°CA. Oxygen radicals abstract hydrogen from methane and thus $CH_3$ and OH radicals are formed. $CH_3$ and its oxidation products undergo several reactions with molecular and atomic oxygen, which end in the formation of $CH_2O$, $HO_2$, and $CH_3OOH$. $CH_2O$ and $CH_3OOH$ do not react further in this temperature range, and $HO_2$ forms $H_2O_2$, then $CH_3OOH$, and then OH radicals. The OH radicals also abstract hydrogen from methane and lead to the formation of water. These reactions take place as long as ozone is present and provides oxygen radicals. This explains the first strong increase in $CH_2O$, $H_2O_2$, and $CH_3OOH$ concentrations. As the concentration of ozone in the mixture is low, methane conversion and temperature increase due to exothermal reactions are but both very small at this time.

*Step 2: methyl hydroperoxide decomposition*

Figure 43 b) shows the most important reaction pathways for H-atoms at -30 °CA and thus the importance of the $CH_3OOH$ decomposition. Due to ongoing compression and the heat release of the reaction, the temperature of the mixture is increasing. At approximately 440°C and -40°CA a threshold is reached at which $CH_3OOH$ decomposes to $CH_3O$ and OH radicals. Consistent with the findings of Kaczmarek et al. [101] this is the main source for OH radicals under such conditions. Molecular oxygen reacts with $CH_3O$ and forms $HO_2$ (and then $H_2O_2$) and $CH_2O$. Additionally, OH radicals abstract hydrogen from methane and this also leads to the formation of $CH_2O$ and $H_2O_2$ via $CH_3OOH$. The latter is therefore a key species for the ongoing conversion of methane and the formation of $CH_2O$ and $H_2O_2$. The increase of $CH_2O$ and $H_2O_2$ formation is thus higher if $CH_3OOH$ is present, which explains the second step in the species profiles.

*Step 3: reaction of formaldehyde and hydrogen peroxide*

The most important reaction pathways for H-atoms at -11°CA are shown in Figure 43 c). The conversion of $H_2O_2$ starts earlier than the conversion of $CH_2O$, as can be seen in Figure 42. With the additional OH radicals the hydrogen abstraction from methane, comparable to step 2, is accelerated further leading then to more $CH_3OOH$ that decomposes as well. The additional $CH_3$ radicals increase the conversion of $CH_2O$ via $HO_2$ to $H_2O_2$ and then lead to more OH radicals.

With increasing temperature, $CH_2O$ is increasingly converted with H radicals to HCO and $H_2$ or with OH radicals to $H_2O$ and HCO. HCO increases the formation of $H_2O_2$ via $HO_2$ and then OH radicals as well. At 5°CA a temperature of 780 °C is reached and $H_2O_2$ decomposes to OH radicals. This finally leads to conditions in which

the OH concentration is high enough to convert a considerable amount of methane whereby the temperature quickly rises and ignition occurs.

The ozone decomposition indirectly accelerates the formation of OH radicals and thus increases the temperature during the late compression stroke. The effectiveness as an additive for ignition depends on a chain of buffer molecules, $CH_3OOH$, $CH_2O$, and $H_2O_2$ all with different thermal stability. In the model, also other "virtual additives" were tested: If instead of ozone the intermediate species $CH_2O$, $H_2O_2$, and $CH_3OOH$ are added separately with initial mole fractions according to their maximum mole fractions before ignition in the case with 2380 ppm ozone, ignition does not occur. The reason is that although $CH_3OOH$ decomposes and OH radicals are present, the temperature increase in the first step (ozone decomposition and $CH_3OOH$ formation) is missing. The temperature necessary for the decomposition of $CH_3OOH$ is reached much later, at -12°CA instead of -40°CA, and this leads to a temperature at TDC that is about 100 K lower – too low for ignition. When more (1775 ppm) of $CH_3OOH$ are used, the same CA20 as for the case with 2380 ppm ozone is observed and the pressure and temperature traces are nearly identical, showing the great importance of $CH_3OOH$ as a buffer molecule or precursor for ignition in the partial oxidation of methane/air/ozone mixtures. Additional $CH_2O$ or $H_2O_2$ are not necessary in this case; these intermediates are formed from $CH_3OOH$ as described above.

Figure 44 illustrates the mole fractions as a function of crank angle after TDC for two cases, a) 12.2 mol% DME and b) the experimentally investigated mixture of 5.3 mol% DME and 75 ppm ozone.

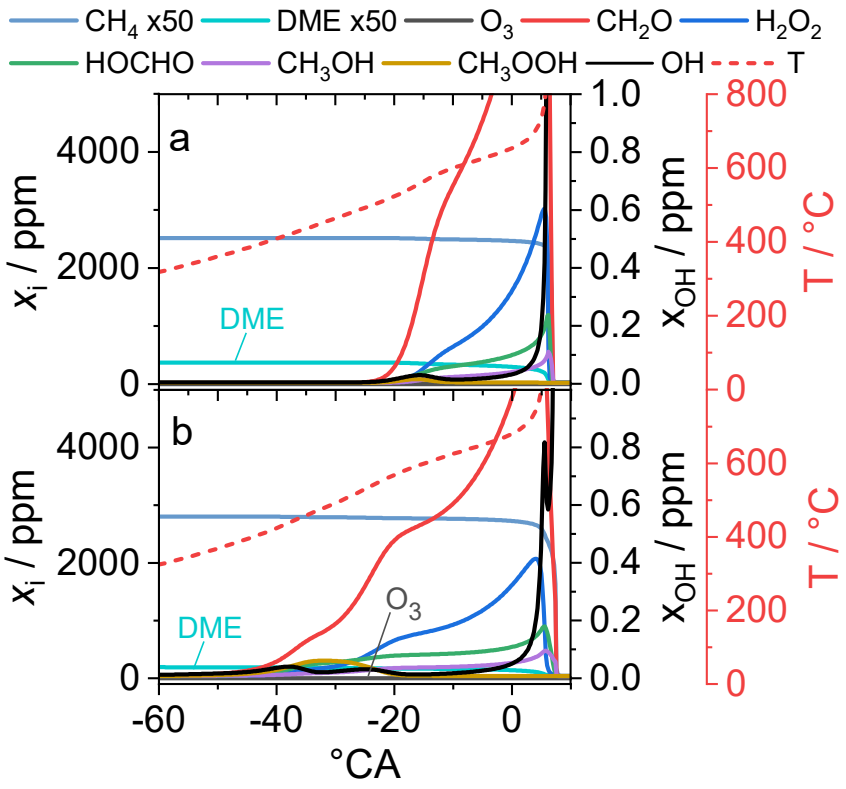


Figure 44: Mole fractions and temperature as a function of crank angle. a)12.2 mol% DME, b) the experimentally investigated mixture of 5.3 mol% DME and 75 ppm ozone.

In case (a) with 12.2% DME as the only additive the maximum mole fractions of $CH_2O$ and $H_2O_2$ are much higher than with ozone as a single additive and their formation is delayed. About 59% of the initial DME is still present at TDC in case (a). With DME as the only additive, the role of $CH_3OOH$ is minor, because it is not a product of the low temperature DME chemistry. Now mainly $CH_2O$ (and $H_2O_2$ from $CH_2O$) and OH radicals are formed. Additionally, DME decomposes at higher temperatures than ozone. A second effect hindering an earlier ignition

with DME is the higher molar heat capacity. With 12.2 mol% of DME in the methane/DME mixture the molar heat capacity increases by 4.4% compared to neat methane which reduces the temperature increase during compression. For ignition, much more DME is thus needed than it would have been the case without this increase of molar heat capacity.

If small amounts of ozone, e.g. 75 ppm are added to the DME, as is shown as case b), $CH_3OOH$ is formed at earlier crank angles; also formaldehyde is formed earlier. Again, the $CH_3OOH$ decomposition leads to $H_2O_2$ formation and both provide the OH radicals needed for ignition. The amount of ozone is not high enough to convert DME completely, but a multi-step reaction appears again.

## 7.4 Conclusions

Ozone is also in the fuel-rich regime an effective ignition-promoting additive in HCCI engines. This was shown experimentally for the first time here for methane/DME fuel mixtures. At the given compression ratio of our HCCI engine, it could not replace DME totally, but reduce the needed DME amount considerably. With this, the energy provided by DME to the fuel mixture can be reduced considerably as well. The modelling provided some insight to the mechanism of this process. From the general kinetics of ozone decomposition it was clear that ozone does not survive the compression process. A more detailed analysis showed that reactions of the decomposition products of ozone with methane lead to the formation of two buffer molecules early in the compression stroke. Under the fuel-rich conditions explored here, these are $CH_3OOH$ and $CH_2O$. The former is converted prior to ignition into $H_2O_2$ and more $CH_2O$, which are also the main intermediates from ozone in fuel-lean HCCI. Without such buffer molecules that survive to relatively high temperatures and then form reactive radicals, ozone would not affect the ignition process. In future work, higher compression ratios will be investigated to reduce the amount of additives needed for ignition further. The use of ozone as a single additive at high compression ratios appears feasible.

# 8 Autothermal reforming in a piston engine

This chapter investigates the fuel-rich combustion of $CH_4/CO_2/O_2$ mixtures in a piston engine. The focus of the experiments is to determine suitable operating parameters in terms of stable engine operation, syngas production, $CO_2$ conversion, and avoiding soot emissions. In particular, the spark timing, $CO_2$ intake mole fraction, equivalence ratio, and compression ratio were varied. Results show stable spark-ignition operation over a wide range of the investigated parameters at a compression ratio of 10. Acceptable operation could be achieved within the spark timing limits of -38° to 10 °CA after top dead center, 7 to 27% $CO_2$ in the inlet and equivalence ratios from 2 to 2.5. A maximum $H_2$ yield of 62% could be achieved at an equivalence ratio of 1.9 and a $CO_2$ intake mole fraction of 4% at a compression ratio of 4.5. Spark time advancing from -10 to -38°CA enhanced the dry reforming reaction and increased the hydrogen yield per methane from 38 to 45%. A significant influence of compression ratio on the amount of soot in the product gas was observed, showing that higher compression ratios increase soot formation.

This chapter is slightly modified from [105]:

> K. Banke, S.A. Kaiser, Syngas production from biogas in a polygeneration process: Simultaneous partial oxidation and dry reforming in a piston engine, Proc. Combust. Inst., 39 (2023) 5011–5020, doi:10.1016/j.proci.2022.08.132.

My contributions include planning, setting up and performing the experiments, the processing, analysis, interpretation, and visualization of the experimental data, and writing the first draft of the manuscript. Sebastian Kaiser was involved in the conceptual design of the study and in reviewing and writing the manuscript.

## 8.1 Introduction

With increasing use of renewables that are not available on demand, a growing concern in energy conversion is the need for flexibility. Usually, power production and chemical conversion are separate, steady-state processes, running at fixed, optimized conditions. Combining the production of several, useful outputs in one single process – "polygeneration"– could provide high exergetic efficiencies and flexibility at the same time. Established polygeneration couples processes for power production and material conversion, each optimized separately and then linked without much flexibility, e.g. in steel production plants [27]. For some applications, more flexibility may be achieved by conducting such a polygeneration process in a piston engine and switching between increased power or syngas production [30].

Methane reforming is the most used industrial process for the production of hydrogen and syngas (hydrogen and carbon monoxide) [106]. In most cases steam is used as reforming agent. The net reaction of such "steam reforming" (SR) is given by eq. (48). It yields syngas with high $H_2$/CO ratios (often around 3 or 4). "Dry reforming" (DR, eq. (49)) uses $CO_2$ as the reforming agent. The use of $CO_2$ as an educt is increasingly seen as an attractive feature of this process. DR is especially interesting for applications that require syngas with a low $H_2$/CO ratio like Fischer-Tropsch or methanol synthesis [107,108]. Both, the SR and the DR processes are highly endothermic, and generally catalysts are used to decrease the temperatures needed for conversion. For DR expensive noble metal catalysts like palladium can be used, but usually less expensive ones like nickel or cobalt are favored although they have a greater tendency for deactivation by coking or oxidation [109–111].

$$CH_4 + H_2O \leftrightarrow CO + 3H_2, \Delta H = 206\frac{kJ}{mol} \tag{48}$$

$$CH_4 + CO_2 \leftrightarrow 2CO + 2H_2, \Delta H = 260 \frac{kJ}{mol} \quad (49)$$

$$CH_4 + 0.5O_2 \leftrightarrow CO + 2H_2, \Delta H = -71 \frac{kJ}{mol} \quad (50)$$

Another method of producing syngas is the partial oxidation (POX) of methane, as given by eq. (50). It uses less complex reactors and does not need a catalyst [112]. In this process a fuel-rich mixture reacts exothermically to produce hydrogen and carbon monoxide. Since oxygen is present, complete oxidation to the products $H_2O$ and $CO_2$ will also occur to a certain extent. The hydrogen yield per methane is much lower for partial oxidation than for steam reforming. Often, partial oxidation is combined with SR or DR. In this case the partial oxidation can provide the enthalpy needed for the reforming reaction. This is also called "autothermal reforming" (ATR). ATR is not as widely used as SR. It yields lower $H_2$/CO ratio syngas and is limited by soot formation [14,113]. However, ATR could potentially decrease the cost of syngas production in a Fischer-Tropsch process [114].

Several approaches for syngas production in piston engines have been investigated. They are based on the combustion of very fuel-rich methane-based mixtures, which tend to have low reactivity. A challenge with those mixtures is stable engine operation, since it can be hard to reach sufficient conversion with low-reactivity mixtures. Szeszich et al. used spark ignition with a compression ratio of $\varepsilon = 4.5$ and an intake mixture of methane and undiluted oxygen at equivalence ratios in the range of $\Phi = 2.5$ to 2.8 [4]. The resulting exhaust gas contained up to 95% syngas after drying. The soot limit was between $\Phi = 2.5$ and 2.6. Karim et al. investigated fuel-rich compression-ignition with pilot-fuel injection [7,36]. The intake air was enriched with variable amounts of oxygen to ensure stable operation. They reported syngas fractions of up to 80% in the dry exhaust. McMillian and Lawson investigated the partial oxidation of natural gas / air mixtures with equivalence ratios up to $\Phi = 1.6$ in spark ignition mode at a compression ratio of $\varepsilon = 13.3$ [5]. They found the operating stability limit at about a maximum $\Phi = 1.6$ with about 11% $H_2$ in the dry exhaust. Lim et al. worked to extend the operating range in spark-ignition mode to equivalence ratios useful for syngas production by strong preheating, spark time advancing, and hydrogen enrichment of the feedstock [6]. With intake temperatures of 480°C and early spark timings between 45-30° CA before top dead center (bTDC) they achieved cycle-to-cycle variability of under 20% at equivalence ratios of $\Phi = 2$. Yang et al. conducted partial oxidation in HCCI mode in a modified diesel engine with compression ratio 18 at equivalence ratios between $\Phi = 3.1$ and 9.1 [37]. They also varied the $O_2$ and $CO_2$ fraction in the mixture and achieved maximum syngas fractions of ~ 41%. Another approach that was studied by Alger et al. is the fue-rich in-cylinder reforming in a dedicated cylinder with exhaust gas recirculation (D-EGR) to the remaining cylinders of a spark ignition engine [115,116]. They found an increase in efficiency and a decrease in pollutant formation by using this approach. The same approach was investigated by Zhu et al. in a natural gas engine [38,117,118] where it lead to accelerated combustion, increased efficiency and decreased pollutant emissions. Simulations of in-cylinder reforming in a HCCI engine were carried out by Zhou et al. [119] who found a retarding effect of the reformate on the HCCI-combustion, providing a possible control parameter. A comprehensive review on reforming in internal combustion engines was given recently by Tartakovsky and Sheintuch [39].

In our own work we demonstrated the partial oxidation of fuel-rich methane-based mixtures with homogeneous charge compression-ignition (HCCI) at compression ratios of $\varepsilon = 10$ and with intake temperatures of 150°C or less, using DME, n-heptane, and ozone as reactive fuel additives to control combustion phasing [8,31,91]. The HCCI mode extended the operating range to $\Phi > 2.8$, which is more favorable for syngas production. However, the soot limit was around $\Phi = 2.0$.

Generally, the nitrogen in the air dilutes the chemically active part of the charge. This limits the maximum in-cylinder pressure, temperature, and especially the pressure rise rates. However, fuel-rich methane mixtures have high heat capacity and low laminar flame speeds [120]. Diluting the mixture with $CO_2$ (for example as found in biogas) exacerbates these issues. This then makes oxygen enrichment reasonable, because the heat release rate is limited anyway in fuel-rich combustion, and increasing the oxygen fraction increases the mixture reactivity. Since the enthalpy needed for the dry reforming is provided by partial oxidation, this may be regarded as ATR in a piston

engine. Such a process was already investigated in experiments in a rapid compression machine (RCM) by Gossler et al. [121]. Using simulations and optimization methods, they found operating points with $CO_2$ conversions of over 50% and confirmed the results in experiments.

Here, we extend that previous work to a reciprocating engine. To that end, our experiments investigate the operating stability, syngas production, soot production, and fuel conversion in an internal combustion engine operated on fuel-rich $CH_4/CO_2/O_2$ mixtures.

## 8.2 Methods

### 8.2.1 Engine and instrumentation

The experiments were conducted the modified single-cylinder BASF-type octane-number research engine described in more detail in chapter 3. The intake temperature was $T_{in}$ = 48°C, and the intake pressure was ambient pressure ($p_{in}$ = 1 bar). Figure 45 shows a schematic of the engine instrumentation.

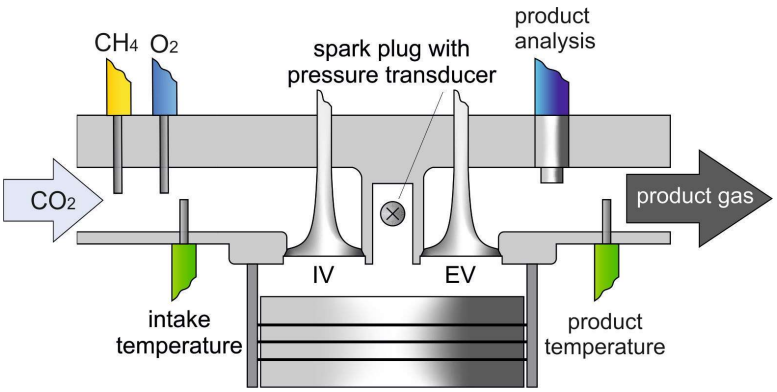


Figure 45: Schematic of the engine instrumentation. Distances in the flow direction are not to scale.

The intake flows were controlled by mass flow controllers (MFC). The $CO_2$ stream was led through a 300 L plenum to balance the pressure fluctuations in the engine intake, and $CH_4$ and oxygen were then added about 50 cm upstream of the intake port. The product gas composition ($H_2$, $CH_4$, CO, $CO_2$) was detected by a commercial exhaust gas analyzer (ABB Advance Optima 2020), while the filter smoke number (FSN) was measured by an AVL smoke meter. To measure the exhaust composition the engine was run in one operating point until the composition was stable.

The pressure data were collected with 0.1°CA resolution by a spark-plug integrated pressure transducer. Based on 140 recorded consecutive cycles, the average indicated mean effective pressure (IMEP), its coefficient of variation (CoV), and the mean of the maximum pressure rise rate ($PRR_{max}$) were calculated. As criterion for stable engine operation a CoV limit of 10% was set. To limit the mechanical stress to the engine a limit for acceptable operation was set at a $PRR_{max}$ of 10 bar/°CA.

### 8.2.2 Experiments

For most experiments, the compression ratio was $\varepsilon$ = 10. A spark timing of -10°CA after top dead center (aTDC), an intake $CO_2$ fraction $x_{CO2,\,in}$ = 20%, and an equivalence ratio $\Phi$ = 2.3 are taken as the reference condition here. Each of these three parameters was varied systematically, keeping the other two constant at their reference value. The spark timing was advanced from -10°CA to -38°CA in 5° increments (apart from the last step), and then

retarded in 5°CA increments from -10°CA to 15°CA. The volume flow of $CO_2$ was varied in increments of 4 standard liter per minute (slm), resulting in 6-7%-points increments in $x_{CO2,\,in}$ within a span of 0 - 33%. The equivalence ratio was varied from $\Phi = 1.9$ to about 2.5. In addition to these three systematic variations, some experiments were done with different compression ratios, but since the other parameters could then not always be kept constant while maintaining stable operation, a systematic variation of this parameter is not included. Nevertheless, these single operating points yielded some interesting results that are included here. Table 8 shows the varied parameter range and reference parameters.

Table 8: Range of parameter variation and reference parameters. Spark timing (ST), $CO_2$ intake mole fraction $x_{CO2,\,in}$, equivalence ratio $\Phi$ and compression ratio $\varepsilon$.

| | ST | $x_{CO2,\,in}$ | $\Phi$ | $\varepsilon$ |
|---|---|---|---|---|
| Varied range | -38 – +15°CA | 0 – 33 % | 1.9 – 2.5 | 4.5 – 13.5 |
| Ref. | -10°CA | 20% | 2.3 | 10 |

## 8.3 Results and discussion

### 8.3.1 Cylinder pressure and operating stability

An important issue in operating a piston engine is how the cylinder pressure behaves, because excessive maximum pressures or pressure rise rates are mechanically harmful for the engine, while low values cycle-to-cycle variations and low thermodynamic efficiency. Figure 46 shows the pressure traces for the three major parameter variations.

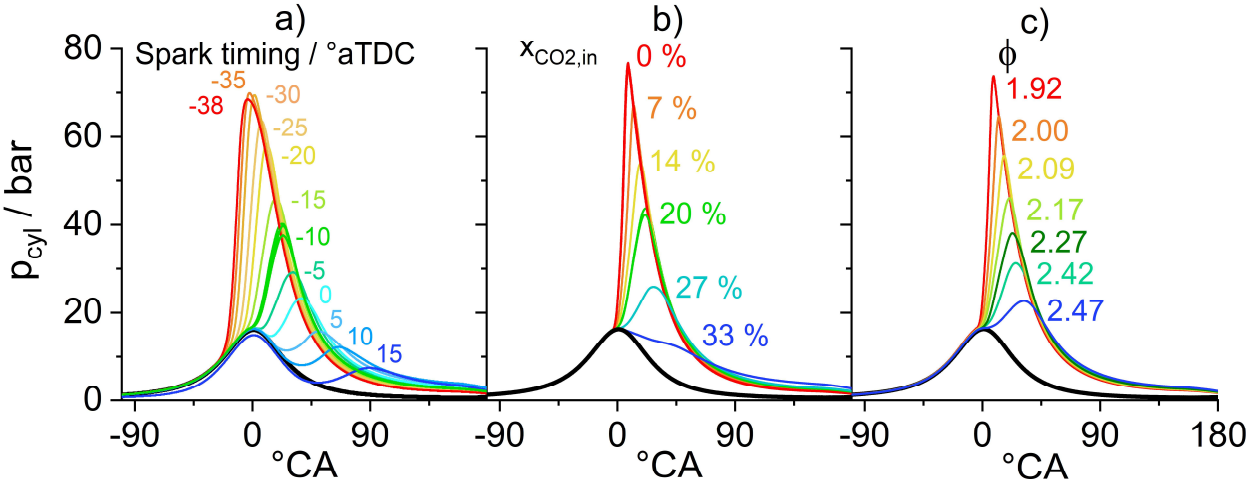


Figure 46: In-cylinder pressure traces for variation in a) spark timing, b) intake mole fraction of $CO_2$, and c) equivalence ratio. The black line represents a motored pressure trace with the reference intake composition ($\Phi = 2.3$, $x_{CO2,\,in} = 20\%$).

In Figure 46 a) the pressure traces for a variation in spark timing show an increase in peak pressure from around 40 bar in the reference case (-10°CA) to about 70 bar maximum pressure for -35°CA spark timing. Even with this spark timing knocking does not occur. Advancing the spark timing further to -38°CA leads to decreasing peak pressure because the increase in heat losses cannot be compensated anymore by the increase in heat release before

TDC. Retarding the spark timing beyond 5°CA decreases the peak pressures to values below the motored TDC pressure, but combustion still occurs. Varying $x_{CO2,\,in}$ results in similar changes of the maximum cylinder pressure, as can be seen in Figure 46 b). For the $CO_2$-free case of $x_{CO2,\,in} = 0\%$ the peak pressure is around 75 bar. Combustion is stable up to $CO_2$ intake mole fractions of 27%. The differences in the pressure trace here originate from those in laminar flame speed and heat capacity of the mixture. Similar results can be seen in Figure 46 c) for varying the equivalence ratio. Again, this shift in combustion phasing is caused by changes in laminar flame speed and heat capacity.

Figure 47 shows the locally averaged cylinder temperature $T_{cyl}$ and the specific heat capacity ratio γ over the crank angle for the same experiments as in Figure 46.

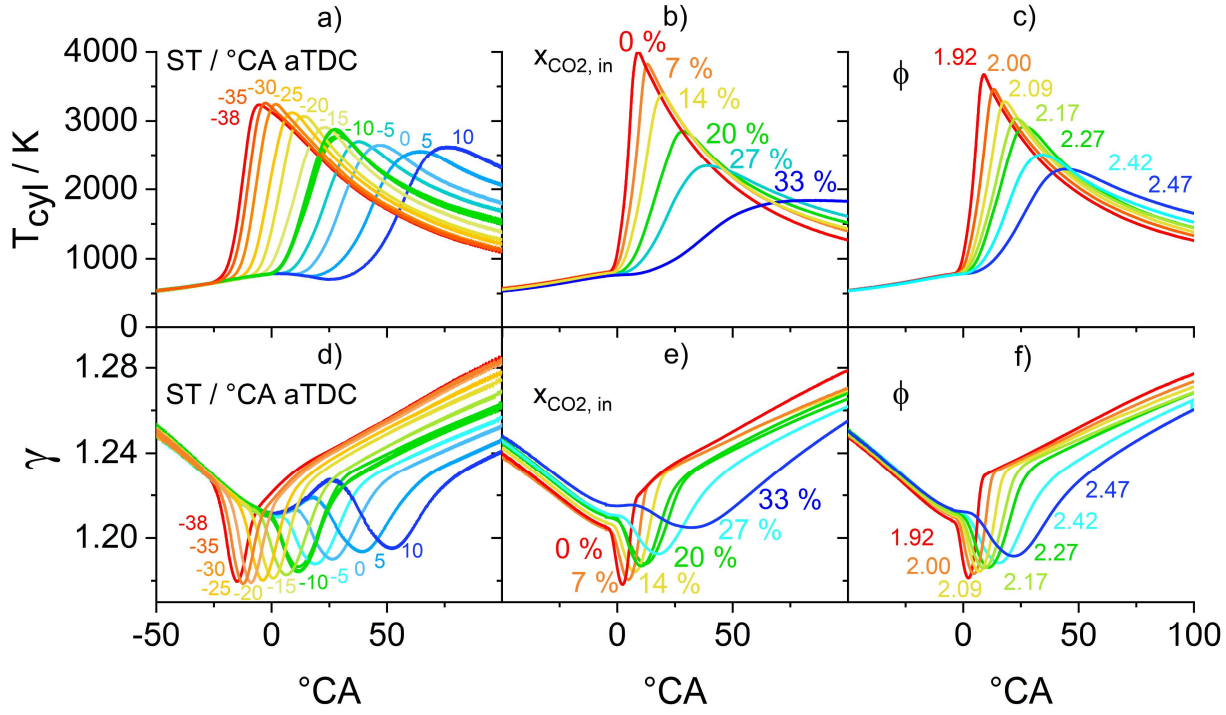


Figure 47: Locally averaged cylinder temperature $T_{cyl}$ and specific heat capacity ratio γ over crank angle for variation in spark timing (ST), $CO_2$ inlet mole fraction $x_{CO2,\,in}$, and equivalence ratio Φ.

The heat capacity ratio γ was calculated using a two-zone model. Two different γ, one for the intake composition and one for the exhaust composition were calculated crank angle (temperature and pressure) dependent using the chemical toolbox "Cantera" for python. Then a combined gamma was calculated by weighting the two using the mass burn function (MBF). Such an approach is described in detail in [24]. The temperature $T_{cyl}$ was calculated using the ideal gas law with the measured averaged pressure traces from Figure 46, the heat capacity ratio of the mixture and the cylinder volume calculated from the engine kinematics.

While in Figure 47 a) a shift in spark timing from -35 to 5°CA reduces the maximum $T_{cyl}$ by around 1000 K a much more drastic effect of the temperature can be seen for the $CO_2$ variation in Figure 47 b). In this case the temperature maximum of 4000 K is reduced to below 2000 K when 33% $CO_2$ is added. The strong reduction can be explained by the higher heat capacity of $CO_2$ as can be seen in Figure 47 e) and also by dilution of the more reactive part of the mixture through the $CO_2$. The temperature decrease for increasing equivalence ratios in Figure 47 c) is similar to the $x_{CO2,\,in}$ variation but less pronounced. The main reason for this is the smaller difference in heat capacity of the different mixtures which can be seen in Figure 47 f).

Figure 48 shows the pressure-based metrics IMEP, CoV and $PRR_{max}$. For the variation of spark timing shown in Figure 48 a) the engine operation is stable with CoV < 10% for all operating points but the most retarded one, 15°CA aTDC. This point shows high cyclic variation with 50% CoV. With early ignition $PRR_{max}$ increases up to 7 bar/°CA. The pressure increases faster with early spark timing because the same heat is released at lower cylinder volume. $PRR_{max}$ does not exceed the limit of 10 bar/°CA in any of the operating points.

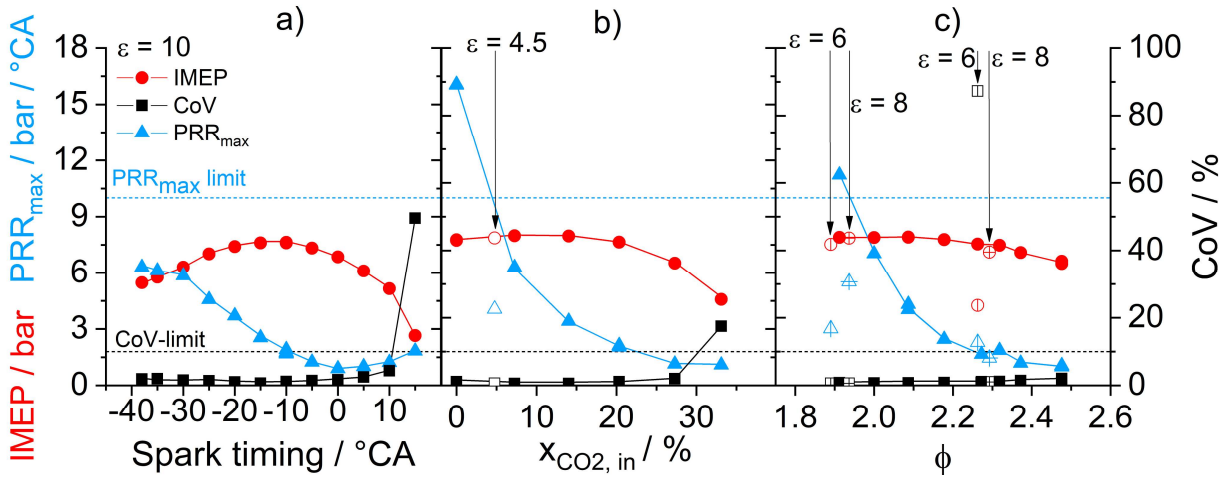


Figure 48: Engine operating parameters for variation in a) spark timing, b) mole fraction of $CO_2$ in the intake mixture and c) equivalence ratio. Dashed lines represent the limits for acceptable operation with less than 10 bar / °CA in $PRR_{max}$ and 10% in the CoV.

This suggests that the mixture's heat capacity is high enough to sufficiently attenuate the pressure rise even for very early combustion. The maximum IMEP of about 8 bar is (by coincidence) at the reference timing of -10°CA. For early spark timings IMEP decreases because of the increasing heat losses, which are unusually large in this knock-testing engine that was never designed for power generation and good efficiency. For later spark timing the IMEP decreases because of heat release at lower maximum pressures and the resulting lower thermal efficiency, and additionally for the latest spark timing because of misfires.

Varying $x_{CO2,\,in}$ (Figure 48 b)), the CoV shows stable operation for compositions except for $x_{CO2,\,in}$ = 33%. In this case the flame speed of the mixture is too slow to ensure sufficient combustion before the expanding volume quenches the reaction. The IMEP is at its maximum at 7 and 14% $CO_2$ in the intake and decreases with less $CO_2$ because of the increased heat losses with early combustion. For higher $CO_2$ intake fractions, it decreases due to the decreasing efficiency and the decreased overall chemical energy in the cylinder. For $x_{CO2,\,in}$ = 0%, $PRR_{max}$ exceeds the limit of 10 bar/°CA. It reaches a value of 16 bar/°CA in this case because of the combined faster combustion and lower heat capacity.

Figure 48 b) shows an additional data point at $x_{CO2,\,in}$ = 4% for the compression ratio of ε = 4.5. This data point shows that stable operation is also possible at this very low compression ratio but with a significantly lower pressure rise rate of 4 bar/°CA instead of over 7 bar/°CA for ε = 10. At first surprisingly, the IMEP is similar to that at ε = 10. This is because of the unusually high heat losses in this engine. These heat losses increase with compression ratio, which counteracts the thermodynamic increase in efficiency.

The effects of variation in equivalence ratio are shown in Figure 48 c). Operation is stable for all points. $PRR_{max}$ exceeds the limit only for the lowest investigated equivalence ratio of Φ = 1.9, i.e., the one closest to stoichiometric conditions. IMEP decreases slightly with increasing equivalence ratio, from 8 to about 7 bar, because of the lower oxygen fraction in the mixture, which is the limiting factor for heat release in the fuel-rich regime. Additional data points for compression ratios ε = 8 and 6 are shown in Figure 48 c). For operation at Φ = 1.9, decreasing the compression ratio yields a significant reduction in the pressure rise rate. For Φ = 2.3 however, operation at ε = 6 is unstable with a CoV of almost 90%.

### 8.3.2 Yields, conversions, and efficiencies

Some important metrics for the usefulness of a chemical process are yields, conversions, and efficiency. The hydrogen yield $Y_{H2}$ is calculated via eq. (52) with the outgoing molar flow of hydrogen $\dot{n}_{H2,out}$, the overall molar flow rate into the system $\dot{n}_{in}$, and the fraction of methane in the intake $x_{CH4,in}$. The conversions $X$ of $CO_2$ and $CH_4$ are calculated via eq. (53) with the molar flows $\dot{n}_{i,\,in}$ and $\dot{n}_{i,out}$ of each species $i$ going into and out of the system, respectively. The calculation of the exergy loss $E_l$ is based on the Gouy-Stodola theorem ($E_l = T_{amb}S_{irr}$) with the ambient temperature $T_{amb} = 298$ K and the entropy production $S_{irr}$ of the engine cycle as described in our previous work [8]. The exergetic efficiency $\eta_{ex}$ is then calculated via eq. (51)

$$\eta_{ex} = \frac{E_l}{m_{CH_4} e_{CH_4}} \tag{51}$$

with the specific chemical exergy of methane $e_{CH4} = 52.281$ MJ/kg.

$$Y_{H2} = \frac{\dot{n}_{H2,out}}{\dot{n}_{in} * (x_{CH4,in} * 2)} \tag{52}$$

$$X_i = \frac{\dot{n}_{i,\,in} - \dot{n}_{i,out}}{\dot{n}_{i,\,in}} \tag{53}$$

The hydrogen yield, the conversions of $CO_2$ and $CH_4$ and the exergetic efficiency are plotted in Figure 49.

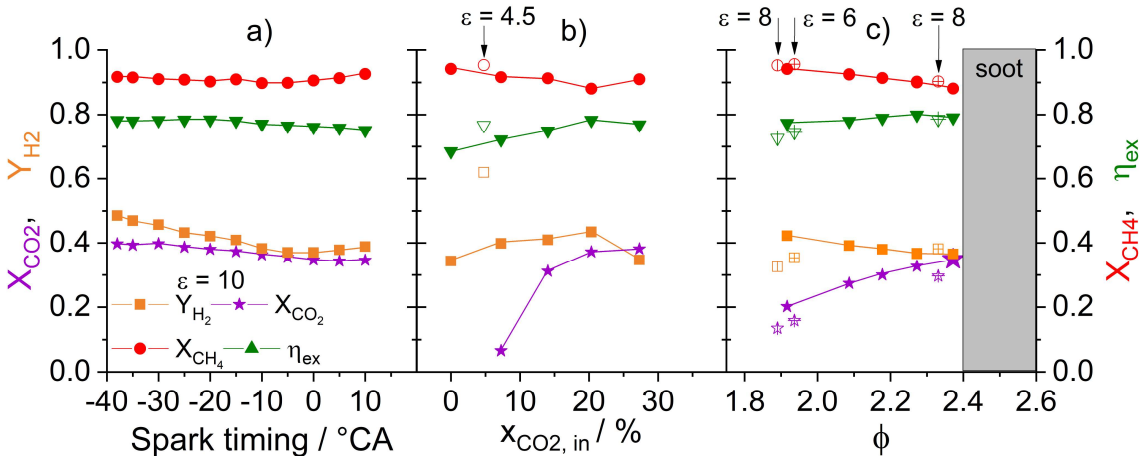


Figure 49: Hydrogen yield, conversions of $CO_2$ and methane, and the exergetic efficiency for variations in a) spark timing, b) intake mole fraction of $CO_2$, and c) equivalence ratio. Negative $CO_2$ conversions are not shown.

For the spark timing variation in Figure 49 a) the minimum $H_2$ yield is at -10°CA. Advancing the spark timing increases the hydrogen yield from 38 to 45% while the $CO_2$ conversion increases from 34 to 38%. The methane conversion is mostly independent from spark timing at values of about 90%. We think that the higher temperatures reached by earlier combustion phasing promote the endothermal dry reforming reaction. The exergetic efficiency is constant at about 78% for spark timings before -10°CA, decreasing slightly for later timings. This is probably caused by the reduction in work output because of the late combustion.

Figure 49 b) shows the effects of varying the $CO_2$ intake mole fraction. The maximum $H_2$ yield is at $x_{CO2,\,in}$ = 20%. It decreases for lower $x_{CO2,\,in}$ because less dry reforming takes place. This can also be seen in the $CO_2$ conversion, which decreases drastically with decreasing $x_{CO2,\,in}$. For low $x_{CO2,\,in}$ more $CO_2$ is in the product than in the educt. $CO_2$ conversions is not shown in this case because conversion is not a reasonable metric if the $CO_2$ output is significantly higher than the input. Increasing $x_{CO2,\,in}$ from 20 to 27% leads to decreasing $H_2$ yield. Probably at this point the peak temperatures are so low that they significantly slow down hydrogen formation. The exergetic efficiency increases with increasing $CO_2$ fractions to a maximum of $\eta_{ex}$ = 78% at $x_{CO2,\,in}$ = 20%. For 27% $CO_2$ it is decreasing again. Methane conversion has its minimum of 88% at $x_{CO2,\,in}$ = 20%, while its maximum is 94% in the $CO_2$-free case. The results for a lower compression ratio of $\varepsilon$ = 4.5 show a significantly higher hydrogen yield of 62% compared to less than 40% at $\varepsilon$ = 10. This suggests that at lower pressures significantly more methane is converted to hydrogen instead of water. This is consistent with lower pressures promoting volume-increasing reactions.

For the equivalence ratio variation shown in Figure 49 c) the maximum hydrogen yield is at the lowest investigated equivalence ratio of $\Phi$ = 1.9. This is counter-intuitive because if all other process parameters were held constant one may expect the hydrogen yield to increase with increasing $\Phi$, because the stoichiometric equivalence ratio of partial oxidation (eq. (50)) is at $\Phi$ = 4 with $\Phi$ based on complete oxidation. Unfortunately, in an engine not everything can be held constant. Since the equivalence ratio is varied and the spark timing is constant, the combustion phasing and the temperature-pressure history the cylinder charge experiences is changing drastically, as seen in Figure 46 c). As already shown in Figure 49 a), the hydrogen yield increases with earlier combustion, because of the promoting effect of the higher temperature on dry reforming. This results also in a higher hydrogen yield for the lower equivalence ratios because the promoting effect of early combustion seems to be predominant over the increase of hydrogen yield with increasing equivalence ratio. The $CO_2$ conversion is increasing with equivalence ratio. This is consistent with the findings of Gossler et al. who found the optimum conditions for $CO_2$ conversion at about $x_{CO2,\,in}$ = 20% for $\Phi$ = 2.8 [121]. The methane conversion in Figure 49 c) is decreasing with increasing equivalence ratio because of the increasing lack of oxygen. Exergetic efficiency is increasing for higher equivalence ratios. For the lower equivalence ratios of $\varepsilon$ = 8 and 6 two significant features can be seen. For $\varepsilon$ = 8 at $\Phi$ = 2.3 a higher hydrogen yield can be found than at $\varepsilon$ = 10 despite the lower $CO_2$ conversion. This is consistent with the result for $\varepsilon$ = 4.5 from Figure 49 b). But for the two points for $\varepsilon$ = 8 and 6 at an equivalence ratio of $\Phi$ = 1.9 the hydrogen yields are lower than for $\varepsilon$ = 10. This suggests that the promotion of hydrogen formation by lower compression ratio is stronger with higher equivalence ratio.

### 8.3.3 Soot in the product

Soot formation is a common problem at fuel-rich conditions. In polygeneration, downstream processing is likely to require a soot-free product stream from the engine, and the less soot needs to be filtered out, the better. For this reason, soot in the product gas was investigated. The FSN is shown in Figure 50.

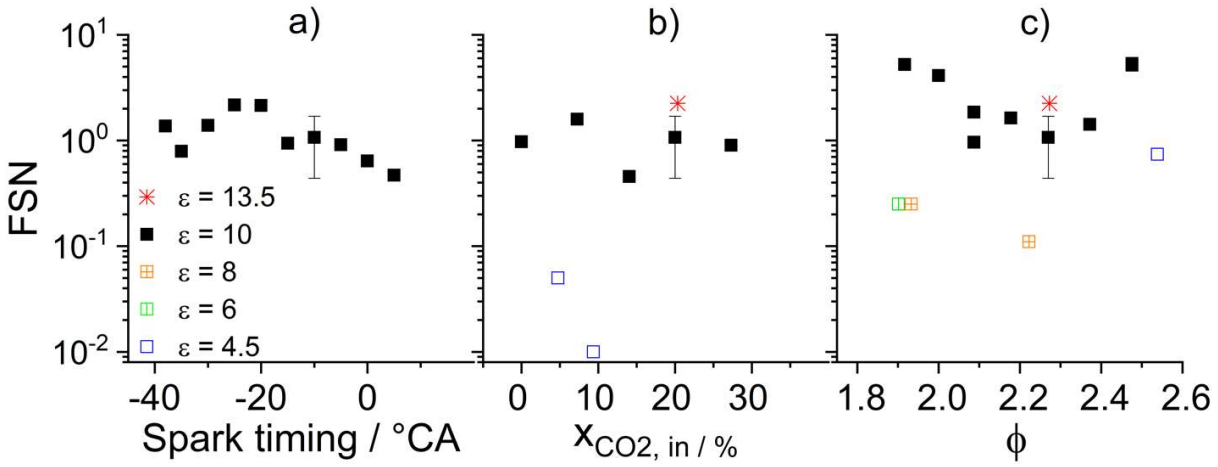


Figure 50: Soot in the product gas for variations in a) spark timing, b) intake mole fraction of $CO_2$, and c) equivalence ratio. The error bar represents the standard deviation of 17 datapoints recorded during 13 different engine runs at reference conditions. The data point at reference conditions is the arithmetic mean of this data. Other data points are the average between 2 FSN measurements conducted at the same engine run.

The most notable feature is the high variance that can be seen in Figure 50 a), b) and c) at reference conditions (-10°CA spark timing, $x_{CO2, in}$ = 20% and Φ = 2.3), where multiple measurements were performed. Especially for small FSN < 1 it is usually suggested to increase the volume of the gas sample that is fed through the filter paper to increase accuracy of the measurement. However, in our case the standard volume of 1000 ccm exhaust used in the smoke meter 415S was held constant. For this reason, we limit the analysis of the data to qualitative conclusions. Also, to accurately capture trends more data over the whole parameter span would be necessary. A few features can be seen anyway. For the variation of spark timing in Figure 50 a) there may be a slight increase of the FSN with earlier timings. The variation in $CO_2$ fraction in Figure 50 b) yields no significant trend. The equivalence ratio in Figure 50 c) however, shows a distinct influence on soot output. Starting at Φ = 2.3, increasing Φ leads to increased soot output with FSN = 5.6 at Φ = 2.47. This is expected. But decreasing the equivalence ratio from Φ = 2.3 to 1.9 also increases soot production. This is counter-intuitive because from a chemical point of view, bringing the equivalence ratio closer to stoichiometric should decrease soot formation. However, varying the equivalence ratio also changes the pressure-temperature history. Reducing the equivalence ratio leads to early combustion and increased pressures and temperatures, as shown in Figure 46 c), and as already seen in Figure 50 a) an early shift in combustion may increase soot formation. In terms of soot, Φ = 2.3 is the optimum here. Varying the compression ratio yields another notable result. The lowest soot concentration is found for a compression ratio of ε = 4.5 at $x_{CO2, in}$ = 10%. The higher compression ratio of ε = 13.5 yields slightly increased soot, and the lower compression ratios of ε = 8 and 6 in Figure 50 c) less soot than ε = 10. Overall, the results in Figure 50 b) and c) indicate that a lower compression ratio significantly decreases soot in the product gas.

## 8.4 Conclusions

The combustion of fuel-rich mixtures of $CH_4/CO_2/O_2$ in a reciprocating piston engine was investigated. Mainly, spark timing, $CO_2$ intake mole fraction, and equivalence ratio were varied at a compression ratio of ε = 10. A few data points for different compression ratios were also recorded. Stable operation of the engine was possible over a wide range in the investigated parameters. For Φ = 2.3 and $x_{CO2, in}$ = 20% operation was stable for spark timings from -38°CA to 10 °CA. At a spark timing of -10°CA operation was stable for $x_{CO2, in}$ = 0 – 27%. For 0%, however, the maximum pressure rise rate exceeded the 10 bar/°CA pressure rise rate limit. The equivalence ratio could be varied from Φ = 1.9 to 2.5 with stable operation, with only the Φ = 1.9 case exceeding the pressure rise rate limit. Early spark timings had positive influence on the $H_2$ yield and $CO_2$ conversion. The variation of $x_{CO2, in}$ showed a maximum $H_2$ yield of $Y_{H2}$ = 43% for $x_{CO2, in}$ = 20%. With $Y_{H2}$ = 62%, the overall highest $H_2$ yield was found for

the very low compression ratio of $\varepsilon = 4.5$. Soot in the product gas increased slightly with early combustion. A significant influence of $x_{CO2,\,in}$ on soot could not be found. The minimum fraction of soot for $\varepsilon = 10$ was found at an equivalence ratio of $\Phi = 2.3$. Lower equivalence ratios produced more soot. The compression ratio showed a significant influence on soot in the product gas, with lower compression ratios drastically decreasing soot output.

The results show that the proposed concept could be suitable for syngas production from $CO_2$-enriched methane. The process yields work, heat, and syngas at the same time, the ratio of which can be adjusted to demand. The use of pure oxygen as the oxidant enables stable fuel-rich operation even at high equivalence ratios and $CO_2$ contents. This makes it possible to use biogas or natural gas with $CO_2$ addition from upstream processes as feed and convert a significant part of the $CO_2$ while still producing power output.

# 9 Conclusions and Outlook

## 9.1 Conclusions

The aim of this work was to investigate strategies for fuel-rich operation of piston engines for polygeneration, i.e., the simultaneous production of mechanical work, heat, and useful chemicals. One important part of these investigations was the fuel rich HCCI operation of engines. It was shown by Wiemann et. al that for operation with air as the oxidizer HCCI operation can extend stable operation to much higher equivalence ratios than SI operation [8]. Hence different ways to enable HCCI operation for very fuel-rich methane-based mixtures and their respective limits were investigated. Also, the conversion of carbon dioxide via dry reforming reaction in the engine was investigated since the use of $CO_2$ as an educt has gained increasing importance. The exothermal reaction of the partial oxidation of methane can be used to drive the endothermal dry reforming reaction – yielding "auto-thermal reforming". $CO_2$ addition to the fuel-rich mixtures further increases auto-ignition resistance because of the high heat capacity of $CO_2$. For this reason, a different operating strategy was chosen. Using pure oxygen as an oxidizer enables fuel-rich operation even in SI mode [4]. Furthermore, it eliminates the nitrogen dilution of the product which occurs when using air. For those reasons the investigation of SI operation with pure oxygen and $CO_2$ addition was also part of this work.

For the experiments in this work a BASF octane number research engine was modified and operated in HCCI and SI mode. The modifications include an injection system for different gases and liquids since several additives with very different properties were used. Other modifications include increasing the compression ratio and redesigning the combustion chamber geometry. Due to the high auto-ignition resistance of the investigated mixtures higher compression ratios were introduced to limit the amount of additive needed for stable engine operation. This was achieved by implementing metal inserts into the combustion chamber and reducing the compressed volume in this way while simultaneously converting the non-ideal "L"-form of the combustion chamber to a more cylindrical one. A modern ignition system was installed for precise variation of the ignition timing, as the outdated mechanics of the engine for setting the ignition timing did not allow this.

Temperature and composition of the intake mixture have a significant influence on auto-ignition. Thus, the influence of these parameters was investigated first. DME was used as additive for these experiments because it is very reactive compared to methane and it can be derived from biomass. A method to determine an acceptable operating range for the engine was introduced. For this purpose, the pressure-based metrics CoV and pressure rise rate were calculated and limits were set for them. The DME fraction was then varied and the influence on CoV and $PRR_{max}$ was investigated. For an intake temperature of 150°C and in the range of $\Phi = 1.66$ to 1.84 the acceptable operating range was found to be at $x_{DME} = 8.6$ to 9.8%. The equivalence ratio was varied from $\Phi = 1.6$ to 2.3. A distinct soot limit was found around $\Phi = 2$. Below that limit, the concentration of soot was below 10 mg/m³, while above it increased significantly. For most of the operating points higher intake temperatures decreased the amount of additive needed for stable operation, as expected. Simulations performed by collaborators could capture the trend from the experiments in combustion phasing when the temperature at start of compression was adjusted by about 10 K, which is within the experimental uncertainty. Also, the flexible use of polygeneration in an engine could be demonstrated. By increasing the equivalence ratio, the work output could be reduced by 20% while simultaneously increasing the exergetic efficiency from 71 to 82%. Maximum selectivities of up to 72% for $H_2$ and 79% for CO were found.

It was shown that polygeneration in ICE is possible when operating in HCCI mode with DME as the additive. In a next step it was investigated which additive would be most suitable. The additives DME, DEE and n-heptane were compared in terms of mole, mass, and energy fraction in the additive-fuel-mixture, the timing and intensity of the heat release, and the operating stability. These additives were chosen because all of them have very high auto-ignition tendency. In terms of operating ranges, the narrowest range was found for n-heptane and the widest for DME. The latter allowed for late, stable combustion. In terms of additive mole, mass, and energy fractions, the lowest fractions needed for stable operation were achieved with DEE. It is the most reactive of the three tested and

proved to be also the most potent ignition enhancer. In terms of mass and energy fraction significantly more n-heptane was needed than DME and DEE. The heat release analysis, which was specifically adjusted to fuel-rich operation for this work showed very similar early heat release behavior for DME and n-heptane, while DEE had significantly less NTC behavior and more heat release at very early crank angles. Additionally, the in-cylinder temperatures and the heat release analysis suggest that the heat capacity of the additive itself has significant influence on the auto-ignition behavior and the amount of additive needed for acceptable operation. For a better comparison of syngas production with the different additives, the dependency of syngas fraction on combustion phasing was investigated. It was found that a shift of combustion phasing within the operating limits could change the $H_2$-fraction in the product by about 1%-point. For a comparison of the influence of the different additives on the syngas fraction in the product the experiments were conducted at a constant CA50 of 15° aTDC. It was found that the choice of additive has no significant influence on the syngas production. The temporal species evolution showed that all three additives basically follow similar reaction pathways and initiate ignition by OH radical formation and H abstraction. However, DEE forms significant amounts of OH much earlier than the other additives. The overall results from this set of experiments suggest that a good additive has high reactivity and releases OH radicals as early as possible while it has a low heat capacity which means high temperature at the end of compression.

The previous experiments showed that even in the case of DEE still over 15% of the heating value of the additive-fuel-mixture came from the additive. This is not desirable since the basic idea is to use methane as an inexpensive base fuel, and the price of the additives is significantly higher. An alternative ignition promoter is ozone. It had been successfully used in lean HCCI [10]. Therefore, it was investigated whether it is similarly effective in fuel-rich HCCI and what the kinetics behind its auto-ignition promoting effect are.

First, DME was consecutively substituted by ozone at a constant CA50. At a compression ratio of $\varepsilon = 10$ and 150°C intake temperature around 5%-points of DME could be replaced with just around 50 ppm of ozone. In this systematic substitution, ozone showed a strong effect when added in small amounts but an exponentially decreasing efficacy with increasing ozone fractions. For the given conditions ozone could not replace the DME completely but the additive energy fraction could be reduced significantly. The modelling by colaborators showed that the ozone decomposes quickly during compression and forms $CH_3OOH$ and $CH_2O$ as buffer molecules that survive to higher temperatures. $CH_3OOH$ further decomposes to $H_2O_2$ and $CH_2O$ during compression. The investigations suggest that ozone is a very potent ignition promoter in small quantities and could be especially useful at higher compression ratios where not much additive is needed.

Second, the compression ratio of the engine was increased systematically. Metal inserts in the combustion chamber increased the range of adjustable compression ratios in the engine from $\varepsilon = 4$ to 10 in its original state to $\varepsilon = 4.5$ to 20 in the modified form. The engine was operated with $CH_4$/DME mixtures in HCCI mode, and the compression ratio was increased in steps of $\varepsilon = 2$ and at the same time the DME fraction in the intake was reduced to maintain stable operation at the acceptable CoV limit. It was found that increasing the compression ratio from $\varepsilon = 10$ to 16 leads to a reduction of the critical DME mole fraction $x_{DME}$ from 9% to below 1%. When the mixture preheating was reduced from 150°C to 50°C, about 2% DME were needed. It was also possible to operate the engine completely without additive with a compression ratio of $\varepsilon = 18$ at $\Phi = 1.4$ and with a compression ratio of $\varepsilon = 19$ at $\Phi = 1.65$. However, then the DME fraction in the intake is lost as a potential control parameter.

It has been shown in RCM experiments and simulations by Gossler et al. that significant amounts of $CO_2$ in the feedstock can be converted via dry reforming reaction in fuel-rich engine operation [121]. As part of this work a process with a fuel-rich mixture and different fractions of $CO_2$ in the intake was investigated to test such an application in a real engine. $CO_2$ has a high heat capacity and further increases the auto-ignition resistance of the fuel-rich methane-based mixture, which is already difficult to ignite. HCCI operation in this case would be difficult to achieve and would require much reactive additives or excessive preheating. For this reason, for the engine experiments SI operation was chosen. To operate the engine stably in SI mode, however, instead of air pure oxygen was used as the oxidant. This strategy also reduces the effort for downstream gas separation of the products since mostly undiluted syngas is produced. The investigations included parameter variations of the equivalence ratio in the range of $1.9 < \Phi < 2.5$, of the $CO_2$ mole fraction in the intake in the range of $x_{CO2,\,in} = 0$ to 33%, and of the

spark timing in the range of -38°CA to 10°CA after top dead center. While these parameter variations were conducted at compression ratios of $\varepsilon = 10$, for some points also different compression ratios were investigated. The results showed stable operation for almost all investigated conditions. $x_{CO2,\,in}$ of 33% led to unstable behavior while operation without $CO_2$ and at $\Phi < 2$ resulted in exceeding the maximum pressure rise rate limit. The maximum $CO_2$ conversion was found to be about 40% at $x_{CO2,\,in} = 20\%$. Hydrogen yields of up to 50% were found at early spark timings for $\varepsilon = 10$. At the very low compression ratio of $\varepsilon = 4.5$, even 62% hydrogen yield could be achieved. It was also found that significantly less soot was produced at low compression ratios.

Overall, it can be concluded that syngas production by fuel-rich engine operation works over a wide range of different operating conditions. The high thermal buffer capacity of fuel-rich methane-based mixtures reduces the pressure rise rates and thus the tendency of HCCI operation to knock or ring and make it a viable operating strategy for syngas production in piston engines since it enables stable operation in the very fuel-rich regime. Compression ratios near the mixtures auto-ignition limit are favorable to reduce the additive demand. For equivalence ratios near the soot-limit, which produce the most syngas without producing excessive soot (at about $\Phi = 2$), without mixture preheating, those would be around $\varepsilon = 18$. In this case only small amounts of additive are needed, and ozone would be a good choice since it is highly effective when added in small amounts. When operation with pure oxygen as oxidizer is employed, SI operation is recommended. The high oxygen content increases the flame speed such that the engine can be spark-operated at very rich equivalence ratios. In this case low compression ratios are favored since they reduce soot formation and increase hydrogen production.

## 9.2 Outlook

The investigations in this work focused on experiments supported by simulations of the chemical kinetics in the engine, the latter performed by collaborators. A next step would be to find an array of possible applications for a flexible polygeneration engine that produces syngas, to narrow down the most promising concept and to simulate and evaluate the entire process concept. The exergetic efficiencies presented in this work are comparably high, but they do not include upstream or downstream processing which have to be taken into account in order to determine the usefulness of the technology. In a next step the efficiencies of an entire process should be evaluated. Also, an economic analysis would be useful to evaluate and show the potential of the technology. Such an analysis should include varying costs for energy and potential storage systems to ensure that the full potential of the flexible polygeneration system can be exploited. Preliminary investigates, not reported here, showed that a wastewater treatment plant could be a good target application. In most wastewater treatment plants biogas produced by the digestion tower is supplied to CHP units to produce power and heat that is needed to run the plant. However, especially in the summer at high temperatures the heat demand of the plant decreases drastically and at some point, the CHP unit needs to be switched off. In this case biogas is flared and energy is wasted. Instead of switching the CHP unit off it could be modified to produce syngas instead decreasing heat and power output and instead producing a useful chemical. The syngas could be used as feedstock for a methanol synthesis yielding an easily storable liquid. In addition, some of the methanol can be used to feed the bacteria of the biological stage of the wastewater treatment plant.

Places where natural gas is flared that otherwise cannot be used are also possibly suitable, as the process concept is also easily scalable to small sizes and can be adopted to mobile applications as for example suggested by Lim et al. [6] who proposed a mobile gas to liquid system using an engine to produce syngas. In addition, plants with varying heat or power requirements may be suitable because they could make use of the process's flexibility. Once a possible process concept is evaluated, the next step is to choose an engine and modify it to run with an operating strategy suitable for polygeneration e.g., as suggested in 9.1. Operating parameters should be optimized to adjust the process to the desired hardware, specifications, and to maximize efficiency.

Investigating aspects of chemical kinetics during the auto-ignition phase in HCCI operation could give better insight in which effects influence ignition and early combustion and how to achieve better control of it. Experiments in an optically accessible engine using UV absorption spectroscopy may elucidate the formation and

conversion of intermediate species like $H_2O_2$ or $CH_2O$ during ignition and early combustion and help gain a better understanding in the effects of different additives on auto-ignition of fuel-rich methane-based mixtures. This could help to identify groups of optimal additives.

# Appendix

## A Uncertainties

To estimate uncertainties of the exhaust gas analysis (EGA), a gas chromatograph (GC) with a mass spectrometer (MS) and a thermal conductivity detector was used. An experiment with $\Phi = 1.9$ in HCCI mode was repeated 10 times and samples of the exhaust were taken. The GC measurements were compared to measurements with the exhaust gas analyzer (EGA) used throughout this thesis work. The results for $H_2$, CO, and $CO_2$ are shown in Figure A 1. The error bars represent the standard deviation over the 10 measurements. The data points are the average of the 10 measurements.

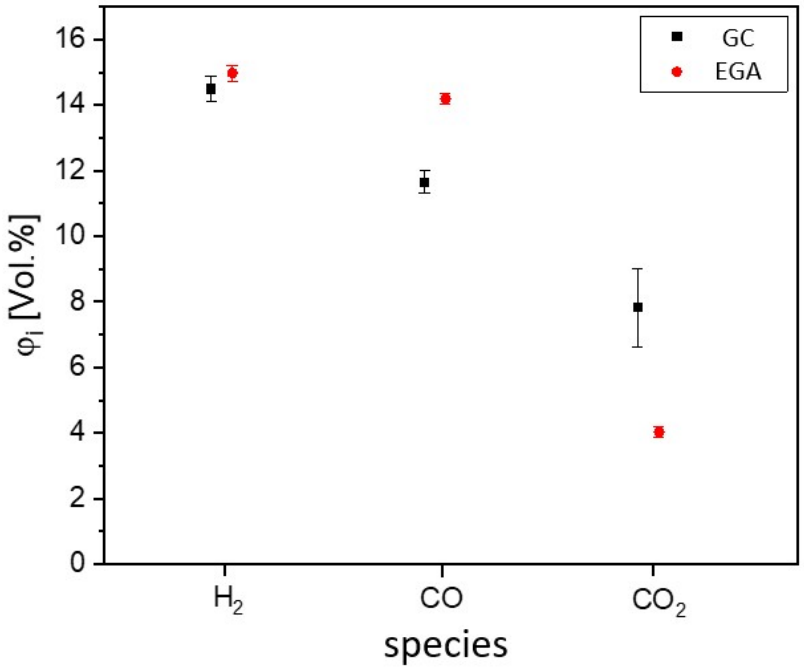


Figure A 1: Comparison of GC and EGA results for $H_2$, CO and $CO_2$

The deviation between GC results and EGA results for $H_2$ is less than 1%-point and within the standard deviation. The deviation for the CO however is above 2-% points and shows that the EGA seems to overpredict the CO fraction. The $CO_2$ fraction measured with the GC is with almost 8 Vol-% much larger than the fraction measured with the EGA.

Figure A 2 shows the results for $CH_4$, $O_2$, and $C_2H_4$.

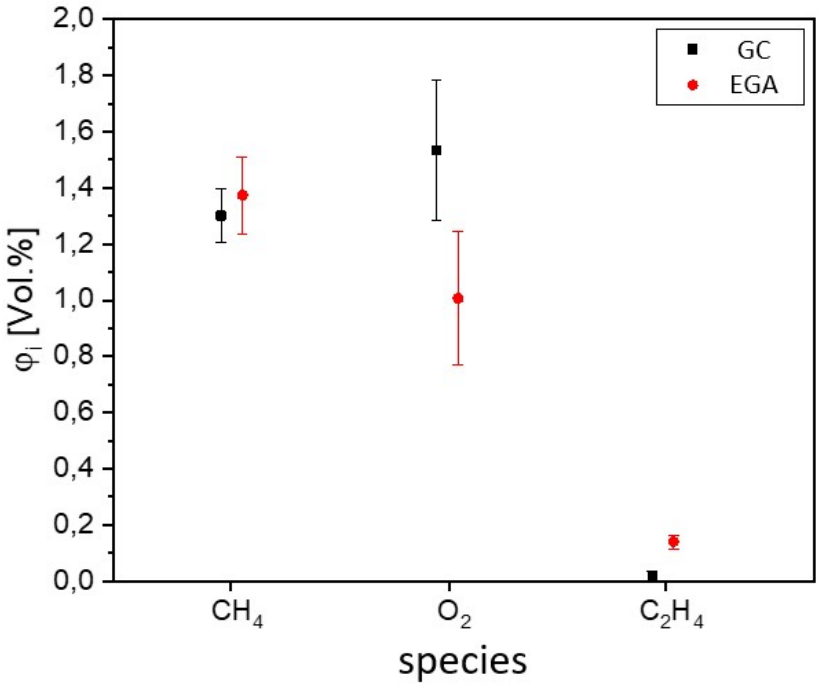


Figure A 2: Comparison of GC and EGA results for $CH_4$, $O_2$ and $C_2H_4$

The difference in the $CH_4$ measurements is less than 0.1 %-points and within the standard deviation. The GC measurements predict significantly more $O_2$ than the EGA. This may indicate a contamination of the GC sample with air. While the EGA predicts a small fraction of $C_2H_4$, no $C_2H_4$ can be detected by the GC. This could be due to a cross sensitivity of one of the EGA's NDIR sensors.

# References

[1] H. Li, H. Hong, H. Jin, R. Cai, Analysis of a feasible polygeneration system for power and methanol production taking natural gas and biomass as materials, Appl. Energy, 87 (2010) 2846–2853, doi:10.1016/j.apenergy.2009.07.001.

[2] A. Simpson, A. Lutz, Exergy analysis of hydrogen production via steam methane reforming, Int. J. Hydrogen Energy, 32 (2007) 4811–4820, doi:10.1016/j.ijhydene.2007.08.025.

[3] B. Atakan, Gas turbines for polygeneration? A thermodynamic investigation of a fuel rich gas turbine cycle, Int J Thermo, 14 (2011), doi:10.5541/ijot.308.

[4] Szeszich, Herstellung von Synthesegas im Otto-Motor bei gleichzeitiger Arbeitsgewinnung, Chemie-Ing.-Techn., 1956 (1957) 191–195, doi:10.1002/cite.330280310.

[5] M. McMillian, S. Lawson, Experimental and modeling study of hydrogen/syngas production and particulate emissions from a natural gas-fueled partial oxidation engine, Int. J. Hydrogen Energy, 31 (2006) 847–860, doi:10.1016/j.ijhydene.2005.08.013.

[6] E.G. Lim, E.E. Dames, K.D. Cedrone, A.J. Acocella, T.R. Needham, A. Arce, D.R. Cohn, L. Bromberg, W.K. Cheng, W.H. Green, The engine reformer: Syngas production in an engine for compact gas-to-liquids synthesis, Can. J. Chem. Eng., 94 (2016) 623–635, doi:10.1002/cjce.22443.

[7] G.A. Karim, N. Moore, Examination of Rich Mixture Operation in a Dual Fuel Engine, SAE Technical Paper 901500 (1990).

[8] S. Wiemann, R. Hegner, B. Atakan, C. Schulz, S.A. Kaiser, Combined production of power and syngas in an internal combustion engine – Experiments and simulations in SI and HCCI mode, Fuel (2018) 40–45, doi:10.1016/j.fuel.2017.11.002.

[9] Sebastian Wiemann, Erzeugung und Verwendung von Synthesegas in Verbrennungsmotoren, Dissertation, University of Duisburg-Essen (2018).

[10] F. Foucher, P. Higelin, C. Mounaïm-Rousselle, P. Dagaut, Influence of ozone on the combustion of n-heptane in a HCCI engine, Proc. Combust. Inst., 34 (2013) 3005–3012, doi:10.1016/j.proci.2012.05.042.

[11] J.-B. Masurier, F. Foucher, G. Dayma, P. Dagaut, Ozone applied to the homogeneous charge compression ignition engine to control alcohol fuels combustion, Appl. Energy, 160 (2015) 566–580, doi:10.1016/j.apenergy.2015.08.004.

[12] K. Liu, C. Song, V. Subramani, Hydrogen and syngas production and purification technologies, Wiley; AIChE, Hoboken N.J., New York (2010).

[13] A.S. Bodke, S.S. Bharadwaj, L.D. Schmidt, The Effect of Ceramic Supports on Partial Oxidation of Hydrocarbons over Noble Metal Coated Monoliths, Journal of Catalysis, 179 (1998) 138–149, doi:10.1006/jcat.1998.2224.

[14] J.R. Rostrup-Nielsen, Syngas in perspective, Catalysis Today, 71 (2002) 243–247, doi:10.1016/S0920-5861(01)00454-0.

[15] A.T. Ashcroft, A.K. Cheetham, M.L.H. Green, P.D.F. Vernon, Partial oxidation of methane to synthesis gas using carbon dioxide, Nature, 352 (1991) 225–226, doi:10.1038/352225a0.

[16] G.P. Merker, Grundlagen Verbrennungsmotoren, Simulation der Gemischbildung, Verbrennung, Schadstoffbildung und Aufladung, 4th ed., Vieweg+Teubner, Wiesbaden (2009).

[17] P. Richards, Automotive fuels reference book, SAE International, Warrendale, PA (2014).

[18] M. Richter, J. Engström, A. Franke, M. Aldén, A. Hultqvist, B. Johansson, The Influence of Charge Inhomogeneity on the HCCI Combustion Process, SAE Technical Paper 2000-01-2868 (2000).

[19] M. Christensen, B. Johansson, A. Hultqvist, The Effect of Combustion Chamber Geometry on HCCI Operation, SAE Technical Paper 2002-01-0425.

[20] M. Mansoury, S. Jafarmadar, M. Talei, S.M. Lashkarpour, Optimization of HCCI (Homogeneous Charge Compression Ignition) engine combustion chamber walls temperature to achieve optimum IMEP using LHS and Nelder Mead algorithm, Energy, 119 (2017) 938–949, doi:10.1016/j.energy.2016.11.047.

[21] F.(Zhao, T.W. Asmus, D.N. Assanis, J.E. Dec, J.A. Eng, P.M. Najt, Homogeneous Charge Compression Ignition (HCCI) Engines, Key Research and Development Issues, Society of Automotive Engineers, Inc., Warrendale, PA (2003).

[22] C. Daw, M. Kennel, C. Finney, F. Connolly, Observing and modeling nonlinear dynamics in an internal combustion engine, Phys. Rev. E Stat. Phys. Plasmas Fluids Relat. Interdiscip. Topics, 57 (1998) 2811–2819, doi:10.1103/PhysRevE.57.2811.

[23] J.B. Heywood, Internal combustion engine fundamentals, McGraw-Hill, New York (1988).

[24] M. Klein, A specific heat ratio model and compression ratio estimation, Dissertation, Linköping (2004).

[25] H.M. Cheung, J.B. Heywood, Evaluation of a One-Zone Burn-Rate Analysis Procedure Using Production SI Engine Pressure Data, SAE Technical Paper 932749 (1993).

[26] F. Calise, G. de Di Notaristefani Vastogirardi, M. Dentice d'Accadia, M. Vicidomini, Simulation of polygeneration systems, Energy, 163 (2018) 290–337, doi:10.1016/j.energy.2018.08.052.

[27] H. Ghanbari, F. Pettersson, H. Saxén, Optimal operation strategy and gas utilization in a future integrated steel plant, Chem. Eng. Res. Des., 102 (2015) 322–336, doi:10.1016/j.cherd.2015.06.038.

[28] D. Schröder, R. Hegner, A. Güngör, B. Atakan, Exergoeconomic analysis of an HCCI engine polygeneration process, Energy Convers. Manage., 203 (2020) 112085, doi:10.1016/j.enconman.2019.112085.

[29] S. Ohler, Entwicklung und Vergleich von Kriterien zur Erkennung der klopfenden Verbrennung in Ottomotoren, Dissertation, Helmut-Schmidt-Universität (2014).

[30] B. Atakan, S.A. Kaiser, J. Herzler, S. Porras, K. Banke, O. Deutschmann, T. Kasper, M. Fikri, R. Schießl, D. Schröder, C. Rudolph, D. Kaczmarek, H. Gossler, S. Drost, V. Bykov, U. Maas, C. Schulz, Flexible energy conversion and storage via high-temperature gas-phase reactions: The piston engine as a polygeneration reactor, Renewable Sustainable Energy Rev., 133 (2020) 110264, doi:10.1016/j.rser.2020.110264.

[31] K. Banke, R. Hegner, D. Schröder, C. Schulz, B. Atakan, S.A. Kaiser, Power and syngas production from partial oxidation of fuel-rich methane/DME mixtures in an HCCI engine, Fuel (2019) 97–103, doi:10.1016/j.fuel.2019.01.076.

[32] F. Calise, M. Dentice d'Accadia, A. Piacentino, Exergetic and exergoeconomic analysis of a renewable polygeneration system and viability study for small isolated communities, Energy, 92 (2015) 290–307, doi:10.1016/j.energy.2015.03.056.

[33] F. Calise, M.D. d'Accadia, A. Macaluso, A. Piacentino, L. Vanoli, Exergetic and exergoeconomic analysis of a novel hybrid solar–geothermal polygeneration system producing energy and water, Energy Convers. Manag., 115 (2016) 200–220, doi:10.1016/j.enconman.2016.02.029.

[34] H. Nishida, T. Tachibana, Homogeneous Charge Compression Ignition of Natural Gas/Air Mixture with Ozone Addition, J. Propul. Power, 22 (2006) 151–157, doi:10.2514/1.14991.

[35] J.-B. Masurier, F. Foucher, G. Dayma, P. Dagaut, Investigation of iso -octane combustion in a homogeneous charge compression ignition engine seeded by ozone, nitric oxide and nitrogen dioxide, Proc. Combust. Inst., 35 (2015) 3125–3132, doi:10.1016/j.proci.2014.05.060.

[36] G.A. Karim, I. Wierzba, The production of hydrogen through the uncatalyzed partial oxidation of methane in an internal combustion engine, Int. J. Hydrogen Energy, 33 (2008) 2105–2110, doi:10.1016/j.ijhydene.2008.01.051.

[37] Y.C. Yang, M.S. Lim, Y.N. Chun, The syngas production by partial oxidation using a homogeneous charge compression ignition engine, Fuel Process Technol, 90 (2009) 553–557, doi:10.1016/j.fuproc.2009.01.002.

[38] L. Zhu, Z. He, Z. Xu, X. Lu, J. Fang, W. Zhang, Z. Huang, In-cylinder thermochemical fuel reforming (TFR) in a spark-ignition natural gas engine, Proc. Combust. Inst., 36 (2017) 3487–3497, doi:10.1016/j.proci.2016.07.058.

[39] L. Tartakovsky, M. Sheintuch, Fuel reforming in internal combustion engines, Prog. Energy Combust. Sci., 67 (2018) 88–114, doi:10.1016/j.pecs.2018.02.003.

[40] R. Hegner, M. Werler, R. Schießl, U. Maas, B. Atakan, Fuel-Rich HCCI Engines as Chemical Reactors for Polygeneration: A Modeling and Experimental Study on Product Species and Thermodynamics, Energy Fuels, 31 (2017) 14079–14088, doi:10.1021/acs.energyfuels.7b02150.

[41] R. Hegner, B. Atakan, A polygeneration process concept for HCCI-engines – Modeling product gas purification and exergy losses, Int. J. Hydrogen Energy, 42 (2017) 1287–1297, doi:10.1016/j.ijhydene.2016.09.050.

[42] A. Inayat, C. Ghenai, M. Naqvi, M. Ammar, M. Ayoub, M. Hussin, Parametric Study for Production of Dimethyl Ether (DME) As a Fuel from Palm Wastes, Energy Procedia, 105 (2017) 1242–1249, doi:10.1016/j.egypro.2017.03.431.

[43] Z. Wang, T. He, J. Li, J. Wu, J. Qin, G. Liu, D. Han, Z. Zi, Z. Li, J. Wu, Design and operation of a pilot plant for biomass to liquid fuels by integrating gasification, DME synthesis and DME to gasoline, Fuel, 186 (2016) 587–596, doi:10.1016/j.fuel.2016.08.108.

[44] D.G. Goodwin, H.K Moffat, R.L. Speth, Cantera: An object- oriented software toolkit for chemical kinetics, thermodynamics, and transport processes.: Version 2.7.1 (2014), http://www.cantera.org.

[45] K. Yasunaga, F. Gillespie, J.M. Simmie, H.J. Curran, Y. Kuraguchi, H. Hoshikawa, M. Yamane, Y. Hidaka, A multiple shock tube and chemical kinetic modeling study of diethyl ether pyrolysis and oxidation, The journal of physical chemistry. A, 114 (2010) 9098–9109, doi:10.1021/jp104070a.

[46] K. Yasunaga, J.M. Simmie, H.J. Curran, T. Koike, O. Takahashi, Y. Kuraguchi, Y. Hidaka, Detailed chemical kinetic mechanisms of ethyl methyl, methyl tert-butyl and ethyl tert-butyl ethers, Combustion and Flame, 158 (2011) 1032–1036, doi:10.1016/j.combustflame.2010.10.012.

[47] F. Sen, B. Shu, T. Kasper, J. Herzler, O. Welz, M. Fikri, B. Atakan, C. Schulz, Shock-tube and plug-flow reactor study of the oxidation of fuel-rich CH4 /O2 mixtures enhanced with additives, Combust. Flame, 169 (2016) 307–320, doi:10.1016/j.combustflame.2016.03.030.

[48] J. Herzler, M. Fikri, O. Welz, C. Schulz, Proceedings of the 7th European Combustion Meeting March 30-April 2 2015, Budapest, Hungary.

[49] J. Herzler, Y. Sakai, M. Fikri, C. Schulz, Shock-tube study of the ignition and product formation of fuel-rich CH4/air and CH4/additive/air mixtures at high pressure, Proceedings of the Combustion Institute, 37 (2019) in press.

[50] D. Nativel, B. Shu, J. Herzler, M. Fikri, C. Schulz, Shock-tube study of methane pyrolysis in the context of energy-storage processes, Proc. Combust. Inst. (2018), doi:10.1016/j.proci.2018.06.083.

[51] J. Zheng, J.A. Caton, Use of a single-zone thermodynamic model with detailed chemistry to study a natural gas fueled homogeneous charge compression ignition engine, Energy Conversion and Management, 53 (2012) 298–304, doi:10.1016/j.enconman.2011.09.005.

[52] G. Woschni, A Universally Applicable Equation for the Instantaneous Heat Transfer Coefficient in the Internal Combustion Engine, SAE Technical Paper 670931 (1967).

[53] H.S. Soyhan, H. Yasar, H. Walmsley, B. Head, G.T. Kalghatgi, C. Sorusbay, Appl. Therm. Eng., 29 (2009) 541–549, doi:10.1016/j.applthermaleng.2008.03.014.

[54] J. Chang, O. Güralp, Z. Filipi, D.N. Assanis, T.-W. Kuo, P. Najt, R. Rask, New Heat Transfer Correlation for an HCCI Engine Derived from Measurements of Instantaneous Surface Heat Flux, SAE Technical Paper 2004-01-2996 (2004).

[55] N.P. Komninos, C.D. Rakopoulos, Heat transfer in HCCI phenomenological simulation models: A review, Applied Energy, 181 (2016) 179–209, doi:10.1016/j.apenergy.2016.08.061.

[56] R.E. Sonntag, C. Borgnakke, G.J. van Wylen, Fundamentals of thermodynamics, 6th ed., Wiley, New York (2003).

[57] T. Kotas, The exergy method of thermal plant analysis, Butterworths, London (1985).

[58] S.-C. Kong, A study of natural gas/DME combustion in HCCI engines using CFD with detailed chemical kinetics, Fuel, 86 (2007) 1483–1489, doi:10.1016/j.fuel.2006.11.015.

[59] H. Kellerer, A. Müller, H.-J. Bauer, S. Wittig, Soot Formation in a Shock Tube under Elevated Pressure Conditions, Combustion Science and Technology, 113 (1996) 67–80.

[60] M. Sjöberg, J.E. Dec, N.P. Cernansky, Potential of Thermal Stratification and Combustion Retard for Reducing Pressure-Rise Rates in HCCI Engines, Based on Multi-Zone Modeling and Experiments, SAE Technical Paper, 2005-01-0113 (2005), doi:10.4271/2005-01-0113.

[61] E. Neshat, R.K. Saray, Development of a new multi zone model for prediction of HCCI (homogenous charge compression ignition) engine combustion, performance and emission characteristics, Energy, 73 (2014) 325–339, doi:10.1016/j.energy.2014.06.025.

[62] N.P. Komninos, Assessing the effect of mass transfer on the formation of HC and CO emissions in HCCI engines, using a multi-zone model, Energy Conversion and Management, 50 (2009) 1192–1201, doi:10.1016/j.enconman.2009.01.026.

[63] L. Gao, H. Li, B. Chen, H. Jin, R. Lin, H. Hong, Proposal of a natural gas-based polygeneration system for power and methanol production, Energy, 33 (2008) 206–212, doi:10.1016/j.energy.2007.10.011.

[64] K. Banke, D. Freund, B. Atakan, S.A. Kaiser, Evaluation of fuel additives for HCCI engines operated on fuel-rich methane/air mixtures: DME, DEE, and n-heptane, Applications in Energy and Combustion Science, 13 (2023) 100112, doi:10.1016/j.jaecs.2023.100112.

[65] M. Izadi Najafabadi, N. Abdul Aziz, Homogeneous Charge Compression Ignition Combustion: Challenges and Proposed Solutions, J. Combust., 2013 (2013) 1–14, doi:10.1155/2013/783789.

[66] R.D. Reitz, G. Duraisamy, Review of high efficiency and clean reactivity controlled compression ignition (RCCI) combustion in internal combustion engines, Prog. Energy Combust. Sci., 46 (2015) 12–71, doi:10.1016/j.pecs.2014.05.003.

[67] J. Patten, T. McWha, Dimethyl ether fuel literature review, National Research Council Canada. Automotive and Surface Transportation (2015).

[68] C. Arcoumanis, C. Bae, R. Crookes, E. Kinoshita, The potential of di-methyl ether (DME) as an alternative fuel for compression-ignition engines: A review, Fuel, 87 (2008) 1014–1030, doi:10.1016/j.fuel.2007.06.007.

[69] H. Abou-Rachid, L. Bonneviot, G. Xu, S. Kaliaguine, On the correlation between kinetic rate constants in the auto-ignition process of some oxygenates and their cetane number: a quantum chemical study, Journal of Molecular Structure: THEOCHEM, 621 (2003) 293–304, doi:10.1016/S0166-1280(02)00676-0.

[70] G.K. Lilik, A.L. Boehman, Effects of Fuel Composition on Critical Equivalence Ratio for Autoignition, Energy Fuels, 27 (2013) 1601–1612, doi:10.1021/ef3016014.

[71] U. Azimov, N. Stylianidis, N. Kawahara, E. Tomita, Characterisation of DME-HCCI combustion cycles for formaldehyde and hydroxyl UV–vis absorption, Fuel, 210 (2017) 578–591, doi:10.1016/j.fuel.2017.09.003.

[72] J. Eble, J. Kiecherer, M. Olzmann, Low-Temperature Autoignition of Diethyl Ether/O2 Mixtures: Mechanistic Considerations and Kinetic Modeling, Z. Phys. Chem., 231 (2017) 1603–1623, doi:10.1515/zpch-2016-0959.

[73] Z. Zhang, E. Hu, C. Peng, Z. Huang, Experimental and Kinetic Study on Ignition Delay Times of Diethyl Ether, SAE Int. J. Fuels Lubr., 8 (2015) 111–118, doi:10.4271/2015-01-0897.

[74] D. Jung, in: M.A. Farrukh (Ed.), Advanced Chemical Kinetics, InTech, 2018, pp. 38–55.

[75] M.H. Morsy, Modeling study on the production of hydrogen/syngas via partial oxidation using a homogeneous charge compression ignition engine fueled with natural gas, Int. J. Hydrogen Energy, 39 (2014) 1096–1104, doi:10.1016/j.ijhydene.2013.10.160.

[76] S. Deng, P. Zhao, D. Zhu, C.K. Law, NTC-affected ignition and low-temperature flames in nonpremixed DME/air counterflow, Combust. Flame, 161 (2014) 1993–1997, doi:10.1016/j.combustflame.2014.01.020.

[77] L.-S. Tran, O. Herbinet, Y. Li, J. Wullenkord, M. Zeng, E. Bräuer, F. Qi, K. Kohse-Höinghaus, F. Battin-Leclerc, Low-temperature gas-phase oxidation of diethyl ether: Fuel reactivity and fuel-specific products, Proc. Combust. Inst., 37 (2019) 511–519, doi:10.1016/j.proci.2018.05.135.

[78] J.-R. Yang, S.-C. Wong, On the suppression of negative temperature coefficient (NTC) in autoignition of n-heptane droplets, Combust. Flame, 132 (2003) 475–491, doi:10.1016/S0010-2180(02)00492-3.

[79] B.M. Gauthier, D.F. Davidson, R.K. Hanson, Shock tube determination of ignition delay times in full-blend and surrogate fuel mixtures, Combust. Flame, 139 (2004) 300–311, doi:10.1016/j.combustflame.2004.08.015.

[80] D.G. Goodwin, H.K. Moffat, R.L. Speth, Cantera: An Object-Oriented Software Toolkit For Chemical Kinetics, Thermodynamics, And Transport Processes, Zenodo (2018).

[81] Victor Salazar, Unburned hydrocarbon emission mechanisms in small engines, Dissertation, University of Wisconsin-Madison (2008).

[82] D. Kaczmarek, J. Herzler, S. Porras, S. Shaqiri, M. Fikri, C. Schulz, B. Atakan, U. Maas, T. Kasper, Plug-flow reactor and shock-tube study of the oxidation of very fuel-rich natural gas/DME/O2 mixtures, Combust. Flame, 225 (2021) 86–103, doi:10.1016/j.combustflame.2020.10.004.

[83] Z. Serinyel, M. Lailliau, S. Thion, G. Dayma, P. Dagaut, An experimental chemical kinetic study of the oxidation of diethyl ether in a jet-stirred reactor and comprehensive modeling, Combust. Flame, 193 (2018) 453–462, doi:10.1016/j.combustflame.2018.04.002.

[84] A. Stagni, A. Frassoldati, A. Cuoci, T. Faravelli, E. Ranzi, Skeletal mechanism reduction through species-targeted sensitivity analysis, Combust. Flame, 163 (2016) 382–393, doi:10.1016/j.combustflame.2015.10.013.

[85] Y. Tsutsumi, A. Iijima, K. Yoshida, H. Shoji, J.T. Lee, HCCI combustion characteristics during operation on DME and methane fuels, Int. J. Automot. Technol., 10 (2009) 645–652, doi:10.1007/s12239−009−0076−3.

[86] U. Burke, K.P. Somers, P. O'Toole, C.M. Zinner, N. Marquet, G. Bourque, E.L. Petersen, W.K. Metcalfe, Z. Serinyel, H.J. Curran, An ignition delay and kinetic modeling study of methane, dimethyl ether, and their mixtures at high pressures, Combust. Flame, 162 (2015) 315–330, doi:10.1016/j.combustflame.2014.08.014.

[87] M. Werler, L.R. Cancino, R. Schiessl, U. Maas, C. Schulz, M. Fikri, Ignition delay times of diethyl ether measured in a high-pressure shock tube and a rapid compression machine, Proc. Combust. Inst., 35 (2015) 259–266, doi:10.1016/j.proci.2014.06.143.

[88] J.E. Dec, W. Hwang, Characterizing the Development of Thermal Stratification in an HCCI Engine Using Planar-Imaging Thermometry, SAE Int. J. Engines, 2 (2009) 421–438, doi:10.4271/2009-01-0650.

[89] J.E. Dec, W. Hwang, M. Sjöberg, An Investigation of Thermal Stratification in HCCI, SAE Technical Paper 2006-01-1518 (2006).

[90] Z. Tang, L. Zhang, X. Chen, G. Tang, Improved Kinetic Mechanism for Diethyl Ether Oxidation with a Reduced Model, Energy Fuels, 31 (2017) 2803–2813, doi:10.1021/acs.energyfuels.6b02010.

[91] D. Schröder, K. Banke, S.A. Kaiser, B. Atakan, The kinetics of methane ignition in fuel-rich HCCI engines: DME replacement by ozone, Proc. Combust. Inst., 38 (2020) 5567–5574, doi:10.1016/j.proci.2020.05.046.

[92] Flynn et al., Premixed Charge Compression Ignition Engine with Optimal Combustion Control, US Patent 6,286,482 B1 (2001).

[93] A. Schönborn, P. Hellier, A.E. Aliev, N. Ladommatos, Ignition control of homogeneous-charge compression ignition (HCCI) combustion through adaptation of the fuel molecular structure by reaction with ozone, Fuel, 89 (2010) 3178–3184, doi:10.1016/j.fuel.2010.06.005.

[94] W. Weng, E. Nilsson, A. Ehn, J. Zhu, Y. Zhou, Z. Wang, Z. Li, M. Aldén, K. Cen, Investigation of formaldehyde enhancement by ozone addition in CH 4 /air premixed flames, Combust. Flame, 162 (2015) 1284–1293, doi:10.1016/j.combustflame.2014.10.021.

[95] H. Yamada, M. Ohtomo, M. Yoshii, A. Tezaki, Controlling mechanism of ignition enhancing and suppressing additives in premixed compression ignition, Int. J. Engine Res., 6 (2005) 331–340, doi:10.1243/146808705X30594.

[96] A. Mohammadi, H. Kawanabe, T. Ishiyama, M. Shioji, A. Komada, Study on Combustion Control in Natural-Gas PCCI Engines with Ozone Addition into Intake Gas, SAE Technical Paper 2006-01-0419 (2006).

[97] F. Contino, J.-B. Masurier, F. Foucher, T. Lucchini, G. D'Errico, P. Dagaut, CFD simulations using the TDAC method to model iso-octane combustion for a large range of ozone seeding and temperature conditions in a single cylinder HCCI engine, Fuel, 137 (2014) 179–184, doi:10.1016/j.fuel.2014.07.084.

[98] S. Sayssouk, D. Nelson-Gruel, C. Caillol, P. Higelin, Y. Chamaillard, Towards control of HCCI combustion by ozone addition: a mathematical approach to estimate combustion parameters, IFAC-PapersOnLine, 49 (2016) 361–368, doi:10.1016/j.ifacol.2016.08.054.

[99] J.-B. Masurier, F. Foucher, G. Dayma, P. Dagaut, Effect of Additives on Combustion Characteristics of a Natural Gas Fueled HCCI Engine, SAE Technical Paper 2014-01-2662 (2014).

[100] V.Y. Basevich, A.A. Belyaev, V.S. Posvyanskii, S.M. Frolov, Kinetic nature of blue flames in the autoignition of methane, Russ. J. Phys. Chem. B, 8 (2014) 326–331, doi:10.1134/S1990793114030026.

[101] D. Kaczmarek, B. Atakan, T. Kasper, Investigation of the partial oxidation of methane/n-heptane-mixtures and the interaction of methane and n-heptane under ultra-rich conditions, Combustion and Flame, 205 (2019) 345–357, doi:10.1016/j.combustflame.2019.04.005.

[102] Y. Wang, L. Wei, G. Jia, M. Yao, A Theoretical Investigation of the Combustion of PRF90 under the Flexible Cylinder Engine Mode, SAE Technical Paper 2017-01-1027 (2017).

[103] H. Zhao, X. Yang, Y. Ju, Kinetic studies of ozone assisted low temperature oxidation of dimethyl ether in a flow reactor using molecular-beam mass spectrometry, Combustion and Flame, 173 (2016) 187–194, doi:10.1016/j.combustflame.2016.08.008.

[104] M.M. Namar, O. Jahanian, Energy and exergy analysis of a hydrogen-fueled HCCI engine, J Therm Anal Calorim, 137 (2019) 205–215, doi:10.1007/s10973-018-7910-7.

[105] K. Banke, S.A. Kaiser, Syngas production from biogas in a polygeneration process: Simultaneous partial oxidation and dry reforming in a piston engine, Proc. Combust. Inst., 39 (2023) 5011–5020, doi:10.1016/j.proci.2022.08.132.

[106] J. Rostrup-Nielsen, in: Natural gas conversion VII: Proceedings of the 7th Natural Gas Conversion Symposium, June 6-10, 2004, Dalian, China, 1st ed., Elsevier, Amsterdam, Boston, 2004, pp. 121–126.

[107] A.Y. Khodakov, W. Chu, P. Fongarland, Advances in the development of novel cobalt Fischer-Tropsch catalysts for synthesis of long-chain hydrocarbons and clean fuels, Chemical reviews, 107 (2007) 1692–1744, doi:10.1021/cr050972v.

[108] A. Giehr, L. Maier, S.A. Schunk, O. Deutschmann, Thermodynamic Considerations on the Oxidation State of Co/γ-Al 2 O 3 and Ni/γ-Al 2 O 3 Catalysts under Dry and Steam Reforming Conditions, ChemCatChem, 10 (2018) 751–757, doi:10.1002/cctc.201701376.

[109] A.W. Budiman, S.-H. Song, T.-S. Chang, C.-H. Shin, M.-J. Choi, Dry Reforming of Methane Over Cobalt Catalysts: A Literature Review of Catalyst Development, Catal Surv Asia, 16 (2012) 183–197, doi:10.1007/s10563-012-9143-2.

[110] O. Corigliano, P. Fragiacomo, Technical analysis of hydrogen-rich stream generation through CO2 reforming of biogas by using numerical modeling, Fuel, 158 (2015) 538–548, doi:10.1016/j.fuel.2015.05.063.

[111] M. Ocsachoque, F. Pompeo, G. Gonzalez, Rh–Ni/CeO2–Al2O3 catalysts for methane dry reforming, Catalysis Today, 172 (2011) 226–231, doi:10.1016/j.cattod.2011.02.057.

[112] B. Albrecht, Reactor modeling and process analysis for partial oxidation of natural gas, Dissertation, University of Twente (2004).

[113] M. Skjøth-Rasmussen, P. Glarborg, M. Østberg, J. Johannessen, H. Livbjerg, A. Jensen, T. Christensen, Formation of polycyclic aromatic hydrocarbons and soot in fuel-rich oxidation of methane in a laminar flow reactor, Combustion and Flame, 136 (2004) 91–128, doi:10.1016/j.combustflame.2003.09.011.

[114] D. Mann, Rice, Steven, D., Autothermal reforming of natural gas to synthesis gas, Reference: KBR paper #2031, Sandia Report SAND2007-2331 (2007).

[115] T. Alger, B. Mangold, Dedicated EGR: A New Concept in High Efficiency Engines, SAE Int. J. Engines, 2 (2009) 620–631, doi:10.4271/2009-01-0694.

[116] C. Chadwell, T. Alger, J. Zuehl, R. Gukelberger, A Demonstration of Dedicated EGR on a 2.0 L GDI Engine, SAE Int. J. Engines, 7 (2014) 434–447, doi:10.4271/2014-01-1190.

[117] Z. Xu, L. Zhu, Z. He, A. Li, Y. Shao, Z. Huang, Performance optimization of in-cylinder thermochemical fuel reforming (TFR) with compression ratio in an SI natural gas engine, Fuel, 203 (2017) 162–170, doi:10.1016/j.fuel.2017.04.109.

[118] Z. He, L. Zhu, Z. Xu, O. Kaario, A. Li, Z. Huang, Effects of ethanol enrichment on in-cylinder thermochemical fuel reforming (TFR) spark ignition natural gas engine, Fuel, 197 (2017) 334–342, doi:10.1016/j.fuel.2017.02.053.

[119] W. Zhou, S. Zhou, H. Xi, M. Shreka, Z. Zhang, Numerical Study on the Effect of Fuel Rich n-Heptane on In-Cylinder Fuel Reforming Characteristics in an HCCI Engine, Int. J. Chem. Eng., 2021 (2021) 1–14, doi:10.1155/2021/2029740.

[120] R. Amirante, E. Distaso, P. Tamburrano, R.D. Reitz, Laminar flame speed correlations for methane, ethane, propane and their mixtures, and natural gas and gasoline for spark-ignition engine simulations, International Journal of Engine Research, 18 (2017) 951–970, doi:10.1177/1468087417720018.

[121] H. Gossler, S. Drost, S. Porras, R. Schießl, U. Maas, O. Deutschmann, The internal combustion engine as a CO2 reformer, Combustion and Flame, 207 (2019) 186–195, doi:10.1016/j.combustflame.2019.05.031.

# Publications

## Peer-reviewed journal articles

- K. Banke, R. Hegner, D. Schröder, C. Schulz, B. Atakan, S.A. Kaiser, Power and syngas production from partial oxidation of fuel-rich methane/DME mixtures in an HCCI engine, Fuel (2019) 97–103, doi:10.1016/j.fuel.2019.01.076.

- K. Banke, D. Freund, B. Atakan, S.A. Kaiser, Evaluation of fuel additives for HCCI engines operated on fuel-rich methane/air mixtures: DME, DEE, and n-heptane, Applications in Energy and Combustion Science, 13 (2023) 100112, doi:10.1016/j.jaecs.2023.100112.

- K. Banke, S.A. Kaiser, Syngas production from biogas in a polygeneration process: Simultaneous partial oxidation and dry reforming in a piston engine, Proc. Combust. Inst., 39 (2023) 5011–5020, doi:10.1016/j.proci.2022.08.132.

- D. Schröder, K. Banke, S.A. Kaiser, B. Atakan, The kinetics of methane ignition in fuel-rich HCCI engines: DME replacement by ozone, Proc Combust Inst, 38 (2020) 5567–5574, doi:10.1016/j.proci.2020.05.046.

- B. Atakan, S.A. Kaiser, J. Herzler, S. Porras, K. Banke, O. Deutschmann, T. Kasper, M. Fikri, R. Schießl, D. Schröder, C. Rudolph, D. Kaczmarek, H. Gossler, S. Drost, V. Bykov, U. Maas, C. Schulz, Flexible energy conversion and storage via high-temperature gas-phase reactions: The piston engine as a polygeneration reactor, Renewable Sustainable Energy Rev, 133 (2020) 110264, doi:10.1016/j.rser.2020.110264.

## Conference contributions (oral presentation)

- K. Banke, S. Wiemann, R. Hegner, B. Atakan, C. Schulz, S.A. Kaiser, Combined production of power and syngas in an internal combustion engine, International Bunsen Discussion Meeting, Bielefeld, Germany, 22.06.2017.

- K. Banke, S.A. Kaiser, Syngas production from biogas in a polygeneration process - simultaneous partial oxidation and dry reforming in a piston engine, 30. Deutscher Flammentag, Hannover-Garbsen, Germany, 28.09.2021.

- K. Banke, S.A. Kaiser, Syngas production from biogas in a polygeneration process - simultaneous partial oxidation and dry reforming in a piston engine, 39th International Symposium on Combustion, Vancouver, Canada, 29.07.2022. (presented by S.A. Kaiser due to illness).

## Conference contributions (poster presentation)

- K. Banke, S.A. Kaiser, Polygeneration by partial oxidation of fuel-rich Methane/air mixtures in an HCCI engine – Different approaches to achieve auto-ignition, Heraeus Seminar, Bad Honnef, Germany, 09.03.2020.

- K. Banke, S.A. Kaiser, Comparison of fuel additives for syngas production from fuel-rich methane HCCI combustion, 9th European Combustion Meeting, Lisbon, Portugal, 15.04.2019.